

Identification and Characterization of EMB1674, as a Novel KNL2 Variant: Revealing its Centromere Targeting Mechanism and Critical Role in Plant- Specific Kinetochore Assembly

Dissertation

zur Erlangung des

Doktorgrades der Naturwissenschaften (Dr. rer. nat.)

der

Naturwissenschaftlichen Fakultät III

Agrar- und Ernährungswissenschaften,

Geowissenschaften und Informatik

Martin-Luther-Universität Halle-Wittenberg

vorgelegt von

Herr Ramakrishna Yadala (M. Tech)

Gatersleben, den 17.01.2025

Gutachter:

Prof. Dr. Andreas Houben

Prof. Dr. Sylvia Erhardt

Tag der öffentlichen Verteidigung: 07.07.2025, Halle (Salle)

Acknowledgements

I would like to express my deepest gratitude to those who have supported and guided me throughout my PhD journey. Firstly, I am profoundly thankful to my supervisor, Dr. Inna Lermontova, for her unwavering support, insightful guidance, and continuous encouragement. Her expertise, patience, and encouragement have been invaluable and instrumental. Without her guidance, the successful completion of this work would not have been possible. She has greatly helped in improving my writing skills, involving me in proposal and paper writing, peer reviewing manuscripts, and supervising students. She has been supportive not only scientifically but also personally, helping me handle critical situations in my personal life like a sister and mother.

I would also like to extend my sincere thanks to Prof. Andreas Houben for accepting to mentor me and defend my PhD thesis under him. I am grateful to Prof. Thorsten Schnurbusch, Assoc. prof. Aleš Pečinka, Prof. Jochen Reif, and Prof. Nils Stein for their encouraging support, motivation, and guidance for career development. I would like to express my heartfelt gratitude to Dr. Ravi Koppolu and Assoc. Prof. Jalaja Naravula for their kindness and guidance in the early stages of my career.

A special thank you to my colleagues at Kinetochore Biology group, collaborators, and friends Amanda, Sheng Zuo, Fen Yang, Dmitri, Bhanu, Ragav, and Saravana for your collaboration, stimulating discussions, and the camaraderie we shared. I would to appreciate and thank all the members of Chromosome Biology theme groups: Agr. CSF (Prof. Houben), Agr. ME (Dr. Heckmann), Agr. ACB (Prof. Jiang), for their support, suggestion and critical evaluation every year during my PhD time. I would also like to thank the radish group at Enza Zaden for their support, particularly Xana Verwek, Chiara Volpi, and other team members.

I am deeply appreciative of the administrative, technical staff and gardeners at IPK, Gatersleben, particularly Pascal, Heike, Bianka, and Ole-Christian, for their assistance and for ensuring that everything ran smoothly. Your behind-the-scenes work does not go unnoticed.

I would like to thank Dr. Rathaiah Lavu and Vignan's Foundation for Science, Technology & Research for their financial support and encouragement, which enabled me to travel to Germany during my master's thesis. Finally, I would like to acknowledge the funding agencies and organizations that provided financial support for my research, including Enza Zaden and the BMBF Wipano program.

Whenever I hear the poem "మరో ప్రపంచం" by Sri Sri, I imagine myself amidst its vivid imagery. The call to move towards a new world, to advance forward with vigor and determination, resonates deeply within me. This poem's spirit of revolution, urging people to march ahead, face challenges, and overcome obstacles, has been a powerful source of motivation in my journey.

Despite the challenging circumstances, I was always inspired by the desire to rise and act for a brighter future. My parents, though uneducated, dreamed big for me. As daily wage laborers, my father worked tirelessly as a lorry cleaner and daily wage laborer during his breaks. My mother, without ever having a moment of rest, prepared us for school before heading to work.

I began my journey as a bright student in the class and had lot of distraction in the journey. Every time I veered off course, it was the unwavering support of my father, mother, and later my wife, that corrected me and guided me back to the path leading here. My wife's words have always been a source of strength and inspiration: "A village boy with not much means, struggling and defying every odd he faces to study and be in a position he dreams. You have got too much work and too little time. But you should know this will be the life till the end. You are supposed to multitask. Life will never be easy on us."

I owe my deepest gratitude to my parents; whose sacrifices and dreams paved the way for my education and success. To my wife, your belief in me and your unwavering support have been my anchor. Your words continue to remind me that perseverance and hard work are the keys to overcoming life's challenges.

This thesis is not just a culmination of my academic endeavors but a testament to the strength, resilience, and unwavering support of my family. Thank you for believing in me and for being my pillars of strength. This achievement is as much yours as it is mine.

Thank you all for your invaluable contributions and being a part of this incredible experience.

మరో ప్రపంచం, మరో ప్రపంచం, మరో ప్రపంచం పిలిచింది! పదండి ముందుకు, పదండి త్రోసుకు! పోదాం, పోదాం పైపైకి!
కదం త్రొక్కుతూ, పదం పాడుతూ, హ్రుదాంతరాళం గర్జిస్తూ- పదండి పోదాం, వినబడలేదా మరో ప్రపంచపు జలపాతం?
దారిపొడుగునా గుండె నెత్తురులు తర్పణ చేస్తూ పదండి ముందుకు! బాటలు నడచి, పేటలు కడచి, కోటలన్నిటినీ దాటండి!
నదీ నదాలూ, అడవులు, కొండలు, ఎడారులూ మన కథలకి? పదండి ముందుకు! పదండి త్రోసుకు! పోదాం, పోదాం, పైపైకి!

- Sri Sri (Srirangam Srinivasa Rao)

Table of contents

Chapter 1: Introduction	1
1.1 Cell: The basic unit of life	2
1.2 The cell cycle and nuclear division: Orchestrating eukaryotic reproduction	2
1.2.1 Cell cycle and endoreplication	2
1.2.2 Mitosis: Vegetative nuclear division	5
1.2.3 Meiosis: Specialized division for sexual reproduction	6
1.3 Gametophyte and seed development in plants	7
1.3.1 Male gamete formation	7
1.3.2 Female gamete formation	9
1.3.3 Pollination and double fertilization in angiosperms	9
1.3.4 Embryo development	10
1.3.5 Endosperm development.....	11
1.4 Chromosome organization and structure	12
1.4.1 Chromosome, centromere structure and function	12
1.4.2 CENH3 loading across eukaryotes	14
1.5 Kinetochore	16
1.5.1 Organization of kinetochore.....	16
1.5.2 Kinetochore Null 2 (KNL2)	18
1.5.3 Centromere targeting mechanism of KNL2 in different organisms	20
Chapter 2: Aims of the thesis	22
Chapter 3: Materials and methods.....	23
3.1 Plant material and growth conditions	23
3.2 DNA isolation.....	23
3.3 Polymerase Chain Reaction (PCR) based genotyping of transgenic plants and T-DNA insertion mutants.....	23
3.4 RNA isolation	25
3.5 cDNA synthesis	25
3.6 Molecular cloning and generation of expression vectors	26
3.6.1 Amplification and purification of genomic fragments or coding sequences (CDS) for molecular cloning	26
3.6.2 GATEWAY-compatible vectors construction for BiFC.....	26
3.6.3 Gateway cloning to generate plant expression vectors	27
3.6.4 Generation of wheat germ expression vector for β KNL2.....	28
3.6.5 Site directed mutagenesis.....	28
3.6.6 Bacterial transformation.....	29

3.6.7 Colony PCR for selection of positive clones	30
3.6.8 Plasmid isolation	30
3.7 Sanger sequencing	31
3.8 Plant transformation	31
3.8.1 Transient transformation of <i>N. benthamiana</i>	31
3.8.2 Stable transformation of <i>A. thaliana</i>	31
3.9 Seeds sterilization	32
3.10 Analysis of T-DNA insertion mutants	32
3.11 Gametophyte and developing embryo analysis	33
3.11.1 FDA staining	33
3.11.2 Hoyer's Clearing	33
3.12 Flow cytometry	33
3.13 Immunostaining	34
3.14 Microscopy analysis	34
3.15 Statistical analysis	35
3.16 Sequence motif analysis	35
3.17 Electrophoretic mobility shift assay	36
3.18 Bimolecular Fluorescence Complementation (BiFC)	36
3.19 Co-Immunoprecipitation (Co-IP)	36
3.20 AlphaFold2 protein predictions and molecular dynamics analysis	37
3.21 Experimental and technical contributions by the collaborators for the present thesis .	40
Chapter 4: Results	41
4.1 <i>KNL2</i> gene underwent independent duplications across plant lineages	41
4.2 <i>Arabidopsis</i> β KNL2 is highly expressed in meristematic tissues and localizes to centromeres despite lacking CENPC-k motif	43
4.3 β KNL2 knockout resulted in an abnormal seed development phenotype	45
4.4 <i>In-vitro</i> recovered β KNL2 homozygous mutants cannot survive beyond seedling stage	46
4.5 <i>Arabidopsis</i> β KNL2 is essential for correct somatic cell division	50
4.6 Loss of β KNL2 impacted nuclear divisions and development of both embryo and endosperm in <i>Arabidopsis</i>	52
4.7 <i>Arabidopsis</i> β KNL2 is required for proper CENH3 loading	55
4.8 Loss of β KNL2 results in cells with high ploidy levels.	57
4.9 SANTA domain and C-terminus of β KNL2 are required for its efficient centromeric targeting	58
4.10 C- terminal motif-III of β KNL2 is required for its nuclear localization	60
4.11 β KNL2 demonstrates <i>in vitro</i> binding to centromeric DNA	64

4.12 Centromeric recruitment of β KNL2 depends on CENPC-k motif containing α KNL2	65
4.13 β KNL2 form homodimer and heterodimer with α KNL2	67
4.14 β KNL2 is highly dynamic and loosely bound to centromeric nucleosome through its SANTA domain and C-terminal conserved motifs	71
Chapter 5: Discussion.....	75
5.1 Duplication of <i>KNL2</i>	75
5.2 The function of β KNL2 in plants	75
5.3 Loss of β KNL2 resulted in abnormal cell divisions	77
5.4 Distinct conserved motifs regulate proper localization of β KNL2.....	78
5.5 β KNL2 is an inner kinetochore protein recruited by CENPC-like motif containing proteins like α KNL2	79
5.6 β KNL2 dimerize to facilitate or support centromere assembly and kinetochore platform	80
Chapter 6: Outlook	82
6.1 Functional roles of β KNL2 domains and SUMOylation beyond centromere targeting.	82
6.2 Tissue dependent centromeric recruitment of β KNL2 governed by CENPC-like motif containing proteins	83
6.3 Bridging the gap: mapping the interaction network of plant kinetochore proteins and their role in chromosome stability	84
6.4 Structural determination of the <i>Arabidopsis</i> CENH3 nucleosome complex with α KNL2 and β KNL2	85
6.5 KNL2 manipulation: A gateway to efficient haploid production.....	85
Chapter 7: Summary.....	87
Chapter 8: Zusammenfassung	88
Chapter 9: References	90
Chapter 10: Appendix	101
Chapter 11: Curriculum vitae	112
Chapter 12: Eidesstattliche Erklärung / Declaration under oath	114

Abbreviation

35S	Cauliflower Mosaic Virus 35S Promoter
3D-SIM	Three-Dimensional Structural Illumination Microscopy
AA	Amino Acid
AGL62	AGAMOUS-LIKE 62
AF2	AlphaFold2
APC/C	Anaphase-Promoting Complex/Cyclosome
BiFC	Bimolecular Fluorescence Complementation
BK Buffer	Bermuda Grass Buffer
bp	Base Pair
BSA	Bovine Serum Albumin
C-term	C-terminal
CBF3	Centromere Binding Factor 3 Complex
CCAN	Constitutive Centromere Associated Network
CDKs	Cyclin-Dependent Kinases
cDNA	Complementary DNA
CENH3	Centromeric Histone 3
CENP	Centromere Protein
ChIP	Chromatin Immunoprecipitation
CLSM	Confocal Laser Scanning Microscope
Co-IP	Co-Immunoprecipitation
DAPI	4',6-Diamidino-2-Phenylindole
ddH ₂ O	Double Distilled Water
DNA	Deoxyribonucleic Acid
dNTPs	Deoxynucleotide Triphosphates

DSSP	Dictionary of Secondary Structure of Proteins
EDTA	Ethylenediaminetetraacetic Acid
EMB	Embryo Defective
EMSA	Electrophoretic Mobility Shift Assay
EYFP	Enhanced Yellow Fluorescent Protein
FIS	FERTILIZATION INDEPENDENT SEED
FC	Flow Cytometry
FDA	Fluorescein Diacetate
FRET	Fluorescence Resonance Energy Transfer
FLIP	Fluorescence Loss in Photobleaching
FRAP	Fluorescence Recovery After Photobleaching
GFP	Green Fluorescent Protein
GW	Gateway
KIP1	Kinase Interacting Protein 1
kDa	Kilodalton
kb	Kilobase Pair
KNL2	Kinetochore Null 2
KMN	Kinetochore Network
LB	Luria-Bertani
LB3.1	Left Border Primer 3.1
M	Molar
MTOCs	Microtubule Organizing Centers
Mis18BP1	Mis18 Binding Protein 1
MS Medium	Murashige and Skoog Medium
mg	Milligram

ml	Milliliter
mM	Millimolar
μ M	Micromolar
μ l	Microliter
μ m	Micrometer
ng	Nanogram
nm	Nanometer
NaCl	Sodium Chloride
N-term	N-terminal
OD	Optical Density
PAGE	Polyacrylamide Gel Electrophoresis
PBS	Phosphate-Buffered Saline
PDB	Protein Data Bank
PLK1	Polo-like Kinase 1
PMC	Pollen Mother Cell
pDNA	Plasmid DNA
PCR	Polymerase Chain Reaction
PPI	Protein Interaction
PTM	Post-Translational Modification
qPCR	Quantitative Polymerase Chain Reaction
Rh	Rhodamine
RMSD	Root Mean Square Deviation
RNA	Ribonucleic Acid
RT	Reverse Transcriptase
SAC	Spindle Assembly Checkpoint

SANTA	SANTA Domain
SDS	Sodium Dodecyl Sulfate
SEM	Scanning Electron Microscopy
seq	Sequencing
SMC_Prok_B	Structural Maintenance of Chromosomes Prokaryotic Bacterial Domain
SUMO	Small Ubiquitin-like Modifier
TAIR	The <i>Arabidopsis</i> Information Resource
T-DNA	Transfer DNA
tocs	<i>Octopine Synthase</i> Gene Terminator
T _m	Melting Temperature
Tris	Tris(hydroxymethyl)aminomethane
Ven	Venus Fluorescent Protein
WB	Western Blot
WGD	Whole Genome Duplication
WT	Wild Type
°C	Degrees Celsius
%	Percent

Chapter 1: Introduction

Observing the diverse forms of life from plants to animals and humans one cannot help but notice profound structural and functional similarities. For instance, the roots of a plant are akin to the legs, providing support to stand, while branches resemble arms, extending outward to interact with the environment. These observations evoke my thoughts on evolutionary processes and the theory of common ancestry.

Charles Darwin's theory of evolution, primarily outlined in *On the Origin of Species* (1859), transitioned the scientific community from a perspective of divine creation to natural selection. Darwin proposed that species evolve through natural selection and common descent (Delisle, 2021) and this idea revolutionized biology by suggesting that variations within a species affect survival and reproduction, allowing advantageous traits to become predominant. The concept "survival of the fittest", describes natural selection as a process where organisms best adapted to their environments are more likely to survive and reproduce (Darwin, 1859).

Before Darwin, the dominant belief was in spontaneous generation, which posited that life could emerge from non-living material. This was challenged by experiments from scientists like Francesco Redi and Louis Pasteur, who demonstrated that life arises from pre-existing life, not inanimate matter, effectively disproving spontaneous generation and setting the stage for biogenesis as the accepted explanation for life's origins (Pasteur and Edelfelt, 1886, Strick, 1997). Post-Darwinian theories further explored life's origins. The Oparin-Haldane hypothesis suggested that life began in a "primordial soup" of organic compounds, a notion supported by Miller and Urey's experiments (Miller, 1953, Xie et al., 2015).

Advances in molecular biology have supported the concept of a universal common ancestry, indicating that all life forms share fundamental molecular components DNA, RNA, and proteins suggestive of a singular origin (Brown et al., 2001). The theory of endosymbiosis provided insights into the evolution of complex cells from simpler ancestors through symbiotic relationships, further emphasizing life's evolutionary complexity (Embley et al., 2003, Poole and Penny, 2007). These hypotheses underscore the understanding of life's chemical and biological origins, painting a complex picture of life from simple organic molecules to complex cellular structures.

1.1 Cell: The basic unit of life

Cells are the foundational units of all life forms; The cell theory proposed by German scientists, Theodore Schwann and Matthias Schleiden was developed over two centuries (Deatherage and Deatherage, 1975, Jacob, 1839, Schwann, 1847). Cells are categorized into two main types: prokaryotic and eukaryotic. Prokaryotic cells, found in bacteria and archaea, are simple, lacking a nucleus and membrane-bound organelles, while eukaryotic cells, found in fungi, plants, and animals, are complex, with a defined nucleus and specialized organelles (Fig. 1A).

One of the most remarkable features of cells is their ability to reproduce. This capability is essential for growth, development, and evolution. All cells arise from the division of pre-existing cells, a principle that was solidified in the cell theory. The reproduction of cells, driven by the accurate transmission of genetic information encoded in DNA, occurs through a carefully coordinated series of events known as the cell cycle. This process ensures the successful duplication and distribution of genetic material to daughter cells, allowing for the continuation of life.

1.2 The cell cycle and nuclear division: Orchestrating eukaryotic reproduction

1.2.1 Cell cycle and endoreplication

The cell cycle is a highly regulated process critical for maintaining proper cell growth, DNA replication, and division. In proliferating eukaryotic cells, this process ensures that the cell increases in size, faithfully replicates its genome, and accurately distributes each copy of the genetic material to two daughter cells. This precise coordination of events is essential for the maintenance of genetic stability and the successful completion of cell division. Cell division is the foundational process through which organisms grow, repair tissues, and reproduce (Abraham, 1939, Mazia, 1961).

The eukaryotic cell cycle comprises four main phases (Fig. 1B) (Howard and Pelc, 1953) that ensure proper cell growth and division. During the G1 phase, the cell grows to an optimal size and accumulates resources necessary for DNA synthesis. Depending on conditions, the cell may either enter the S phase for DNA replication or enter a non-dividing state, G0, if factors like nutrient supply are unfavorable (Vermeulen et al., 2003b, Vermeulen et al., 2003a). In the S phase, chromosomes are duplicated into sister chromatids, with accuracy being crucial to prevent genetic errors. Following this, in the G2 phase, the cell continues to grow and synthesizes proteins needed for mitosis, with a checkpoint to ensure that DNA replication is complete and intact. Finally, in the M phase, the cell undergoes either mitosis, producing two

identical daughter cells, or meiosis, resulting in gametes with half the parental chromosome number.

During the interphase (G1-S-G2), cells that have duplicated their DNA pass through a critical checkpoint before entering the M phase, during which chromosomes become visibly organized. Variations in the standard G1–S–G2–M cell cycle can result in an endoreplication or endomitosis, or cell cycle arrest (Fig. 1B).

Endoreplication is a process where cells replicate their DNA without undergoing mitosis, resulting in increased DNA content through genome doublings. Endoreplication is common in various organisms, including plants and animals, and plays a crucial role in cell growth and differentiation (Lee et al., 2009, Tourdot et al., 2023, Shu et al., 2018). Despite the potential risks to genome integrity, endoreplication is essential for normal development. Many organisms utilize endoreplication during terminal differentiation to generate the nutrients and proteins essential for embryogenesis. This process is particularly important in structures like plant endosperm and suspensor cells, which play critical roles in supporting the developing embryo (Tourdot et al., 2023, Yeung and Meinke, 1993). The increase in DNA content supports the high metabolic demands of these cells by switching from the mitotic cell cycle to an endoreplication after fertilization (Grafi and Larkins, 1995, Leiva-Neto et al., 2004).

Endomitosis is a process similar to endoreplication but involves incomplete mitosis. Unlike endoreplication, endomitotic cells display early mitotic markers such as phospho-histone H3 (Hendzel et al., 1997). For instance, endomitotic megakaryocytes reach metaphase or anaphase but do not separate sister chromatids (Nagata et al., 1997, Vitrat et al., 1998). These cells replicate their DNA and initiate mitosis but do not complete cytokinesis, resulting in cells with multiple nuclei or a single enlarged nucleus (Lee et al., 2009).

The regulation of mitosis and endoreplication involves cyclin-dependent kinases (CDKs) and their regulatory partners, cyclins (Imai et al., 2006, Lilly and Spradling, 1996, Levan and Hauschka, 1953). In endoreplication, the suppression of mitotic CDK activity is crucial and is often mediated by proteins that activate the anaphase-promoting complex/cyclosome (APC/C) to degrade mitotic cyclins, thereby preventing mitosis (Marrocco et al., 2009, Genschik et al., 2014, Roodbarkelari et al., 2010, Su'udi et al., 2012, Mathieu-Rivet et al., 2010, Cebolla et al., 1999, Serralbo et al., 2006). Dysfunction or loss of critical cell cycle or checkpoint proteins can lead to abnormal endoreplications or endomitosis (Demidov et al., 2014, Lilly and Spradling, 1996).

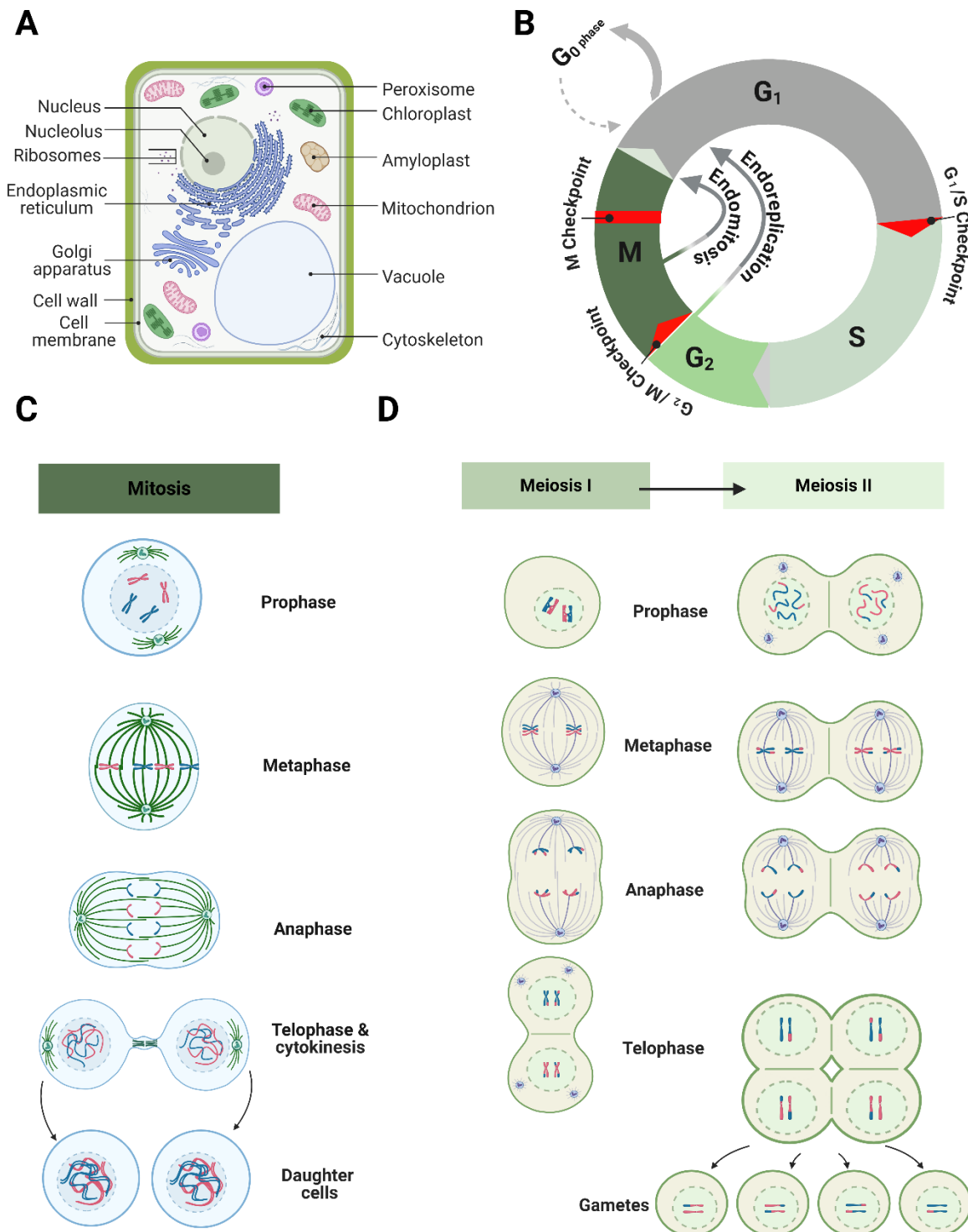


Figure 1. Overview of cell division processes in eukaryotic cells.

(A) A schematic representation of a typical plant cell, highlighting essential organelles involved in cellular functions. (B) The cell cycle is depicted, outlining the progression through different phases: G₁ (first gap phase), S (synthesis phase), G₂ (second gap phase), and M (mitosis) phase. The checkpoints that ensure proper cell cycle progression, including the G₁/S checkpoint, G₂/M checkpoint, and the M checkpoint. The diagram also shows the pathways of endoreplication and endomitosis, which diverge from the standard mitotic cycle. (C) The stages of mitosis, including prophase, metaphase, anaphase, telophase, and cytokinesis, are depicted. The process results in the formation of two daughter cells, each genetically identical to the parent cell. (D) The stages of meiosis, divided into Meiosis I and Meiosis II, are illustrated. Meiosis I involve the separation of homologous chromosomes, while Meiosis II resembles a mitotic division, resulting in four gametes, each with half the number of chromosomes as the original cell, essential for sexual reproduction.

1.2.2 Mitosis: Vegetative nuclear division

Mitosis in plant cells involves a series of well-coordinated steps, starting with the condensation of chromosomes in prophase (Fig. 1C) (Polymenis, 2022, Hiraoka et al., 1990). As chromosomes condense, transcription halts, and the nucleolus disassembles (DiMario, 2004, Vikal and Kaur, 2017). Unlike animals, plant cells do not have centrosomes. Instead, microtubules are nucleated from microtubule organizing centers (MTOCs) that are dispersed around the nuclear envelope region. Microtubules form distinct structures, including the preprophase band, the mitotic spindle, and the phragmoplast (Smertenko, 2018, Pickett-Heaps and Northcote, 1966). In early or late prophase, the nuclear envelope breaks down allowing microtubules to attach kinetochores (McIntosh, 2016, Beaudouin et al., 2002). Kinetochores, essential for chromosome segregation, form on the centromeric regions. These multi-protein complexes serve as attachment points for spindle microtubules.

The breakdown of the nuclear envelope marks the beginning of prometaphase, facilitated by the phosphorylation of nuclear envelope proteins by CDKs (Dorée and Galas, 1994, Lilly and Spradling, 1996, Silva et al., 2012). Unlike animals, plants lack lamin proteins, which play a key role in nuclear envelope breakdown (Fiserova and Goldberg, 2010). Instead, they have CRWN proteins which localize to the nuclear periphery and nucleoplasm (Dittmer et al., 2007, Sakamoto and Takagi, 2013, Wang et al., 2013).

Spindle microtubules grow towards chromosomes and attach to kinetochores. The capture and stabilization of microtubules by kinetochores are crucial for aligning chromosomes at the metaphase plate. Initially, spindle microtubules interact laterally with kinetochores. This lateral interaction is the first contact between microtubules and kinetochores. These initial lateral attachments are then converted into stable end-on attachments, where the plus ends of the microtubules directly attach to the kinetochore (Foley and Kapoor, 2013, Liu and Palevitz, 1991). This conversion is crucial for generating proper tension and stabilizing the kinetochore-microtubule interactions (Rosas-Salvans et al., 2022, Liu and Lee, 2022, Pickett-Heaps and Northcote, 1966, Bouck and Brown, 1973, Foley and Kapoor, 2013).

During metaphase, chromosomes align at the cell's equator, with kinetochores facing opposite spindle poles (McIntosh, 1985, Hiraoka et al., 1990, Ferreira and Maiato, 2021, Franklin and Cande, 1999). Any attachment errors are corrected through the action of Aurora kinase, which destabilizes incorrect microtubule connections, allowing for reattachment (Cimini et al., 2006, Cimini, 2007, Su et al., 2021). This error correction is vital to prevent aneuploidy (Demidov et

al., 2014, Demidov et al., 2019). Abnormal expression of key kinetochore genes can lead to misalignment of chromosomes at the metaphase plate, disrupting proper cell division and leading to genetic instability (Deng et al., 2024, Paganelli et al., 2015, Shin et al., 2018, Lermontova et al., 2013, Ravi et al., 2011, Umbreit et al., 2012, DeLuca et al., 2006).

The spindle assembly checkpoint (SAC) ensures all chromosomes are correctly attached to microtubules before anaphase (McAinsh and Kops, 2023). Unattached kinetochores signal to inhibit the APC/C, preventing securin and cyclin B degradation (Kamenz and Hauf, 2014, Holder et al., 2020). Once alignment is achieved, the APC/C degrades securin, releasing separase, which then cleaves the cohesin and initiate anaphase. (Izawa and Pines, 2011). During anaphase, sister chromatids are pulled towards opposite poles as kinetochore microtubules shorten, powered by motor proteins and the depolymerization of tubulin subunits.

Anaphase bridges are formed when chromosomes fail to segregate properly during cell division. This typically occurs due to abnormalities in chromosome structure, unresolved recombination intermediates, telomere dysfunction or abnormal kinetochore function (Varas et al., 2017, Yang et al., 2021, Lermontova et al., 2013, Higgins et al., 2005, Riha et al., 2001, Jaške et al., 2013). All of which are essential for the accurate attachment of spindle microtubules to chromosomes. Telophase follows, characterized by the reformation of the nuclear envelope, decondensation of chromosomes, and reassembly of the nucleolus.

1.2.3 Meiosis: Specialized division for sexual reproduction

Meiosis is a specialized cell division process that generates four gametes with half the chromosome content of the original cell, crucial for sexual reproduction (Fig. 1D). Meiosis differs from mitosis in that it includes two separate rounds of chromosome segregation after the DNA replication in the S-phase: meiosis I and meiosis II.

In meiosis I, homologous chromosomes pair up and engage in recombination, characterized by double-strand breaks that allow for the exchange of genetic material. This recombination reshuffles the genetic information, introducing variability essential for evolution and adaptation (Zickler and Kleckner, 1999, Petronczki et al., 2003). Following this, meiosis II, which resembles mitotic division, separates the sister chromatids into four distinct haploid cells. Similar to a mitotic division, meiosis II involves the separation of the sister chromatids, now individual units, into four distinct haploid cells. In plants, the formation of male and female gametes via meiosis involves distinct pathways within the reproductive structures of the flower.

1.3 Gametophyte and seed development in plants

1.3.1 Male gamete formation

Pollen development in plants is a complex, tightly regulated process essential for plant reproduction. This process, known as microsporogenesis and microgametogenesis (Fig. 2), occurs within the anthers and involves several stages leading to the formation of mature pollen grains capable of fertilization. Microsporogenesis begins with the differentiation of archesporial cells in the anther's locules, forming a mass of sporogenous tissue. Each sporogenous cell differentiates into a pollen mother cell (PMC), or microsporocyte, which undergoes meiosis. This meiotic division produces a tetrad of haploid microspores, each encased in a callose wall. Meiosis I and meiosis II result in four haploid microspores (Owen and Makaroff, 1995).

Following meiosis, the enzyme *callase* degrades the callose wall, releasing the microspores. The microspore nucleus initially resides in the center of the cytoplasm. As a large central vacuole forms, it pushes the nucleus toward the periphery, marking the transition of the microspore into a young pollen grain. Each pollen undergoes two critical mitotic divisions to form a mature pollen grain. The first asymmetric mitosis in pollen development leads to the formation of a smaller generative cell and a larger vegetative cell (Berger and Twell, 2011). This initial pollen mitosis produces a lens-shaped generative cell with its nucleus positioned near the pollen wall (Halbritter et al., 2018). Subsequently, the generative cell detaches from the wall and becomes embedded within the cytoplasm of the vegetative cell. The generative cell, lacking in organelles, gradually assumes a spindle shape, with the generative nucleus altering its shape accordingly. The generative cell undergoes a second mitotic division, producing two sperm cells (Ma, 2005). In plants like *Petunia*, *Lilium* and some other species has unique pathway like the second mitotic division occurs in the pollen tube after pollen germination (Ma, 2005, Sax and O'Mara, 1941). At maturity, pollen grains may be either two-celled, with one vegetative cell and one generative cell, or three-celled if the generative cell has already divided into sperm cells within the pollen grain.

Kinetochore proteins are crucial for accurate chromosome segregation during the meiotic and mitotic divisions of pollen development. Mutations or mis-expression of kinetochore genes like *CENH3* and *KNL2* can lead to severe defects in pollen development resulting reduced viability or partial fertility (Lermontova et al., 2011, Lermontova et al., 2013, Yang et al., 2021, Deng et al., 2024).

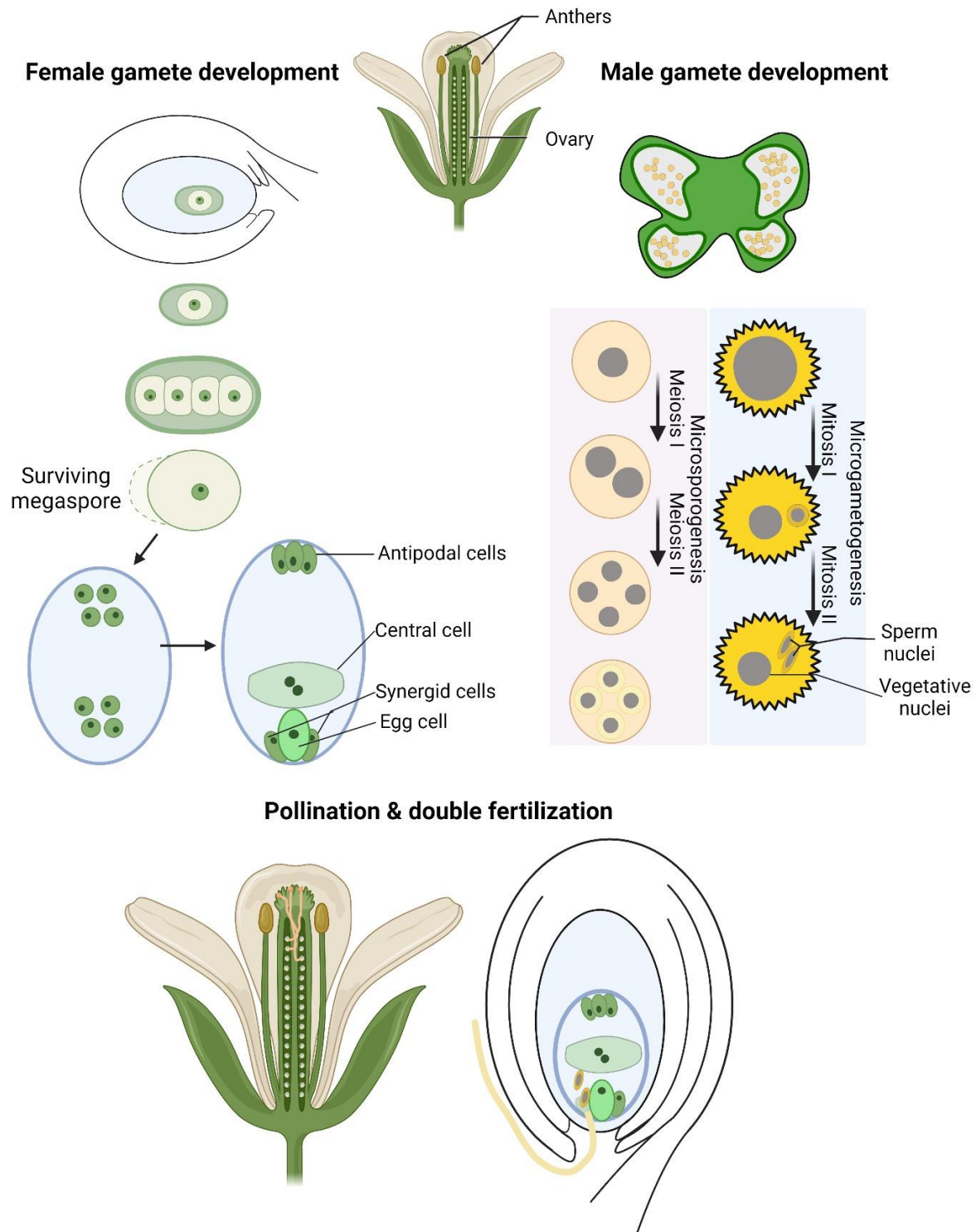


Figure 2. Overview of flower development and gametogenesis in plants

This figure illustrates the overall structure of a mature flower, highlighting key stages in the development of male and female gametophytes. Cross-sections of the anther (right) and ovule (left) are shown, depicting the development of pollen and ovules. The stages of male and female gametophyte development are detailed, beginning with the microspore and megaspore mother cells within the anther and ovule undergoing meiosis. This process produces microspores and megaspores, which subsequently develop into pollen grains and the embryo sac, respectively, each containing the male and female gametes (sperm and egg cells). The fertilization process is also depicted, showing how pollen grains land on the stigma, grow a pollen tube down the style, and deliver sperm cells to the ovule, leading to fertilization, and the initiation of seed development.

1.3.2 Female gamete formation

Female gamete development in angiosperms occurs within the ovules housed in the ovary at the base of the pistil (Fig. 2). This process involves two stages: megasporogenesis and megagametogenesis. Initially, a diploid megasporocyte within the ovule undergoes meiosis to produce four haploid megaspores. In most plants, including *Arabidopsis*, three of these megaspores degenerate, leaving one functional megaspore. This process is known as megasporogenesis (Caryl et al., 2003).

The remaining functional megaspore undergoes three mitotic divisions, resulting in an eight-nuclear embryo sac composed of different cell types with specialised functions. At the micropylar end are the egg cell required for fertilization and two synergid cells that guide the pollen tube to the egg, and at the chalazal end are three antipodal cells that support early development of the embryo and endosperm but normally degenerate after fertilization (Doronina et al., 2022, Song et al., 2014). In the centre is a homodiploid cell with two identical haploid nuclei, completing the structure of the mature germ sac (Drews and Koltunow, 2011). The egg and central cells exhibit polarity, with their nuclei positioned in close proximity due to a large central vacuole. This spatial arrangement facilitates the simultaneous fertilization of both cells by the two sperm nuclei. This entire developmental process, from a functional megaspore to a differentiated embryo sac, is called megametogenesis and is the basis for fertilization and early development in angiosperms (Caryl et al., 2003, Drews and Koltunow, 2011). Any abnormalities in embryo sac development can result in reduced seed set (Drews and Koltunow, 2011).

1.3.3 Pollination and double fertilization in angiosperms

After gamete formation, pollination can lead to fertilization. Pollen grains germinate on the stigma of the carpel and extend a pollen tube through the style to reach the ovule (Fig. 2). The generative cell splits into two sperm cells, if it hasn't already, and reaches the ovule with the help of the pollen tube. The pollen tube's growth towards the embryo sac is guided by attractants from the synergids and enters through the micropyle (Bleckmann et al., 2014). Enclosed within the pollen tube, sperm cells have thin cell walls essential for fusion. Upon release into the embryo sac, the sperm cells move through the degenerated synergid cell to the space between the egg and central cell. There, they shed their outer membrane and expand their vacuole in preparation for fusion.

Inside the ovule, one sperm cell fertilizes the egg cell, forming a diploid zygote that will develop into an embryo. The other sperm cell merges with the two polar nuclei of the central cell,

forming a triploid cell that develops into the endosperm. This process, called double fertilization, is unique to flowering plants and is crucial for initiating seed formation (Higashiyama, 2002, Hamamura et al., 2011). Double fertilization ensures the formation of a diploid embryo and a triploid endosperm, essential for the development of the seed and future plant growth (Hamamura et al., 2011). Post-fertilization, mechanisms prevent further sperm entry, allowing the ovule to develop into a seed while the surrounding ovarian tissues mature into fruit, encapsulating the seed.

1.3.4 Embryo development

Embryo and endosperm develop simultaneously in a precisely orchestrated process, transforming from a fertilized zygote into a mature embryo capable of germination (Fig. 3). Following fertilization, the single-celled zygote undergoes an asymmetric division. The smaller apical cell and a larger basal cell, establishing the apical-basal axis essential for subsequent growth (Peris et al., 2010). Apical cells develop into the embryo or embryonic leaves, while basal cells form the suspensor to support the embryo, which may degenerate in mature seeds (Johri and Ambegaokar, 1984). *Arabidopsis* embryo development follows a sequence of stages, reflecting the transformation from a fertilized zygote into a mature embryo (Armenta-Medina et al., 2021). The developmental stages are:

Zygote Stage: The zygote undergoes an asymmetric division, resulting in a smaller apical cell and a larger basal cell, setting the stage for the embryo's growth pattern.

Globular Stage: The embryo takes on a spherical shape as cells continue to divide without significant expansion, establishing the apical-basal axis.

Heart Stage: The embryo assumes a heart-like shape with the formation of cotyledons. Tissue differentiation becomes more apparent, with the development of protoderm, ground meristem, and procambium.

Torpedo Stage: The embryo elongates and resembles a torpedo. Rapid cell division and elongation occur, with cotyledons extending upward. The internal organization of the shoot and root apical meristems is established.

Bent Cotyledon Stage: The cotyledons bend due to the confined space within the seed coat. The embryo nearly fills the seed, and maturation processes, including the accumulation of storage compounds take place.

Mature Embryo Stage: The embryo fills the seed coat and growth ceases, entering dormancy until germination. The mature embryo has a well-defined axis with a shoot apical meristem nestled between the cotyledons and a root apical meristem at the opposite end.

The loss of key proteins in various pathways can lead to a defective embryo phenotype (EMB) (Meinke, 2020). The term "embryo defective" encompasses a broad spectrum of mutants exhibiting abnormal development in embryos, endosperm, gametes, and fertilization (Muralla et al., 2011, Wu, 1999, Meinke, 2020). EMB mutants result in seeds with abnormal shapes, sizes, and colors compared to normal seeds. There are over 2,200 embryogenesis mutants across more than 1,800 loci in the *Arabidopsis* mutant collection, with an estimated 500-1000 total EMB genes (Best et al., 2023, Meinke, 2020). Disruptions of kinetochore proteins like CENH3, CENP-C, KNL2 result in abnormal cell proliferation and differentiation. Similarly, defects in proteins involved in cell signaling pathways, hormonal responses, nuclear divisions, cell wall formation and maintenance can impair endosperm and embryo development (Meinke, 2020).

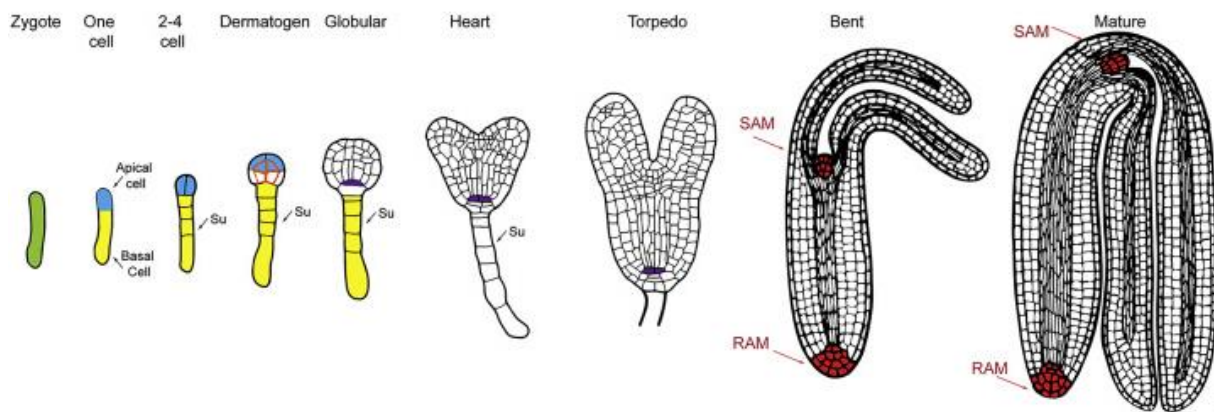


Figure 3. Embryo development in *Arabidopsis thaliana*.

Adapted from Armenta-Medina et al. (2021). The fertilized zygote undergoes an initial asymmetric division, producing a smaller apical cell, which develops into the embryo proper, and a larger basal cell that forms the suspensor (Su), anchoring the embryo to maternal tissues. The embryo then progresses through distinct developmental stages, including dermatogen, globular, heart, torpedo, and bent cotyledon, ultimately reaching maturity. The shoot apical meristem (SAM) and root apical meristem (RAM), are specified.

1.3.5 Endosperm development

In *Arabidopsis*, primary role of endosperm is to support the developing embryo by synthesizing and storing nutrients. Post-fertilization, the endosperm development begins as a syncytium, where rapid, free nuclear divisions create a multinucleate structure without cell wall formation (Olsen, 2004). This phase is crucial for metabolic efficiency and nutrient distribution essential for embryo development. Nuclei are evenly distributed within the central cell's cytoplasm by the cytoskeleton, preparing for later cellularization when cell walls encase each nucleus (Boisnard-Lorig et al., 2001). Microtubules position these nuclei to ensure uniform spacing, essential for subsequent developmental stages (Brown and Lemmon, 2007).

The genetic regulation of endosperm development in *Arabidopsis* is complex and involves a network of imprinted genes whose expression is determined by their parental origin. The maternal genome usually restricts growth while the paternal genome promotes it, thus the balance between maternal and paternal genomes is crucial for normal seed development. Specifically, the majority of endosperm genes are expressed in a 2:1 maternal to paternal ratio (Gehring, 2013).

Endosperm cellularization occurs once a sufficient number of nuclei are established at a defined time point in plants. In *Arabidopsis*, it happens during the heart stage embryo, around the fifth day after pollination (Adams et al., 2000). This transition regulated by key genes like *FIS* (*FERTILIZATION INDEPENDENT SEED*) and disruption of these genes can affect endosperm development and seed viability (Chaudhury et al., 1997, Luo et al., 2000). Post-cellularization, the endosperm diminishes and is largely consumed by the growing embryo, with only remnants remaining around the cotyledons by seed maturation in many eudicots, like *Arabidopsis*. Whereas in monocots, the endosperm is the major part of the seed at maturity (Armenta-Medina et al., 2021). While there's no direct evidence that embryo formation depends on the endosperm cellularization, abnormalities in this could negatively impacts embryo (Peris et al., 2010, Hehenberger et al., 2012).

1.4 Chromosome organization and structure

1.4.1 Chromosome, centromere structure and function

In the late nineteenth century, Flemming, Boveri, and Sutton made significant advances in genetics by discovering chromosomes. Walther Flemming first visualized chromosomes as threadlike structures called chromatin, identifying centromeres as constricted regions. Early cytogenetic studies highlighted the crucial role of centromeres in sister chromatid cohesion and chromosome segregation during mitosis and meiosis (Murray and Szostak, 1983).

Eukaryotic cells compact their extensive genomic DNA into chromatin to fit within the micrometer-sized nucleus, enabling regulation and protection of genetic information. The nucleosome, the basic unit of chromatin, consists of ~147 base pairs of DNA (10 nm) wrapped around an octamer of histone proteins (Fig. 4) (Câmara et al., 2024). This octamer includes two copies each of the core histones: H2A, H2B, H3, and H4 (McGhee and Felsenfeld, 1980, Luger et al., 1997a, Luger et al., 1997b). In interphase nuclei, chromosomes are organized into topologically associated domains (TADs), which help structure the chromatin and regulate gene expression. These regions can include both gene-rich euchromatin and compact

heterochromatin (Dixon et al., 2012, Misteli, 2020, De Nooijer et al., 2009). Heterochromatin is densely packed and enriched with repetitive DNA such as centromeric repeats.

Centromeres serve as the assembly site for the kinetochore and are defined by a combination of factors, including repetitive DNA sequences, specific protein complexes, and epigenetic markers (Fig. 4). In most plants and animals, centromeres are typically assembled on tandem repeats of satellite DNA sequences. However, the presence of neocentromeres lacking these repetitive sequences demonstrates that specific DNA sequences are not essential for centromere identity (Nishimura et al., 2019). Instead, centromeres are often epigenetically defined by the histone H3 variant CENH3 (CENP-A), which replaces canonical histone H3 within the nucleosome, altering chromatin structure to enable kinetochore assembly (Black and Cleveland, 2011, McKinley and Cheeseman, 2016, Blower et al., 2002). While CENP-A is crucial for centromere identity, it is not universally required for centromere specification (Mellone and Fachinetti, 2021). Additionally, the interaction between CENP-B and CENP-C can anchor the kinetochore to the centromere independently of CENP-A (Hoffmann et al., 2016).

Chromosomes exist in two primary forms: monocentric and holocentric (Schubert et al., 2020). Monocentric chromosomes, typical in most eukaryotes, feature a single centromere evident as a primary constriction during metaphase. Holocentric chromosomes show centromere activity along almost their entire length. Centromere size and composition can vary greatly among species. In yeast, point centromeres are about 125 base pairs of specific DNA sequences, while in humans and many plants, regional centromeres span several megabases of repetitive DNA sequences (Talbert et al., 2002, Henikoff et al., 2001).

Centromere evolution is complex. Unlike monocentric chromosomes with a single centromere, holocentric chromosomes have multiple centromere units along their length. In typical monocentric chromosomes, CENH3 is crucial for kinetochore assembly. However, in holocentric species like *Cuscuta*, CENH3's role varies. In *Cuscuta europaea*, CENH3 is present in heterochromatin, but kinetochore complexes disassemble during mitosis, indicating an altered role (Oliveira et al., 2020, Neumann et al., 2023). Whereas in *Cuscuta epithymum*, CENH3 is depleted possibly due to the absence of KNL2, necessary for CENH3 loading, yet chromosome segregation remains unaffected (Oliveira et al., 2020, Neumann et al., 2023). This suggests a CENH3-independent mechanism for kinetochore function in holocentric species. Interestingly, in monocentric plants and animals, depletion of KNL2 and CENH3 levels lead to severe defects in development and growth due to abnormal chromosome segregation (Fujita et

al., 2007, Zuo et al., 2022, Boudichevskaja et al., 2019, Lermontova et al., 2013, Lermontova et al., 2011).

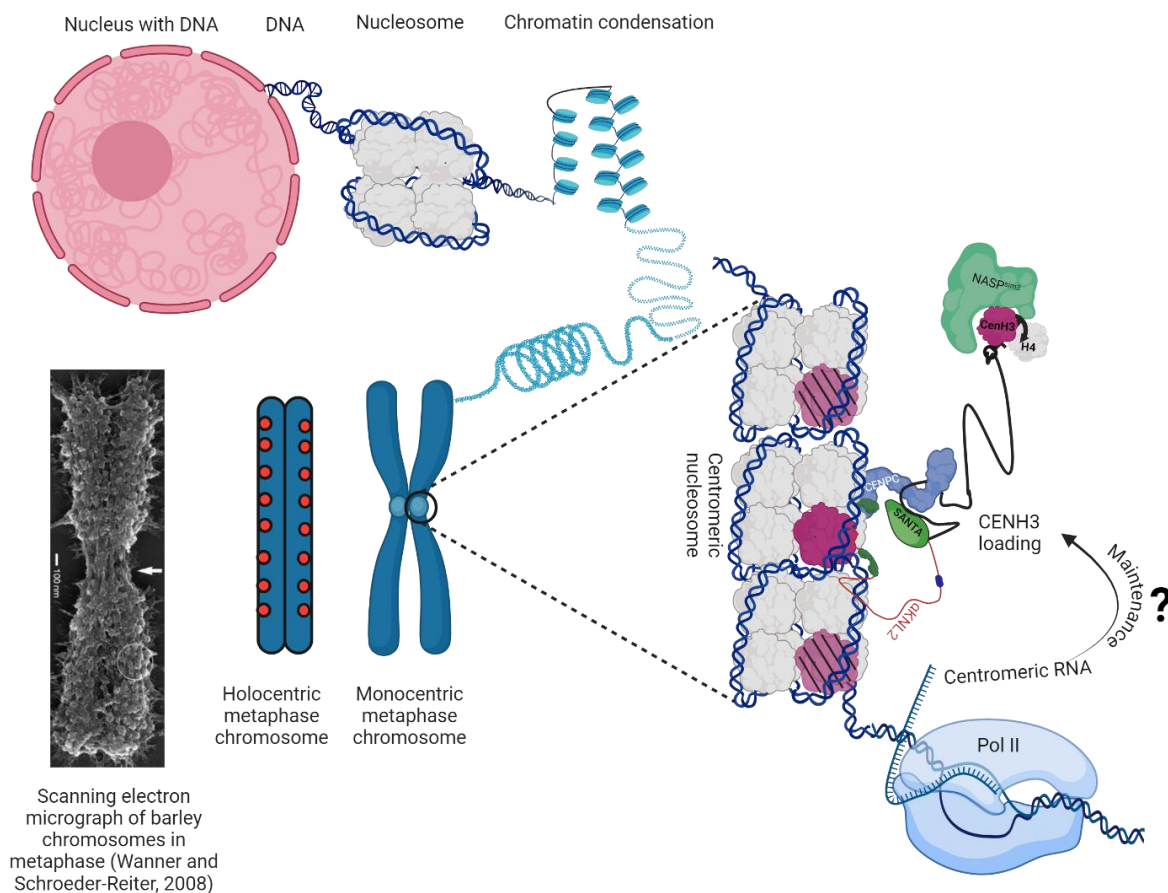


Figure 4. Chromosome structure and CENH3 nucleosome assembly.

This figure illustrates the organization of DNA within the nucleus, its condensation into nucleosomes, and the structure of chromosomes. It contrasts monocentric chromosomes, with a single centromere, and holocentric chromosomes, with centromeric activity along their length. A scanning electron micrograph of barley chromosomes in metaphase provides a real-world view of chromosome structure. The right section focuses on the centromeric nucleosome, where the histone variant CENH3 replaces canonical H3, facilitated by the KNL2 protein and NASP chaperone. The figure also depicts the role of centromeric RNA and interactions with CENP-C in regulating CENH3 loading and maintenance.

1.4.2 CENH3 loading across eukaryotes

Centromeric chromatin is characterized by interspersed arrays of CENP-A/CENH3 and canonical histone H3 nucleosomes. In eukaryotic cells, replication-independent loading of centromeric histones requires the prior removal of placeholder nucleosomes containing H3 and H3.3, which were established during the preceding S-phase. CENH3 is loaded into centromeres in a process varying subtly between animals and plants. In plants, CENH3 is loaded during late G2, while in animals, it occurs in early G1, immediately following sister centromere separation (Lermontova et al., 2007). It involves the KNL2 protein, crucial for guiding CENH3 to the centromere, ensuring its integration into the chromatin (Lermontova et al., 2013). CENH3 plays

critical role in the cascade steps of kinetochore assembly initiation (Lermontova et al., 2015). Its loading onto centromeres involves initiation, deposition, and maintenance stages (De Rop et al., 2012).

Centromere licensing: Centromere functionality begins with an initiation phase, where centromeric regions are marked epigenetically, preparing them for CENH3 loading. This involves a protein complex that alters the chromatin to accept CENH3, such as the Mis18 complex in humans and the KNL2 protein in plants (Hayashi et al., 2004, Fujita et al., 2007, Lermontova et al., 2013).

CENH3 deposition: Following this, the deposition phase sees CENH3 brought to the centromere by specific chaperones. CENH3 specific chaperones, including HJURP in humans, CAL1 in *Drosophila*, Scm3 in yeast, and NASP in *Arabidopsis*, are essential for the targeted delivery of CENP-A to the centromere (Fig. 4) (Stirpe and Heun, 2023). These chaperones engage with CENH3 in its pre-nucleosomal CENH3-H4 heterodimeric form and are frequently directed by the Mis18 complex, a process supported by existing CENH3 nucleosomes that reinforce centromere identity (Hayashi et al., 2004, Hirai et al., 2022). Post-translational modifications, such as phosphorylation, SUMOylation, and ubiquitination at specific residues on CENH3 loading factors, may inhibit their centromere localization, thereby restricting CENH3 deposition (Renaud-Pageot et al., 2022). Conversely, modifications at alternate residues can protect these CENH3 loading factors from degradation or inactivation, ensuring the stability and functionality essential for effective centromere assembly.

CENH3 maintenance at centromeres: To ensure the continuity of centromere functionality through cell divisions, CENH3 within centromeric chromatin must be preserved. This process involves the semi-conservative replication of CENH3-containing nucleosomes, assisted by the existing nucleosomes which guide new CENH3 deposition (Black and Cleveland, 2011, Pidoux et al., 2009, Probst et al., 2009). However, the deposition of CENP-A is not entirely dependent on its prior presence, as CENP-C and CENP-B can facilitate its de novo assembly when CENH3 is absent (Salinas-Luypaert and Fachinetti, 2024). Recent studies indicate that the *MCM2-7 helicase*, alongside other chaperones, plays a crucial role in recycling parental nucleosomes during DNA replication (Huang et al., 2015, Yuan et al., 2017, Zasadzińska et al., 2018, Bobkov et al., 2020, Petryk et al., 2018). Additionally, transcripts from centromeric regions contribute to the stability of these nucleosomes (Fig. 4) (Talbert and Henikoff, 2018, Ramakrishnan Chandra et al., 2023). In humans and flies, SPT6 has been identified as a maintenance factor

for CENP-A (Bobkov et al., 2020). However, in plants, research on these mechanisms is limited and further studies are needed to understand these processes.

1.5 Kinetochore

1.5.1 Organization of kinetochore

The kinetochore was first described by Walther Flemming in 1882 as "strange bodies" located at chromosome centromeres during cell division. By the 1930s, electron microscopy helped reveal its distinctive structure and essential role at centromeres. The term "kinetochore" was first used in 1934 by Lester Sharp following a suggestion from J.A. Moore, and later popularized by Franz Schrader (Schrader, 1936, Sharp, 1934). Kinetochores show remarkable conservation across species, from yeast to humans, highlighting their fundamental role in cell division. However, variations exist, particularly between organisms, reflecting evolutionary adaptations to the kinetochore's structure and function (Meraldi et al., 2006).

Kinetochore architecture varies across organisms and has been primarily elucidated through transmission electron microscopy (TEM). In animal cells, reveals a characteristic three-layered structure with distinct inner and outer layers separated by a clear middle zone. During mitosis, when microtubule attachment is required, a fibrous corona appears on the outer layer, which disassembles during interphase (Kops and Gassmann, 2020). In contrast, plant kinetochores exhibit a "ball-and-cup" structure, where a uniform kinetochore "ball" is embedded in a "cup" of chromatin, enabling microtubule attachment. This unique configuration allows plant kinetochores to function consistently throughout the cell cycle, without the distinct stratified layers typical in animal kinetochores (Dawe et al., 2005, Yu et al., 2000).

The kinetochore is a multi-protein structure that assembles in a highly regulated manner (Cheeseman and Desai, 2008). It consists of inner and outer plates that form the core, with CENH3 serving as a foundational component for recruiting other kinetochore proteins (Fig. 5) (Earnshaw and Rothfield, 1985, Foltz et al., 2006). The inner kinetochore is formed by the Constitutive Centromere Associated Network (CCAN) (Table 1). This inner kinetochore contacts centromeric DNA and is crucial for the initial assembly of kinetochore structures, providing a foundation for other kinetochore proteins. This layer includes proteins that recognize and bind to specialized nucleosomes containing the CENH3/CENP-A. In plants, only four CCAN components are conserved (Pettkó-Szandtner et al., 2024). Among these, CENP-C

localizes to the kinetochores throughout the cell cycle, whereas the other three (CENP-O, CENP-S, and CENP-X) are predominantly found in the cytoplasm during mitosis.

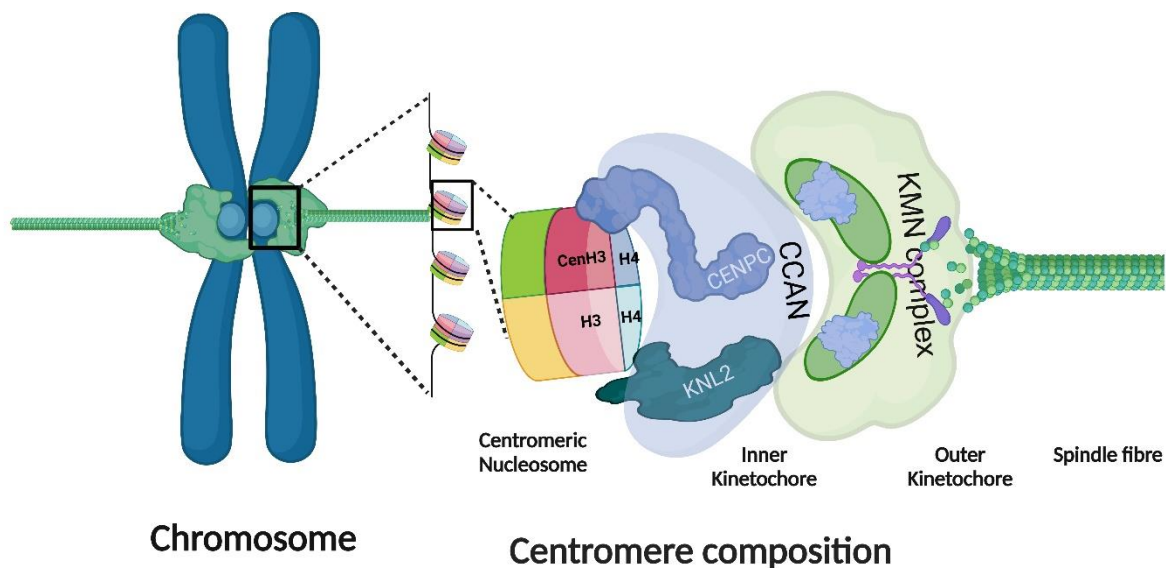


Figure 5. Organization of the kinetochore structure

The figure illustrates the organization of the kinetochore on the centromere, highlighting specialized nucleosomes containing the CENH3 histone variant. Inner kinetochore is composed of the Constitutive Centromere Associated Network (CCAN), which directly interacts with centromeric DNA. Key components, such as CENP-C and KNL2, are highlighted. The outer kinetochore is primarily composed of the KMN network, which includes the KNL1, Mis12, and Ndc80 complexes. This structure is crucial for microtubules binding and facilitating chromosome movement during cell division.

The outer kinetochore, formed by the KMN network (comprising the KNL1, Mis12, and Ndc80 complexes), interacts with the mitotic spindle microtubules, playing a key role in chromosome movement and signal transduction during cell division (Musacchio and Desai, 2017). Interestingly, Pettkó-Szandtner et al. (2024) demonstrated that in *Arabidopsis*, all KMN network components consistently localize to the kinetochore throughout the cell cycle.

Table 1. List of identified kinetochore proteins

Protein	Function	Availability in Plants
Inner kinetochore components		
CENP-A	Essential for chromatin incorporation at centromeres	HTR12/CENH3 AT1G01370
CENP-B	Recognizes and binds to CENP-B box in the centromeric alpha satellite	Not present/ identified
CENP-C	Links centromeric DNA and kinetochore structures	AT1G15660
CENP-H	Part of a complex involved in kinetochore assembly	Not present/ identified
CENP-I	Works with CENP-H to stabilize the kinetochore	Not present/ identified
CENP-K	Part of the inner kinetochore structure	Not present/ identified

CENP-L	Contributes to the cohesion and function of the kinetochore	Not present/ identified
CENP-M	Essential for kinetochore assembly and chromosome segregation	Not present/ identified
CENP-N	Binds directly to CENP-A, helping to anchor additional proteins	Not present/ identified
CENP-O	Part of a subcomplex that aids in the overall architecture	AT5G10710
CENP-P	Works with other CENP proteins to maintain kinetochore integrity	Not present/ identified
CENP-Q	Interacts with components of the outer kinetochore	Not present/ identified
CENP-R	A component of the core kinetochore	Not present/ identified
CENP-S	Forms a nucleosome-like structure with CENP-T, CENP-W, and CENP-X	Defective cytokinesis/ KOR1 AT5G49720/ AT5G50930
CENP-T	Essential for kinetochore and spindle attachment	Not present/ identified
CENP-U (50)	Plays a critical role in kinetochore composition and stability	Not present/ identified
CENP-V	Involved in kinetochore function, specific role less known	Not present/ identified
CENP-W	Works with CENP-T to form functional structures	Not present/ identified
CENP-X	Collaborates in nucleosome-like structure formation at the kinetochore	MHF2 /AT1G78790
Plant specific components		
α KNL2	CENH3 loading and kinetochore assembly	AT5G02520
β KNL2	CENH3 loading and kinetochore assembly	AT1G58210
Outer kinetochore components		
NDC80 (Hec1)	Key component of the kinetochore-microtubule attachment	AT3G54630
NUF2	Partners with NDC80 to connect to microtubules	AT1G61000
SPC24	Integral part of the NDC80 complex	SPC24.1/ MUN1/AT3G08880 SPC24.2/AT5G01570
SPC25	Integral part of the NDC80 complex	AT3G48210
KNL1	Connects kinetochore to spindle microtubules	AT2G04235
MIS12	Core component of the kinetochore	AT5G35520
NSL1	Part of the Mis12 complex	NSL1.1/ AT4G00525 NSL1.2/AT1G01715
DSN1	Part of the Mis12 complex	AT3G27520
PMF1	Part of the Mis12 complex	NNF1 EMB3006 AT4G19350

1.5.2 Kinetochore Null 2 (KNL2)

Depletion of essential kinetochore components such as CENP-A and CENP-C leads to a kinetochore-null phenotype in *C. elegans*, as demonstrated by Oegema et al. (2001). Further investigation into kinetochore regulators identified three additional candidates: KNL1, KNL2, and KNL3. Notably, KNL2, which contains a Myb domain, was established to function

upstream of CENP-A in both *C. elegans* and human cell lines, marking a significant discovery in kinetochore biology (Maddox et al., 2007). KNL2, also known as Mis18BP1, is pivotal in kinetochore functions across various species, primarily associated with CENH3 loading and kinetochore assembly (Moree et al., 2011, Lermontova et al., 2013). Recent studies have demonstrated that in *C. elegans* oocytes, KNL2 coordinates with CENP-A and MEL-28 to assemble the outer kinetochore during meiosis, ensuring accurate chromosome attachment and segregation (Bellutti et al., 2024). Meiosis I rely on this non-redundant kinetochore assembly pathway, which involves both KNL-2 and MEL-28 in conjunction with the CENP-A/CENP-C pathway.

KNL2 functions in association with MIS18 complex for recruitment and loading of CENH3 (Maddox et al., 2007, Fujita et al., 2007). The Mis18 complex is pivotal for centromere assembly and maintenance during cell division. This complex formed out of oligomers of Mis18 α , Mis18 β , and M18BP1/KNL2, crucial for its operational integrity (Hayashi et al., 2004, Fujita et al., 2007, Barnhart-Dailey and Foltz, 2014, Maddox et al., 2007, Smith and Maddox, 2017). In human cells, a hexamer of Mis18 α and Mis18 β in a 4:2 ratio, assisted by Yippee domains, effectively binds two M18BP1/KNL2 molecules (Stellfox et al., 2016, Pan et al., 2017).

In *Saccharomyces*, homologs of KNL2 have not been identified, although other components of the Mis18 complex are conserved in *S. pombe*. The outer kinetochore Dam1-DASH complex and the inner kinetochore CBF3 complex functionally compensate for KNL2 by facilitating the centromere localization of Cse4 (Ho et al., 2014, Zhang et al., 2018, Lechner and Carbon, 1991). In *Drosophila*, HJURP and the Mis18 complex are absent, and instead, the protein CAL1 proposed to integrate both CENP-A chaperone and centromere-targeting functions.

Contrastingly, in plants, particularly *Arabidopsis*, only KNL2 was identified and characterized as an upstream component of CENH3 loading. The counterparts to Mis18 α and Mis18 β remain unidentified despite the presence of seven Yippee domain-containing proteins (AT4G27745, AT4G27740, AT5G53940, AT2G40110, AT3G11230, AT3G55890, AT3G08990). Notably, none of these proteins co-precipitate with KNL2 or CENH3 (unpublished).

KNL2 proteins are characterized by the presence of the Swi3-Ada2-NCoR-TFIIIB-associated (SANTA) domain, which is about 90 amino acids (AA) long (Zhang et al., 2006). While metazoans contain a single gene encoding a protein with a SANTA domain, plants possess two such genes. Early studies primarily focused on *At5g02520*, while *At1g58210* was initially

overlooked due to its atypical domain composition for a KNL2 protein (Lermontova et al., 2013). The SANTA domain often associated with a SANT/Myb-like putative DNA-binding domain and/or a CENPC-like motif (Sandmann et al., 2017, Hori et al., 2017). The role of SANT domains in DNA interaction remains unclear as SANT containing KNL2 homologues have not yet shown direct DNA binding. The Myb domain's critical DNA-binding residues differ in the SANT domain (Boyer et al., 2004, Mo et al., 2005). Interestingly, *Arabidopsis* KNL2, lacking this domain, has demonstrated DNA-binding capability *in-vitro* and is associated with the centromeric repeat *pAL1 in-vivo* (Sandmann et al., 2017).

The N-terminal SANTA domain is believed to regulate chromatin remodeling by interacting with other proteins (Zhang et al., 2006). Yet, the ability of the SANTA domain to bind DNA has not been demonstrated in any organism. Deletion of the SANTA domain in *Arabidopsis* KNL2 does not affect its DNA interaction (Lermontova et al., 2013, Sandmann et al., 2017). In *Xenopus* and chicken, direct interactions of M18BP1/KNL2 with CENH3 nucleosomes occur independently of the SANTA domain (French et al., 2017, Jiang et al., 2022). However, in *Xenopus*, M18BP1/KNL2 binds to CENP-C at centromeres during metaphase before CENH3 loading, utilizing the SANTA domain (French and Straight, 2019). In plants and non-mammalian vertebrates, KNL2 is distinguished by a highly conserved CENPC-like motif, which is essential for its localization to the centromere (Sandmann et al., 2017, Hori et al., 2017).

1.5.3 Centromere targeting mechanism of KNL2 in different organisms

The centromere targeting mechanisms of KNL2 proteins demonstrate considerable diversity across organisms, highlighting an evolutionary adaptation that aligns with centromere structure and kinetochore complexity. KNL2, while conserved in function, has evolved distinct combinations of conserved domains, motifs, and regions across different species to mediate its centromeric localization and interaction with other kinetochore proteins.

In monocentric organisms such as vertebrates, the centromere localization of KNL2 is primarily regulated by its interaction with CENP-C, mediated through a conserved SANTA domain. For example, in *Xenopus laevis*, M18BP1 localizes to centromeres during metaphase through interaction with CENP-C via the SANTA domain, prior to CENH3 loading (French and Straight, 2019). In non-mammalian vertebrates, centromere targeting often involves a CENPC-like motif on M18BP1 that is essential for its centromere targeting (French et al., 2017, Hori et al., 2017). However, this motif is absent in eutherian mammals, indicating species-specific

variations in KNL2's structure and function. In humans, Mis18 components (Mis18 α :Mis18 β 4:2 hexamer) guided by Yippee domains, binds two M18BP1 copies (Pan et al., 2017, Stellfox et al., 2016). Human M18BP1 requires N-terminus, SANTA domain and the CENP-C binding domain for centromeric recruitment (Stellfox et al., 2016). Additionally, the recruitment and assembly of KNL2 at the centromere are tightly regulated by cell-cycle-dependent phosphorylation by kinases such as CDK1 and PLK1, which control M18BP1's interaction with the Mis18 complex for centromere localization (Silva et al., 2012, McKinley and Cheeseman, 2014).

In holocentric species such as *Caenorhabditis elegans*, KNL2 exhibits a unique functional relationship with CENP-A, unlike monocentric organisms where KNL2 acts upstream of CENP-A. In *C. elegans*, KNL2 and CENP-A (HCP-3) are interdependent for centromere localization, illustrating a co-dependent centromere targeting mechanism adapted for the holocentric structure (Maddox et al., 2007). KNL2 interacts directly with CENP-A's N-terminal tail and is essential for chromosome condensation and CENP-A loading (de Groot et al., 2021, Wenda et al., 2021, Prosée et al., 2021). Furthermore, in *C. elegans* oocytes, KNL2 and the nucleoporin MEL-28 show interdependence for kinetochore localization during meiosis, adding another layer to KNL2's role in centromere dynamics in holocentric chromosomes (Bellutti et al., 2024).

In plants, particularly *Arabidopsis thaliana*, KNL2 has distinct structural features, including the absence of the C-terminal SANT domain, typically linked to chromatin binding in vertebrates. *Arabidopsis* KNL2 relies on a CENPC-like CENPC-k motif for centromeric targeting (Sandmann et al., 2017). Even a single conserved residue alteration in this motif can cause KNL2 mis-localization. Recent studies in *Arabidopsis* have demonstrated that DNA-binding regions are crucial for centromere targeting along with the CENPC-k motif (Yalagapati et al., 2024). The conserved SANTA domain exclusion did not affect the centromeric targeting and DNA binding (Sandmann et al., 2017). Although KNL2 plays a critical role in CENH3 loading and kinetochore assembly in plants, *knl2* mutants are viable, suggesting compensatory mechanisms that sustain essential centromere functions despite KNL2 depletion.

This underscores the evolutionary flexibility of KNL2's structure and interactions across species, enabling centromere targeting and kinetochore assembly to meet specific cellular and chromosomal requirements. In the present thesis, we identified and characterized a new variant, β KNL2, which similarly functions in CENH3 loading and kinetochore assembly in *Arabidopsis*, providing insights into the role of KNL2 variations in plants.

Chapter 2: Aims of the thesis

The kinetochore is a multi-protein complex that assembles on centromeres facilitating the attachment of chromosomes to spindle microtubules. The loss of centromere or kinetochore function can lead to cell death (Fachinetti et al., 2013, Barra and Fachinetti, 2018, McKinley and Cheeseman, 2016). CENH3 marks centromeres epigenetically for the functional assembly of the kinetochore (Talbert et al., 2002). KNL2, along with other proteins, plays a key role in regulating the deposition of CENH3 at centromeres. KNL2 proteins contain a conserved SANTA domain, sometimes accompanied by a SANT/Myb-like DNA-binding domain. In *Arabidopsis*, two SANTA-containing proteins exist, but only one was initially characterized. The second protein was excluded due to annotation errors.

Depletion of KNL2 across different organisms impacts CENH3 loading and kinetochore assembly (Lermontova et al., 2013, French et al., 2017, Fujita et al., 2007). Interestingly, unlike in mammals, homozygous *knl2* mutants in *Arabidopsis* remain viable despite reduced CENH3 levels, though they exhibit mitotic and meiotic abnormalities that result in reduced growth and fertility. The fact that CENH3 still localizes at centromeres in the *knl2* mutant suggests alternative mechanisms for CENH3 loading. To explore the KNL2 evolution, we reconstructed the evolutionary history of KNL2 proteins and identified a KNL2 variant. We designated it as β KNL2 and the previously characterized KNL2 as α KNL2. This study aims to understand the role of β KNL2 in kinetochore assembly, plant growth, and development by performing the following:

1. Reconstruct the evolutionary history of *KNL2* genes.
2. Classify and characterize *KNL2* gene clades.
3. Characterize the localization and functional characterization of β KNL2
4. Investigate the β KNL2 role in CENH3 loading.
5. Examine the structural requirements of domains and motifs for efficient centromeric targeting of β KNL2.
6. Investigate dimerization properties of β KNL2 and its interactions with centromeric DNA and α KNL2.
7. Assess β KNL2's dependency on CENPC-like motif proteins for centromeric localization.
8. Provide insights into plant-specific kinetochore assembly, emphasizing on the role of β KNL2.

Chapter 3: Materials and methods

3.1 Plant material and growth conditions

All experiments were performed using *Arabidopsis thaliana* or *Nicotiana benthamiana*. Columbia-0 (Col-0) ecotype of *Arabidopsis* served as the wild-type (WT). Stable *Arabidopsis* transformants were generated either in the Col-0 background or in T-DNA insertion mutants of *βkn12* and *akn12* using the floral dip method, as described by (Clough and Bent, 1998).

Arabidopsis seeds were sown in a single pot, placed at 4 °C for 2 days for stratification, and then transferred to short-day conditions (8 h light/16 h dark, 18 °C) until germination. After 2-3 weeks, seedlings were transplanted into individual pots and maintained under short-day conditions for an additional 3-4 days to allow them to acclimate before being transferred to long-day conditions. The two-week-old seedlings were then transferred to long-day conditions (16 h light/8 h dark, 21 °C) and grown until seed setting was complete. Once seed setting was achieved, plants were covered with either Aracons or plastic triangle covers and moved to a drying area.

N. benthamiana plants were grown in a greenhouse under 16 h light/8 h dark at 22 °C for 2-4 weeks and these young plants were used for transient expression experiments.

3.2 DNA isolation

DNA isolation from seedlings was performed by following the protocol described by Edwards et al. (1991). In short, the plant material was homogenized in Edwards buffer (containing 200 mM Tris, 25 mM EDTA, 250 mM NaCl, and 0.5% SDS (w/v), pH 8) to release cellular contents. After vortexing and centrifugation at 13,000 revolutions per minute (rpm), the supernatant was transferred to a new tube and mixed with an equal volume of chilled isopropanol to precipitate the DNA. The mixture was centrifuged again, and the DNA pellet was washed with 700 µL 70% ethanol, followed by air drying. The purified DNA was resuspended in 30-70 µL sterile ddH₂O for further analysis.

3.3 Polymerase Chain Reaction (PCR) based genotyping of transgenic plants and T-DNA insertion mutants

PCR amplification

PCR amplification was performed to confirm the presence of transgenes in *A. thaliana* transformants and the presence and zygosity of T-DNA insertions. Depending on the need we

used GoTaq (Promega, M3001), Qiagen (201203), Phusion polymerases (Thermo Scientific, F530). A master mix was prepared by following manufacturer's instructions. All the primers used in the present thesis are listed in Appendix Table 1. The reaction mixture, excluding the template DNA, was first prepared and then aliquoted into PCR tubes (9 μ L per tube). Subsequently, 1 μ L of template DNA, isolated from *Arabidopsis*, was added to each tube to achieve a final reaction volume of 10 μ L. The PCR reactions were carried out using a thermal cycler with a specific program (Table 2). The annealing temperature was determined using the IDT OligoAnalyzer tool (<https://www.idtdna.com/pages/tools/oligoanalyzer>). If amplification proved challenging, the annealing conditions were optimized for each primer pair based on the melting temperature (T_m). Upon completion of the PCR run, products were analyzed by agarose gel electrophoresis to verify successful amplification.

Table 2. PCR conditions

Temperature	Time	
95 °C	5 mins	
95 °C	40 sec	} 35×
55-65 °C	40 sec	
72 °C	X	
72 °C	10 min	
18	∞	
x- 30-60 sec/1Kb size amplification		

Agarose gel electrophoresis

Agarose gels were prepared at appropriate concentrations for different purposes: 0.8% for genomic DNA verification, 1% for PCR products (excluding genotyping products), and 1.5% for genotyping products. To dissolve the agarose, it was mixed with 0.5 \times or 1 \times TAE buffer and heated in a microwave until no solid particles remained. After cooling to approximately 60 °C, Intas HDGreen Plus DNA stain was added (5 μ L per 100 mL of agarose solution). The mixture was then poured into a gel tray with combs inserted to create wells and allowed to solidify at room temperature (RT). Once solidified, the gel was placed in an electrophoresis chamber filled with 0.5 \times or 1 \times TAE buffer. DNA samples were prepared by mixing 2 μ L of DNA with 0.4 μ L of 6 \times loading dye, and 5 μ L of PCR products were loaded into the wells. In the left lane, 5 μ L of a DNA ladder (100 bp or 1 kb, depending on the sample) was loaded to estimate the size of the PCR products. Electrophoresis was carried out at 100 V for 30 to 40 minutes, depending on the size of the DNA fragments, until the bands were sufficiently resolved for analysis.

3.4 RNA isolation

RNA was isolated from unopened young flower buds or seedlings. Prior to extraction, surfaces were cleaned with RNase Zap to prevent RNase activity. The samples were homogenized using mortar and pestle in liquid nitrogen and mixed with 1 mL of TRIzol™ Reagent (Invitrogen, 15596026) (stored at 4 °C) to inhibit RNase activity. The mixture was incubated for 5 minutes at RT on a belly dancer shaker. Following this, 200 µL of chloroform was added, and the mixture was incubated for 3 minutes at RT before being centrifuged at 12,000 rpm and 4 °C for 15 minutes. Approximately 650 µL of the upper aqueous phase was transferred to new tubes containing 500 µL of RT isopropanol. The tubes were gently inverted 20 times, incubated on ice for 15 minutes, and then centrifuged for 10 minutes at 12,000 rpm and 4 °C. The resulting supernatant was discarded, and the pellet was washed with 70% ethanol by centrifuging at 12,000 rpm and 4 °C for 5 minutes. After removing the ethanol, the pellet was air-dried at RT and dissolved in 30-50 µL of ddH₂O.

RNA quality and integrity were evaluated using a 1% agarose gel. Agarose gel was prepared as detailed in section 3.3. For electrophoresis, 1–2 µL of RNA was mixed with 1 µL of loading dye and loaded alongside a molecular weight ladder. The gel was run at 100 V for 30 minutes, and RNA bands were visualized under UV light.

RNA concentration and purity were measured using a nanodrop spectrophotometer. The instrument was calibrated with 1 µL of ddH₂O as a blank. For each sample, 1 µL was used to measure absorbance at 260 nm (A₂₆₀) for quantification. A₂₆₀/A₂₈₀ and A₂₆₀/A₂₃₀ ratios of ~2.0 indicated high purity. RNA with acceptable quality and purity was stored at -80 °C or used for downstream applications like cDNA synthesis.

3.5 cDNA synthesis

To prepare the cDNA library, the first strand cDNA synthesis kit (Thermo Scientific, K1632) was used. The RNA samples (1-2 µg) were mixed with 1 µL of polydT primer. The mixture was gently mixed and briefly spun down before incubating at 70°C for 5 minutes, and then immediately transferred to ice. This pre-heating and snap chilling step melts secondary structures and prevents their reformation. The mixture was centrifuged for 30 seconds and kept on ice. A master mix was prepared by adding 4 µL of 5× buffer, 1 µL of RNase inhibitor, and 2 µL of 10 mM dNTP mix. This 7 µL master mix was added to each sample, which was then incubated at 37 °C for 5 minutes and subsequently kept at RT. Next, 1 µL of *H minus M-MuLV RT* enzyme was added, and the mixture was incubated at 42 °C for 60 minutes. The reaction

was inactivated by heating at 70 °C for 10 minutes. The resulting cDNA was tested by amplifying the housekeeping genes *actin 2* (AT3G18780) or *EF1B* (AT5G19510) with the gene specific primers (Appendix Table 1) to confirm successful synthesis and stored at -20 °C.

3.6 Molecular cloning and generation of expression vectors

3.6.1 Amplification and purification of genomic fragments or coding sequences (CDS) for molecular cloning

Primers specific to the desired construct, designed with attB sites for Gateway cloning or with specific restriction sites for restriction cloning, are used to target the sequence of interest. Either genomic DNA or complementary DNA (cDNA) serves as the template, depending on the application. Amplification is carried out using Phusion polymerase, following the protocol outlined in section 3.3.

To purify the PCR product, 50 µL of the PCR reaction was mixed with 200 µL of TE buffer (10 mM Tris-HCl, 1 mM EDTA, pH 8.0) and 125 µL of 30% PEG 8000 solution. The mixture was gently mixed and incubated on ice for 20-30 minutes to allow DNA precipitation. Following the incubation, the sample was centrifuged at 13,000 rpm for 30 minutes at 4 °C. After centrifugation, the supernatant was carefully discarded, and the DNA pellet was washed with 500 µL of 70% ethanol. The tube was centrifuged again at 13,000 rpm for 5 minutes, and the ethanol was removed. The pellet was then air-dried at RT before being resuspended in 30-50 µL of nuclease-free water for further use.

3.6.2 GATEWAY-compatible vectors construction for BiFC

The GATEWAY-compatible BiFC vectors generated based on the highly efficient and small binary vector pPZP200BAR (Jozefkiewicz et al., 2016). To this end, the cauliflower mosaic virus 35S promoter (35S) was assembled with the terminator sequence of the *octopine synthase* gene (*tocs*) from *Agrobacterium tumefaciens* via overlap extension PCR (Appendix Table 1). The overlap primers were designed to create a 5'-*EcoRI-SpeI-XbaI*-3' multiple cloning site (MCS) between the promoter and terminator sequences, and the resulting 35S:MCS:*tocs* fusion product was additionally flanked with restriction sites for *BamHI* and *PstI*.

After restriction enzyme digestion using *BamHI/PstI* the 35S:MCS:*tocs* cassette was ligated into the accordingly linearized pPZP200BAR binary vector. To facilitate PPI analyses with the Venus fluorescent protein in all possible orientations (Waadt and Kudla, 2008), the coding sequences of both the VN (residues 1-173) and VC (residues 156-239) of Venus were amplified

by PCR using primers (Appendix Table 1) suitable to create *EcoRI* and *SpeI* restriction sites for N-terminal fusions or *SpeI* and *XbaI* restriction sites for C-terminal fusions.

Additionally, a c-MYC epitope tag was attached to both VN variants and a hemagglutinin (HA) epitope tag to all VC variants. The PCR fragments of the truncated Venus variants were cloned into the previously assembled binary 35S:MCS:ocs-pPZP200BAR vector using the aforementioned restriction sites. To modify the resulting BiFC binary vectors into GATEWAY-compatible destination vectors, a *SpeI* flanked PCR-fragment containing a GATEWAY *ccdB* gene cassette for LR was ligated into the linearized plasmids through digestion with *SpeI*. The final set of GATEWAY-compatible BiFC destination vectors, including 3'Ven-N-pBAR GW and 3'Ven-C-pBAR GW, was verified by Sanger sequencing. These vectors were generated and kindly provided by Dr. Tobias Meitzel.

3.6.3 Gateway cloning to generate plant expression vectors

The Gateway cloning system was invented to clone multiple DNA fragments in high-throughput formats (Hartley et al., 2000, Walhout et al., 2000). In this system, two distinct enzymes responsible for a specific type of recombination reaction. The BP clonase enzyme recombines *attB* sites with *attP* sites to produce *attL* and *attR* sites. The LR clonase enzyme reverse BP reaction, recombining *attL* and *attR* sites back into *attB* and *attP* sites.

The complete open reading frame of β KNL2 (AT1G58210) was amplified from *Arabidopsis* flower buds as described above (section 3.4 and 3.5). For complementation studies, the genomic fragment was amplified from *Arabidopsis* WT genomic DNA using primers (Appendix Table 1). The amplified product was purified (section 3.6.1) and subsequently cloned into the pDONR221 vector (Invitrogen, 12536017) through a BP reaction using the Gateway cloning system (Invitrogen, 11789020). The resulting entry clones were confirmed via colony PCR (section 3.6.7) and Sanger sequencing (section 3.7). These entry clones were either subjected to site-directed mutagenesis or subcloned into expression vectors via LR reactions (Invitrogen, 11791020) for plant transformation. For localization studies, the pGWB641, pGWB642, pGWB640, and pGWB659 vectors were used (Nakamura et al., 2010), while for interaction studies, the 3'Ven-N-pBAR GW and 3'Ven-C-pBAR GW vectors (section 3.6.2) served as expression vectors. All the clones were verified at each step through colony PCR using *attB* primers and further confirmed by Sanger sequencing (Appendix Table 1).

Both BP and LR reactions were performed by adding 1-7 μ l of purified PCR product/entry clone (50-150 ng, based on the formula below), 150 ng of destination vector, and 2 μ L of BP/LR

Clonase enzyme. The reaction mix was made up to 10 μ L with 1 \times TE buffer (pH 8.0) and incubated at 25 °C for 4 hours to overnight. To terminate the reaction, 2 μ g of Proteinase K was added, followed by incubation at 37 °C for 10 minutes.

$$\text{Entry vector concentraion(ng/reaction)} = \frac{\text{Destination vector concentration (ng/}\mu\text{L)} \times \text{entry vector size (bp)}}{\text{Destination vector size (bp)}} \times 2$$

3.6.4 Generation of wheat germ expression vector for β KNL2

To clone β KNL2 for wheat germ expression, restriction cloning was performed using the Flexi enzyme blend (*SgfI* & *PmeI*, Promega, R1851) by following the manufacturer's instructions. The PCR product of β KNL2, amplified with FLAG-tagged primers, was digested with *SgfI* and *PmeI*. The reaction, containing the 5 \times Flexi digest buffer, PCR product, enzymes, and water, was incubated at 37 °C for 30 minutes and then heat-inactivated at 65 °C for 20 minutes. Concurrently, the pF3A WG acceptor vector was digested in the same manner. The digested PCR product was purified using QIAquick PCR purification kit (QIAGEN, 28104), washed with ethanol, and eluted in nuclease-free water. The ligation was carried out by combining the digested product, vector, ligase buffer, and T4 DNA ligase, and incubated for one hour at RT. The ligated product was transformed into *E. coli*, plated, and screened via colony PCR (section 3.6.7) and Sanger sequencing (section 3.7).

3.6.5 Site directed mutagenesis

For the localization and PPI studies, various constructs (β KNL2 Δ SANTA, β KNL2 Δ N, β KNL2 Δ C, β KNL2(C), β KNL2 Δ motif-I, β KNL2 Δ motif-II, β KNL2 Δ motif-III, β KNL2 Δ motif-III new) were generated through site-directed mutagenesis using the β KNL2 cDNA cloned in pDONR221.

Site-directed mutagenesis was performed using the entry clone pDONR221- β KNL2 with the Phusion site-directed mutagenesis kit (Thermo Scientific, F541), following the manufacturer's instructions. Forward and reverse primers were designed as described by manufacturer and custom synthesized with 5' phosphorylation for all constructs requiring mutagenesis. The PCR master mix (Table 3) and conditions (Table 4) were prepared accordingly. After PCR amplification, *DpnI* digestion was carried out to remove the unmutagenized parental plasmid, followed by a ligation reaction and bacterial transformation.

Table 3. Master mix composition

Component	Volume (μL)
ddH ₂ O	32.5
5X Phusion HF Buffer	10
10 mM dNTPs	1
Forward primer	2.5
Reverse primer	2.5
Template DNA	1
Phusion Hot Start DNA polymerase	0.5

Table 4. PCR conditions for site directed mutagenesis

Temperature	Time
98 °C	5 mins
98 °C	30 sec
65-72 °C	30 sec
72 °C	X
72 °C	5 min
18	∞
x- 30 sec/1Kb size amplification	

For localization studies, entry plasmids were then subcloned into pGWB641 expression vector and for PPI studies, into 3'Ven-N-pBAR GW and 3'Ven-C-pBAR GW vectors via LR reaction. All the clones were verified at each step through colony PCR (section 3.6.7) using *attB* primers (Appendix Table 1) and further confirmed by Sanger sequencing (section 3.7).

3.6.6 Bacterial transformation

For transformations involving BP or LR recombination mixtures exceeding 2 μL, the samples were first dialyzed using a 0.025 μm membrane (Millipore, VSWP02500) for 1 hour prior to electroporation to reduce salt concentration. Afterward, the recombination mixtures or plasmids were introduced into competent *E. coli* cells, and transformation was performed using either electroporation or heat shock.

For electroporation, TOP10 electrocompetent cells (Invitrogen, C404050) were mixed with the plasmid and transferred to a pre-chilled electroporation cuvette, followed by a short electrical pulse (typically 1.8 kV). For heat shock, a mixture of plasmid DNA and DH5α chemically competent cells (Thermo Scientific, EC0112) was incubated on ice for 30 minutes, subjected to a 42°C heat shock for 45 seconds, and then placed back on ice for 2 minutes. DB survival cells (Invitrogen, A10460) were used to propagate vectors containing the *ccdB* gene, and for the

expression of constructs in plants, *Agrobacterium* GV3101 electrocompetent cells (Gentaur, 774128212) were employed.

Post-transformation, cells were allowed to recover in 1 mL of SOC medium at 37°C (for *E. coli*) or 28°C (for *Agrobacterium*) with shaking (250-300 rpm) for 1-2 hours. Following recovery, 50-100 µL of the *E. coli* culture or 10-20 µL of the *Agrobacterium* culture was plated onto Luria-Bertani (LB) agar for *E. coli* (10 g/L tryptone, 5 g/L yeast extract, 10 g/L NaCl, 15 g/L agar; pH 7.0) or yeast extract broth (YEB: 5 g/L beef extract, 1 g/L yeast extract, 5 g/L peptone, 5 g/L sucrose, 0.49 g/L MgSO₄·7H₂O; pH adjusted to 7.2) medium for *Agrobacterium*, both containing the appropriate antibiotics. Plates were incubated overnight at 37°C for *E. coli* or for two days at 28°C for *Agrobacterium*.

3.6.7 Colony PCR for selection of positive clones

Colony PCR was utilized to identify positive clones containing the desired inserts. To initiate the screening process, 2–4 colonies were selected using sterile toothpicks. Each colony was first resuspended in 5 µL of ddH₂O, and the same toothpick was used to inoculate 5 mL of LB liquid medium supplemented with appropriate antibiotics. The cultures were incubated overnight at 37 °C with shaking at 240 rpm to ensure adequate growth.

A PCR master mix was prepared using *attB* or insert-specific primers, as outlined in section 3.3. Subsequently, PCR amplification was performed according to the protocol detailed in section 3.3. The PCR products were analyzed on a 1% agarose gel to confirm the presence of bands corresponding to the expected insert size. Colonies confirmed to carry the desired construct were further processed for plasmid isolation and further downstream applications.

3.6.8 Plasmid isolation

Plasmid DNA was isolated using GeneJET plasmid miniprep kit (Thermo Scientific, K0502) according to the manufacturer's instructions. As per the protocol, the cultures were harvested by centrifuging at 8000 rpm for 2 minutes, and the supernatant was decanted, with the remains removed by pipetting. The pelleted cells were resuspended in 250 µL of resuspension solution, followed by 250 µL of lysis solution, and the tubes were gently inverted 4-6 times. Neutralization solution was then added, and the tubes were gently inverted 4-6 times. The mixture was centrifuged for 5 minutes at 13000 rpm, and the supernatant was transferred to a column. After centrifuging for 1 minute, the flow-through was discarded. The columns were washed with 500 µL of Wash Solution and centrifuged for 1 minute. The flow-through was

discarded, and the wash step was repeated. 50 μ L of water was added to the center of the column and incubated for 5 minutes. Finally, the column was centrifuged for 2 minutes at 13000 rpm, and the flow-through was collected. To increase DNA concentration, the elution step was repeated using the collected flow-through.

3.7 Sanger sequencing

The plasmid DNA was sent for Sanger sequencing to LGC Genomics GmbH. Sequencing was performed on purified PCR products or isolated plasmids using 200-400 ng of PCR product or 1 μ g of plasmid DNA, respectively. Each sample was combined with 20 μ M primer and adjusted to a final volume of 14 μ L with ddH₂O. Sequence analysis was conducted using Serial Cloner 2.6.1. For entry clones or PCR products, the exact sequence of the construct was verified. In the case of expression clones, both the construct sequence and the tags were verified to ensure they were in the correct frame by translating the sequence.

3.8 Plant transformation

3.8.1 Transient transformation of *Nicotiana benthamiana*

The functionality of all constructs was tested via *Agrobacterium*-mediated transient expression in *N. benthamiana* following the protocol of Yadala et al. (2022). As per the protocol, *A. tumefaciens* strain GV3101 carrying the desired constructs were cultured overnight at 28 °C in YEB medium with appropriate antibiotics. The bacterial culture was pelleted and resuspended in *Agrobacterium* infiltration medium (AIM: 10 mM MES, 10 mM MgCl₂, and 150 μ M acetosyringone) to an OD₆₀₀ of 0.8. The bacterial suspension was incubated at RT for 1-2 hours to allow the acetosyringone to induce the virulence genes.

Young leaves of 4-6-week-old *N. benthamiana* plants were infiltrated by gently pressing the suspension into the abaxial side of the leaves using a 1 ml syringe without a needle. Plants were then kept in greenhouse for 48 hours before tissue collection for further analysis, such as fluorescence microscopy, protein extraction, or Western blotting.

3.8.2 Stable transformation of *A. thaliana*

For the stable transformation of *A. thaliana*, *Agrobacterium*-mediated floral dip transformation was performed according to Clough and Bent (1998). Bacterial suspension (800 mL) for each vector was prepared from a pelleted 500 mL *Agrobacterium* culture. The culture was centrifuged at 7000 rpm for 20 minutes, and the pellet was resuspended in infiltration medium.

Acetosyringone (150 μ M) and Silwet L-77 (0.02% v/v) were added to enhance *Agrobacterium*-mediated transformation efficiency by improving bacterial attachment to plant tissues and facilitating infection. Inflorescences of *Arabidopsis* plants were dipped into this suspension for approximately 10 seconds, ensuring that the plants were gently swirled to facilitate complete coverage.

After dipping, the plants were laid down horizontally on trays and covered with wet tissue paper and a lid to maintain humidity. They were then placed in the dark overnight to promote *Agrobacterium* infection. The following day, the plants were returned to a standing position and transferred to short-day conditions (8 h light/16 h dark) under low light. To prevent stress from direct light, the light shelf was switched off to avoid intense illumination, allowing the plants to recover. The following day, the plants were transferred back to standard growth conditions under long-day light (16 h light/8 h dark).

Once the plants had set seeds, the seeds were harvested and positive transformants were selected on $\frac{1}{2}$ Murashige and Skoog (MS) medium with appropriate antibiotics. Successful transformants were further confirmed by PCR and Sanger sequencing.

3.9 Seeds sterilization

For the germination and segregation experiments, seeds from individual siliques were harvested into single tubes and germinated on $\frac{1}{2}$ MS medium plates. *Arabidopsis* seeds were sterilized by immersing them in 70% ethanol for 5 minutes. After removing the ethanol, continued the sterilization with 5% sodium hypochlorite and 0.1% Tween for 7-8 minutes, ensuring the seeds are continuously mixed using a head-over-head shaker. Following sterilization, the seeds were washed 3-4 times with distilled water for 10 minutes each in head-over-head shaker. Next, seeds were mixed in 2 ml of 0.1% agarose and dropped onto $\frac{1}{2}$ MS plates using cut tips. The seeds were refrigerated for 2 days to synchronize germination and break dormancy, either in agarose or on the plate. The seeds were transferred to a cultivation room with growth conditions: 21 °C 8 h light/18 °C 16 h dark or 21 °C 16 h light/18 °C 8 h dark for germination.

3.10 Analysis of T-DNA insertion mutants

Seeds of T-DNA insertion lines were acquired from the European Arabidopsis Stock Centre (<http://arabidopsis.info/>). PCR was performed to verify the presence of T-DNA insertions. Gene-specific primer pairs flanking the predicted insertion sites comprising a left primer (LP) and a right primer (RP) along with T-DNA end-specific primers (LBb3.1, Appendix Table 1),

were used to distinguish between heterozygous and homozygous insertions. In the heterozygous SALK_135778 lines, both LP+RP (1186 bp) and LB+RP (814 bp) bands were amplified, while in homozygous mutants, only the LB+RP (814 bp) band was present. For SALK_091054 lines, the LP+RP product was 1090 bp and the LB+RP product was 761 bp. WT lines, lacking the T-DNA insertion, showed no amplification for the LB+RP product.

3.11 Gametophyte and developing embryo analysis

3.11.1 FDA staining

For pollen viability analysis, fluorescein diacetate (FDA) staining was performed as described by Yang et al. (2021). The FDA buffer was prepared by mixing 2 µg of FDA stock solution (Sigma-Aldrich, F7378) with 1 mL of BK buffer (10 mM HEPES (pH 7.0), 5 mM KCl, 1 mM CaCl₂, 0.75 mM MgSO₄, 10 mM glucose). FDA staining was carried out on at least three plants per genotype. A 20 µL aliquot of the FDA buffer was placed onto a microscope slide, and yellow anthers from a single opened flower were immersed in the buffer. The fluorescein fluorescence was observed after 20 minutes using an inverted microscope (Olympus IX 83) at 543/620 nm wavelengths.

3.11.2 Hoyer's Clearing

Clearing of ovules using Hoyer's solution was conducted as outlined by Yang et al. (2021). The anthers from unpollinated flowers were manually emasculated. The ovules were carefully dissected by slitting the ovary, taking care not to damage them two days after emasculation. The dissected ovules were then placed on a microscope slide, and 20 µL of Hoyer's solution was added. A coverslip was gently placed over the ovules without applying pressure. The slides were stored at 4 °C overnight or longer, and subsequently examined under an inverted microscope (Olympus IX 83).

For embryo analysis, same Hoyer's clearing was followed by manually pollinating the emasculated flowers.

3.12 Flow cytometry

For the analysis of ploidy levels of immature seeds, white and green seeds were selected from the same silique of the heterozygous mutant and compared with the green seeds of the WT. For the analysis of ploidy levels in seedlings, one leaf from 2-week-old heterozygous mutant and WT seedlings was used. Seeds and leaf tissue were chopped with a razor blade in 300 µl of

nuclei extraction buffer (CyStain UV Ploidy; Sysmex-Partec). The resulting nuclei suspension was filtered through a 50 µm disposable CellTrics filter (Sysmex-Partec), incubated for 10 minutes on ice and measured on BD Influx cell sorter (BD Biosciences).

3.13 Immunostaining

Immunostaining was performed as described in Ahmadli et al. (2022b). Two-week-old *Arabidopsis* seedlings were harvested and fixed in 4% paraformaldehyde in Tris buffer (10 mM Tris-HCl, 10 mM Na₂-EDTA, 100 mM NaCl, 0.1% Triton X-100, pH adjusted to 7.5 with NaOH) under vacuum for 5 minutes, followed by 30 minutes incubation on ice. After fixation, seedlings were washed three times in chilled Phosphate-Buffered Saline (PBS, 137 mM NaCl, 2.7 mM KCl, 10 mM Na₂HPO₄, 1.8 mM KH₂PO₄, pH 7.4) for 5 minutes each. Nuclei were prepared by chopping the seedlings in LB01 buffer (15 mM Tris-HCl, 2 mM Na₂EDTA, 0.5 mM spermine, 80 mM KCl, 20 mM NaCl, 0.1% Triton X-100, 15 mM 2-Mercaptoethanol pH 7.5, (Dpooležel et al., 1989)) and filtering the suspension through a 50 µm nylon mesh. The suspension was then transferred to glass slides using a cytopspin centrifuge, and the slides were kept in PBS until blocking.

Samples were blocked with 5% Bovine Serum Albumin (BSA) in PBS for 1-2 hours at RT in a moist chamber to prevent nonspecific binding. Primary antibodies (anti-CENH3 and anti-GFP) were diluted in 2% BSA and applied to the slides, followed by overnight incubation at 4 °C. The next day, the slides were washed three times in chilled PBS to remove unbound primary antibodies. Following the washes, secondary antibodies conjugated with fluorescent dyes were diluted in 2% BSA and applied to incubate for 1 hour at 37 °C in the dark. After incubation, the slides were washed again three times in PBS followed by dehydration in an ethanol series of 70%, 85%, 96%. The nuclei were counterstained with DAPI and mounted with anti-fade medium. Fluorescent signals were visualized using a fluorescence microscope to assess CENH3 and βKNL2-EYFP co-localization.

3.14 Microscopy analysis

Seeds of *Arabidopsis* transformants stably expressing EYFP fusion constructs were germinated on agar medium. The roots of 7-10-day-old seedlings were analyzed for the presence of EYFP fusion proteins using a 40× water objective (N.A. 1.2). For time-lapse microscopy, seedlings were grown in cover slip chambers (Nalge Nunc International) for 7–10 days and analyzed with an LSM 510 META confocal laser scanning microscope (Carl Zeiss GmbH).

To investigate the interphase nucleus and centromeric chromatin structures at high resolution, spatial structural illumination microscopy (3D-SIM) was employed. The microscopy analysis was conducted using an Elyra PS.1 super-resolution microscope system (Carl Zeiss GmbH) with a 63×/1.40 objective. DAPI (staining whole chromatin) and rhodamine (marking CENH3 signals) were excited using 405 nm and 561 nm lasers, respectively, as previously described by Weissbart et al. (2016) and Kubalová et al. (2021) respectively.

Confocal fluorescence imaging was performed using a Zeiss LSM780 confocal laser scanning microscope (Carl Zeiss Jena GmbH, Germany). EYFP was visualized using a 488 nm laser for excitation, with a 490–550 nm bandpass filter for detection. Images were analyzed using the Zeiss LSM software ZEN Black edition. Fluorescence loss in photobleaching (FLIP) and fluorescence recovery after photobleaching (FRAP) experiments were conducted using a 20× water objective (N.A. 0.8), with a zoom of 4.0 and an image size of 512 × 80 pixels. The pixel dwell time was set to 1 µs, and a pinhole setting of 2 airy units was applied. For bleaching experiments, the laser intensity was set at 100%.

FRAP experiments began with three to five pre-scans, followed by bleaching of an area of interest. The number of iterations was adjusted to achieve a 50-70% reduction in fluorescence. Fluorescence recovery was monitored until stability was reached. For FLIP experiments, a small region was repeatedly bleached with 1 or 5 iterations until a stable fluorescence loss was achieved.

3.15 Statistical analysis

All statistical analyses were performed in Microsoft Excel using F-test and two-tailed t-test functions. Box plots were generated using the online tool BoxPlotR (<http://shiny.chemgrid.org/boxplotr/>, Team RC, 2013).

3.16 Sequence motif analysis

Protein sequences of plant KNL2s were retrieved and analyzed for additional conserved motifs using the MEME Suite v5.1.0 (Bailey et al., 2009). The dataset was then submitted to the MEME server (<http://meme-suite.org/>), where conserved domains and motifs were identified using the MAST motif search algorithm (Bailey and Gribskov, 1998).

3.17 Electrophoretic mobility shift assay

FLAG- β KNL2 was expressed using the TnT SP6 High-Yield Wheat Germ Protein Expression System (Promega, L3260) following the manufacturer's instructions. The expression reaction was incubated at 25 °C for 2 hours. The expressed protein was confirmed by Western blot analysis using anti-FLAG-tag antibodies (Sigma-Aldrich, SAB4301135). The centromeric repeat *pAL1* was amplified from *Arabidopsis* genomic DNA using IRD700 labeled and unlabeled oligos, serving as the probe and competitor, respectively. Amplicons were purified using the oligonucleotide purification kit (BioRad, 7326300EDU).

The binding reaction was set up using the Odyssey EMSA kit (LICOR, 829-07910) with a protocol adapted from Eysholdt-Derzsó et al. (2023). Motif-III extended peptide from brassica species (Lifetain) was included in the reaction for peptide DNA binding ability testing. The expressed FLAG- β KNL2 and motif-III extended peptides with the *pAL1* labeled probe was incubated for 30 minutes at RT. The reaction was then loaded onto a 5% native polyacrylamide gel and run at 4 °C with a voltage of 70 V until the dye reached the bottom. Gel images were captured using a LICOR Odyssey scanner.

3.18 Bimolecular Fluorescence Complementation (BiFC)

The BiFC assay was conducted following Yadala et al. (2022). *Agrobacterium* containing one interaction partner cloned in the 3'Ven-C-pBAR-GW vector and the other in the 3'Ven-N-pBAR-GW vector (or vice versa) were mixed in equal proportions. The combined cultures were incubated for 1 hour at RT before infiltration, as described in section 3.8.1. Following infiltration, fluorescence was observed after 48 hours using a Zeiss Observer fluorescence microscope (Carl Zeiss Jena GmbH, Germany), with a 514 nm laser line for excitation and a 505–550 nm band-pass filter for detection.

3.19 Co-Immunoprecipitation (Co-IP)

Co-IP was conducted using the anti-HA tag magnetic agarose trap kit (Proteintech, atma), following the manufacturer's instructions. For the experiments, β KNL2 was fused to a MYC tag, while its interaction partners were fused to an HA tag. Leaves from 2–3-week-old *N. benthamiana* plants were co-infiltrated with *Agrobacterium* carrying the respective plasmids, as described in section 3.18.

After 48 hours post-infiltration, 2–4 grams of leaf tissue were harvested for total protein extraction. The leaves were ground in liquid nitrogen, and proteins were extracted using a

phosphate buffer (50 mM NaH₂PO₄, 1 mM β -mercaptoethanol, 100 mM NaCl, 0.5% Nonidet-P40, pH 7.0–7.5). Non-infiltrated leaves served as a negative control to ensure specificity. The protein extracts were incubated on ice for 30 minutes, followed by centrifugation at 13,000 rpm for 10 minutes at 4°C. The resulting supernatant was diluted 1:3 (g:mL) and incubated with 50 μ L of MYC-trap agarose for 2 hours at room temperature, or overnight at 4°C.

The MYC-trap agarose beads were washed three times with extraction buffer to remove non-specifically bound proteins. Bound proteins were eluted by boiling the beads at 95°C for 5 minutes in 60 μ L of 2 \times PLB loading buffer (125 mM Tris-HCl, pH 6.8, 4% SDS, 20% glycerol, 10% β -mercaptoethanol, 0.02% bromophenol blue).

Eluted proteins (10 μ L per sample) were separated by SDS-PAGE on a 10% acrylamide gel at 120–130 V for 1–2 hours, depending on the protein size, until the dye front reached the bottom of the gel. After separation, proteins were electro-transferred onto PVDF membranes (Thermo Scientific, 88518) at 49 mA for 90 minutes using a wet transfer system.

The membranes with proteins transferred from acrylamide gels were blocked for 1 hour at room temperature in 5% (w/v) non-fat milk dissolved in PBS containing 0.1% Tween-20 (PBS-T). Blocked membranes were incubated overnight at 4°C with primary antibodies (anti-HA, Proteintech 51064-2-AP and anti-cMYC) diluted 1:10,000 in blocking buffer.

The membranes were washed three times with PBS-T (5 minutes per wash), followed by incubation with a secondary goat anti-rabbit antibody conjugated to IRDye 800CW (LI-COR Biosciences, 926-32211) at a 1:5000 dilution for 1 hour at room temperature in the dark. After secondary antibody incubation, the membranes were washed three more times with PBS-T to remove unbound antibodies. Protein bands were visualized using the LI-COR Odyssey imaging system.

3.20 AlphaFold2 protein predictions and molecular dynamics analysis

A local installation of AlphaFold2 was utilized for all structural predictions in this study. We predicted the structures of β KNL2, α KNL2 and CENP-A/CENH3 and their combinations in different complexes (Appendix Fig. 1). To model β KNL2 and α KNL2 bound to the nucleosome, the centromeric histone octamer, consisting of CENP-A/CENH3, H2AW6, H2BHTB9, and H4, was first predicted using AlphaFold2. Next, this structure was superposed with the recently resolved *Arabidopsis* euchromatic nucleosome (PDB code 7ux9 (Lee et al., 2023)), and found that, the AlphaFold2 predicts a nearly identical structure, with RMSD of 1.2 Å for the 391

aligned residues. Following this, an attempt was made to predict the histone octamer in complex with β KNL2 and α KNL2 (Fig. 6).

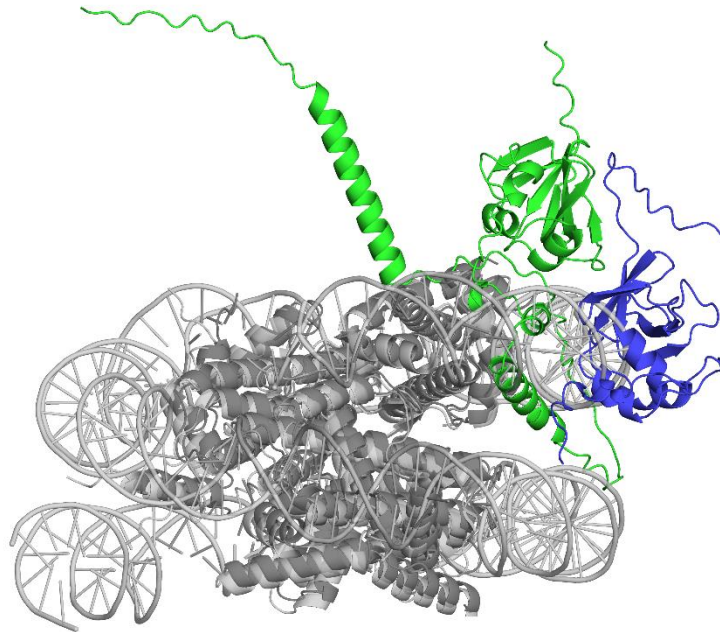


Figure 6. The predicted model of β KNL2(green) and α KNL2 (blue) with the octameric histones superposed with *Arabidopsis* euchromatic nucleosome (blue) (PDB code 7ux9 (Lee et al., 2023)). The structural alignment was performed with PyMOL, which aligned 391 residues from H2AW6 and H2BHTB9 monomers with the solved nucleosome, with a RMSD of 1.201 Å.

Some previously predicted disordered regions of the histones and of α KNL2 were neglected in the prediction of the complex to decrease computational costs. This prediction was superposed with the chicken CENP-A nucleosome in complex with KNL2, recently resolved by cryo-EM (pdb code 7y71) (Jiang et al., 2022). AlphaFold2 correctly placed the CENPC-k motif of α KNL2 in a similar position of the experimentally resolved CENPC-like motif of chicken KNL2. β KNL2 and α KNL2 were consistently predicted to be bound by their SANTA domains, but interacting with the octameric histones in a place that would collide with the DNA and not interacting with CENP-A/CENH3. To address this, a model of the nucleosome was constructed, incorporating β KNL2, α KNL2, and the CENPC-k motif of α KNL2 by combining different models predicted by AlphaFold2. These models demonstrated consistent characteristics and aligned well with experimental observations.

The proposed model was generated in 5 steps.

1. The initial model was constructed using centromeric nucleosome made of the predicted octameric histones (CENP-A/CENH3, H2AW6, H2BHTB9 and H4) with the DNA

from the superposed *Arabidopsis* euchromatic nucleosome. The CENPC-k motif of α KNL2 was retained in the same position predicted to bind to the histones core.

2. Next, the heterotrimer model of β KNL2, α KNL2 and CENP-A/CENH3 was superposed with the CENP-A/CENH3 from the octameric nucleosomes opposed to the CENPC-k motif of α KNL2.
3. The heterodimer of β KNL2 and α KNL2 was superposed with the β KNL2 of the heterotrimer and rotated it by 25° around the second α -helix of CENP-A/CENH3, next to Loop1. This way potential clashes between β KNL2, α KNL2, and the histones were avoided, while preserving what appears to be a crucial interaction between β KNL2 and CENP-A/CENH3 near Loop1.
4. The extended α -helix of motif-III (residues 213-281), that appeared in the predicted models of different dimer and trimers, was incorporated by superposing residues 208-218 of β KNL2, which folded into an α -helix in both models (the β KNL2 and α KNL2 heterodimer and the homotetramer).
5. A molecular dynamics of 150 ns in equilibrium was performed, starting from the thus assembled chimeric model, to remove small clashes and check the stability of the proposed model. The model presented is the last conformation of the molecular dynamics.

The molecular dynamics was performed with GROMACS software (Abraham et al., 2015). CHARMM36 all-atom force field (Huang et al., 2017) was used with an updated port for GROMACS (http://mackerell.umaryland.edu/charmm_ff.shtml#gromacs). Periodic boundary conditions and explicit solvation were used with SPC water model and neutralizing salt ions to fill a cubic box circumscribing the model with 10 Å from its edge. Minimization was performed with 100 ps pressure (NVT) and 100 ps volume (NPT) equilibrations prior to the 100 ns dynamics, all steps with Particle Mesh Ewald long-range electrostatics, velocity rescale thermostat, isotropic Parrinello-Rahman pressure coupling (for NPT and dynamics) and Verlet cutoff-scheme for neighbor searching with steps of 2 fs.

The Dictionary of Secondary Structure of Proteins (DSSP) method is widely used to analyze the secondary structure of proteins based on their atomic-resolution three-dimensional structures. DSSP assigns secondary structures to AA residues within a protein and provides detailed information about the protein's conformation.

The models by its secondary structure were analyzed with DSSP algorithm (Kabsch and Sander, 1983) and by its interchain interactions as the distance of a query residue to the closest residue

of another chain, measured by their alpha carbons and with a cutoff of 20 Å. Pictures of the structures were made with PyMOL (The PyMOL Molecular Graphics System, Version 3.0 Schrödinger, Inc.). Charge distribution surfaces were calculated with APBS Electrostatics method inside PyMOL and PDB2PQR for calculation of Poisson-Boltzmann electrostatics (Dolinsky et al., 2004).

In this study, DSSP was used to analyze the secondary structure of β KNL2 in combination with different kinetochore proteins. This analysis allowed us to determine the changes and rearrangement of secondary structure elements in β KNL2 based on its various binding partners. The results helped us hypothesize the protein's function by examining the structural changes resulting from its interaction with other molecules.

3.21 Experimental and technical contributions by the collaborators for the present thesis

The results presented in this thesis are based on and include findings from our articles Yadala et al. (2022), Zuo et al. (2022), and Yadala et al. (2024) with the exception of sections 4.5 and 4.6. Sections 4.1 and 4.2 were significantly contributed to by Dr. Sheng Zuo and Dr. Martin Lysak's lab. Sections 4.5 and 4.6 were generated through collaboration with Dr. Fen Yang and Assoc. Prof. Ales Pecinka's lab, with Dr. Yang also providing support in sections 4.3 and 4.4. For section 4.11, Surya Prakash Yalagapati, supported with EMSA experiments. Sections 4.13 and 4.14 were supported by Dr. Amanda Camara for the AlphaFold2 predictions. Dr. Twan Rutten contributed to the microscopic analyses, including FLIP, FRAP, mutant sectioning, confocal and scanning electron microscopy (SEM). Viet Schubert assisted with super-resolution microscopic images of CENH3 immunostaining in section 4.8, and Joerg Fuchs provided support with flow cytometry, section 4.7.

Chapter 4: Results

4.1 *KNL2* gene underwent independent duplications across plant lineages

All identified M18BP1/*KNL2* proteins typically feature the SANT-associated domain (SANTA) (Fig. 7A) (Zhang et al., 2006, Stellfox et al., 2013). This domain is often accompanied by a SANT domain and/or a CENPC-like motif. In eudicots, and grasses, two genes encoding proteins with SANTA domain have been identified (Zhang et al., 2006), but previously, only one has been characterized as *KNL2* (*At5g02520*) in *Arabidopsis* (Lermontova et al., 2013). The other gene was overlooked due to its atypical features, such as the protein interaction kinase domain 1 (KIP1) and the chromosome maintenance structural domain (SMC_Prok_B). This gene, *AT1G58210* or EMB1674 (Embryo Defective 1674) was identified to have embryo-lethal phenotype in large-scale seed mutant screens. Recent updates to the TAIR website, integrating Araport-11 and Phytozome 13 databases, show that the *AT1G58210* gene encodes a 281 AA protein with the SANTA domain but lacking KIP1 and SMC_Prok_B (Appendix Fig. 2). The re-annotated protein is designated as β *KNL2*, while the previously characterized protein as α *KNL2* (Fig. 7A).

To investigate the origin and evolution of *KNL2* genes across different plant lineages, 148 homologous conceptual protein sequences were identified based on the presence of the SANTA domain. These sequences were collected from various plant groups, including bryophytes, lycophytes, ferns, gymnosperms, and angiosperms (Appendix Table 2). These sequences were used to construct a phylogenetic tree (Fig. 7B), revealing that *KNL2* proteins cluster into two branches within three plant clades—heterosporous water ferns (Salviniaceae), eudicots, and grasses (Poaceae). This clustering suggests ancient gene duplications. In angiosperms, gene duplication occurred ~100 Ma (Angiosperm Phylogeny Website: <http://www.mobot.org/MOBOT/research/APweb/>; (Friis et al., 2016)). This event led to the formation of α *KNL2* and β *KNL2* genes in *Arabidopsis* and their orthologs in other eudicots. Interestingly, while most monocots have only one *KNL2* gene copy, the presence of two paralogs in grasses suggests an additional duplication event in their ancestor ~100 Ma (Wu et al., 2018), leading to the formation of γ *KNL2* and δ *KNL2*.



Figure 7. Domain organization and evolutionary relationships of KNL2 homologs in land plants. (A) Domain organization of M18BP1/KNL2 in various species: The schematic illustrates the domain structure of M18BP1/KNL2 proteins across different species. In non-mammalian vertebrates, M18BP1/KNL2 includes SANTA (magenta) and SANT (yellow) domains, along with a CENPC-like motif (purple). In mammals, the SANTA and SANT domains are separated by the CENP-C binding region (thick black line). In *Arabidopsis thaliana*, α KNL2 (598 amino acids) contains both the SANTA domain and a CENPC-k motif (blue), while β KNL2 (281 amino acids) is characterized solely by the SANTA domain. (B) Maximum likelihood phylogenetic analysis of KNL2 homologs in land plants: This phylogenetic tree was constructed using IQ-tree based on protein alignments of KNL2 homologs across land plants. KNL2 genes form two distinct clusters in three plant clades: heterosporous water ferns (Salviniaceae), eudicots, and grasses (Poaceae), suggesting ancient gene duplication events (indicated by arrows). In eudicots and grasses, KNL2 homologs are further classified into two major groups: α KNL2 and β KNL2 in eudicots, and γ KNL2 and δ KNL2 in grasses. Bootstrap values (bb) obtained from 1,000 ultrafast bootstrap replicates are displayed on the tree branches. The scale bar represents the number of substitutions per site, and the tree is arbitrarily rooted between bryophytes and tracheophytes.

4.2 *Arabidopsis* β KNL2 is highly expressed in meristematic tissues and localizes to centromeres despite lacking CENPC-k motif

In *Arabidopsis*, both α KNL2 and β KNL2 are present, and they share a conserved SANTA domain. Unlike β KNL2, the α KNL2 contains a CENPC-k motif at the C-terminus. The CENPC-k motif is a highly conserved motif essential for centromere targeting. Even a single residue modification can abolish α KNL2's centromere targeting capability (Appendix Fig. 3, (Sandmann et al., 2017)).

To determine the expression profiles of *KNL2* genes, expression analysis was performed. β KNL2 was initially omitted from the eFP genome browser analysis, possibly due to annotation errors. To rectify this, RNA-seq data was sourced from *Arabidopsis* (Klepikova et al., 2016), applying the correct β KNL2 annotation. The expression levels of the genes were normalized against the reference gene *MONENSIN SENSITIVITY1* (*MON1*; *AT2G28390*). Our findings indicate that *KNL2*, *CENH3*, and *CENP-C* genes exhibit enriched transcripts in meristematic active cells (Fig. 8A), indicating their crucial roles in cell division. Notably, β KNL2 exhibited higher expression levels than α KNL2 across nearly all tissues.

To analyze the *in-vivo* subcellular localization of β KNL2 in *Arabidopsis*, transgenic lines stably expressing the β KNL2-EYFP and EYFP- β KNL2 fusion construct under the CaMV 35S promoter were generated. Fluorescence microscopy of seedlings from selected transgenic lines revealed distinct fluorescent signals localized at centromeres as well as dispersed within the nucleoplasm of nuclei in root tip cells (Fig. 8B). Both N- and C-terminal fusions of EYFP exhibited similar localization patterns. Immunostaining with anti-GFP and anti-CENH3 antibodies confirmed the co-localization of β KNL2-EYFP with CENH3 at centromeres (Fig. 8B). Live cell imaging demonstrated that β KNL2 is present at centromeres during interphase, becomes nearly undetectable just before mitosis, and reappears during the M phase (Fig. 8C). In contrast, α KNL2 was not detectable during prophase, metaphase, and early anaphase in *Arabidopsis* root tip cells (Lermontova et al., 2013).

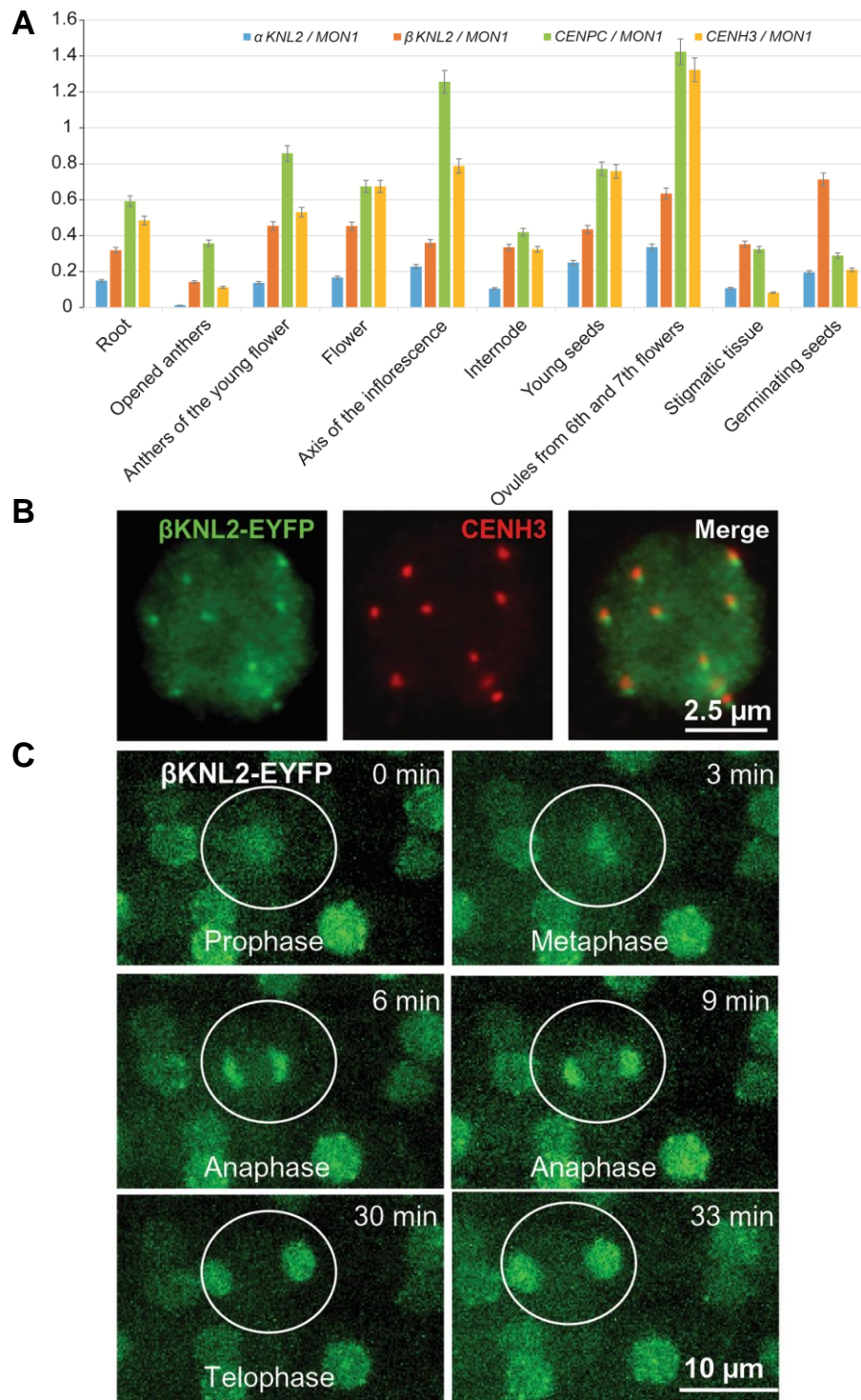


Figure 8. Gene expression profiles of *CENH3*, *CENP-C*, and *KNL2* variants, and subcellular localization of β KNL2 in *Arabidopsis*.

(A) Expression levels of *CENH3*, *CENP-C*, and *KNL2* genes: Column charts display the expression levels of *CENH3*, *CENP-C*, and *KNL2* genes across various tissues enriched for dividing cells. The relative expression levels are presented as fragments per kilobase of exon per million mapped fragments (RPKM), normalized to the reference gene *MON1* from RNA-seq data sets. (B) Subcellular localization of β KNL2: Immunostaining of nuclei isolated from β KNL2-EYFP transformant seedlings is shown. The left panel displays the signal from anti-GFP antibodies (β KNL2-EYFP), the middle panel shows the signal from anti-CENH3 antibodies, and the right panel presents the merged image of both signals. (C) Live imaging of root tip cells: Root tip cells of *Arabidopsis*, transformed with the β KNL2-EYFP fusion construct, are shown. A cell undergoing mitosis is highlighted with a circle, illustrating the localization of β KNL2 during cell division.

4.3 $\beta KNL2$ knockout resulted in an abnormal seed development phenotype

To investigate the function of $\beta KNL2$ in plants, two T-DNA insertion lines, SALK_135778 and SALK_091054, were obtained from the *Arabidopsis* Biological Resource Center (ABRC) and named $\beta knl2-1$ and $\beta knl2-2$, respectively (Fig. 9A). The insertions are located within the single exon of $\beta KNL2$, at positions 270 and 335 nucleotides downstream from the transcription start site. Specifically, the insertion in $\beta knl2-1$ is positioned upstream of the region encoding the SANTA domain, while in $\beta knl2-2$ it disrupts this region directly (Fig. 9A). PCR-based genotyping showed the absence of homozygous mutants in soil-grown plants from both populations obtained from the ABRC seed stock (n=26 for $\beta knl2-1$ and n=38 for $\beta knl2-2$; data not shown). Similar results were found in subsequent generation (n=195 and n=220, respectively; data not shown), suggesting that homozygous $\beta KNL2$ knockout may be lethal.

Therefore, the siliques of heterozygous $\beta knl2$ mutants were examined and abnormal seed phenotype was observed. In contrast to WT plants, which produce normal green seeds, heterozygous $\beta knl2$ mutants exhibit approximately $11 \pm 1\%$ seeds that are larger, whitish and glossy (Fig. 9B-C). Additionally, the $\beta knl2-1$ line displayed an ovule abortion phenotype not seen in $\beta knl2-2$ (Fig. 9D). Analysis revealed that SALK_135778 ($\beta knl2-1$) harbors additional T-DNA insertions in genes *AT1G76850* and *AT3G13920*, which influence ovule development and pollen acceptance (Bush et al., 2015, Safavian et al., 2015). Using primers specific to these additional T-DNA insertions, $\beta knl2-1$ plants without additional insertions were isolated. These selected lines did not exhibit the ovule abortion phenotype and were used for further analyses (Fig. 9B).

To determine the effect of the heterozygous or homozygous state of these mutations on seed development, reciprocal crosses between WT and heterozygous mutants of $\beta knl2-1$ and $\beta knl2-2$ were conducted. All crosses resulted in less than 3% abnormal seeds (Fig. 9E-F, Appendix Table 3), similar to WT self-pollinated rates. This suggests that the abnormal seed phenotype in heterozygous siliques results from homozygous mutations of $\beta knl2$, indicating that the abnormal seed phenotype is of a recessive nature. This also confirms that the gametes are not the cause; instead, abnormalities arise during postzygotic development.

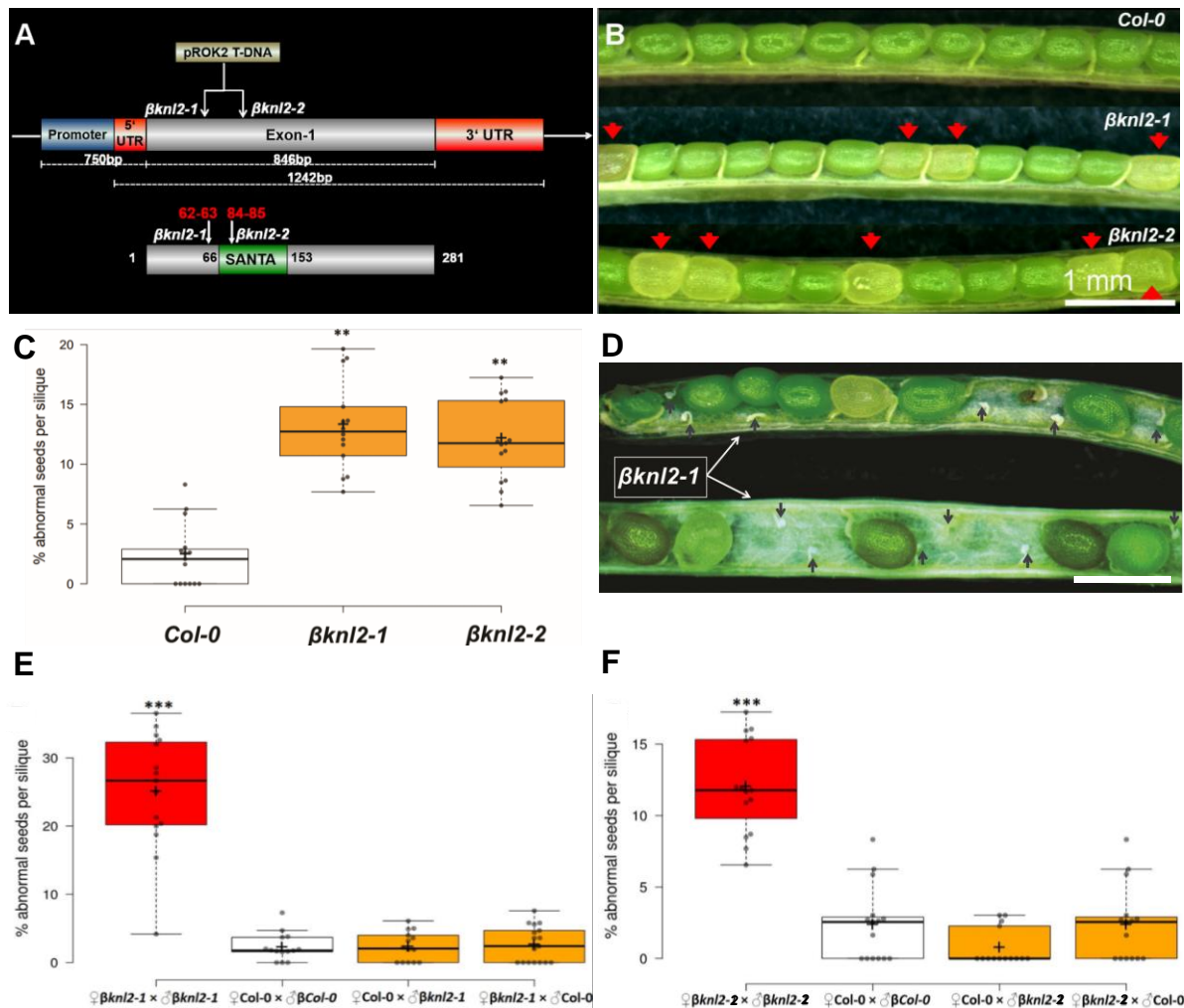


Figure 9. $\beta knl2$ heterozygous mutants show embryo defective phenotype.

(A) Schematic representation of the T-DNA insertion positions within the $\beta KNL2$ gene in *Arabidopsis thaliana*. The insertions in $\beta knl2-1$ is before the SANTA domain and in $\beta knl2-2$ after the SANTA domain disrupting the gene's coding sequence. (B) Representative siliques from heterozygous $\beta knl2-1$ and $\beta knl2-2$ plants, displaying abnormal seeds marked by red arrowheads. The abnormal seeds are characterized by a whitish, glossy appearance, distinguishing them from normal green seeds in WT plants. Scale bar: 1 mm. (C) Box plot analysis showing the percentage of abnormal seeds per silique in heterozygous $\beta knl2-1$ and $\beta knl2-2$ mutants compared to WT. Both $\beta knl2-1$ and $\beta knl2-2$ mutants exhibit a significant increase in abnormal seed formation. (D) Siliques from a heterozygous $\beta knl2-1$ plant showing early ovule abortion, along with abnormal whitish seeds and normal green seeds. Early ovule abortion is caused due to the T-DNA insertions in the other loci than $\beta KNL2$ gene. Scale bar: 1 mm. (E-F) Box plots depicting the frequency of abnormal seeds per silique in reciprocal crosses between WT and heterozygous $\beta knl2-1$ (E) and $\beta knl2-2$ (F) plants. The crosses demonstrate a significant increase in abnormal seeds in self-pollinated $\beta knl2$ mutants compared to crosses with WT plants. (* $P \leq 0.05$, ** $P \leq 0.01$, *** $P \leq 0.001$).

4.4 *In-vitro* recovered $\beta KNL2$ homozygous mutants cannot survive beyond seedling stage

Homozygous $\beta knl2$ mutants could not be isolated from soil-grown plants due to their non-viability. Therefore, abnormal seeds, presumably homozygous for the $\beta knl2$ mutation, were assessed for their ability to germinate under controlled *in-vitro* conditions. This could minimize the environmental stresses and competition, allowing better observation of seedling growth.

In both mutants, abnormal seedlings characterized by stunted growth and poor root development were observed (Fig. 10A). These abnormal seedlings were confirmed to be homozygous mutants through genotyping and observed at a frequency of 2-6% among all sown seeds. Attempts to transfer these homozygous seedlings to soil consistently resulted in their death (Fig. 10B), whereas heterozygous seedlings appeared indistinguishable from WT (Fig. 10A).

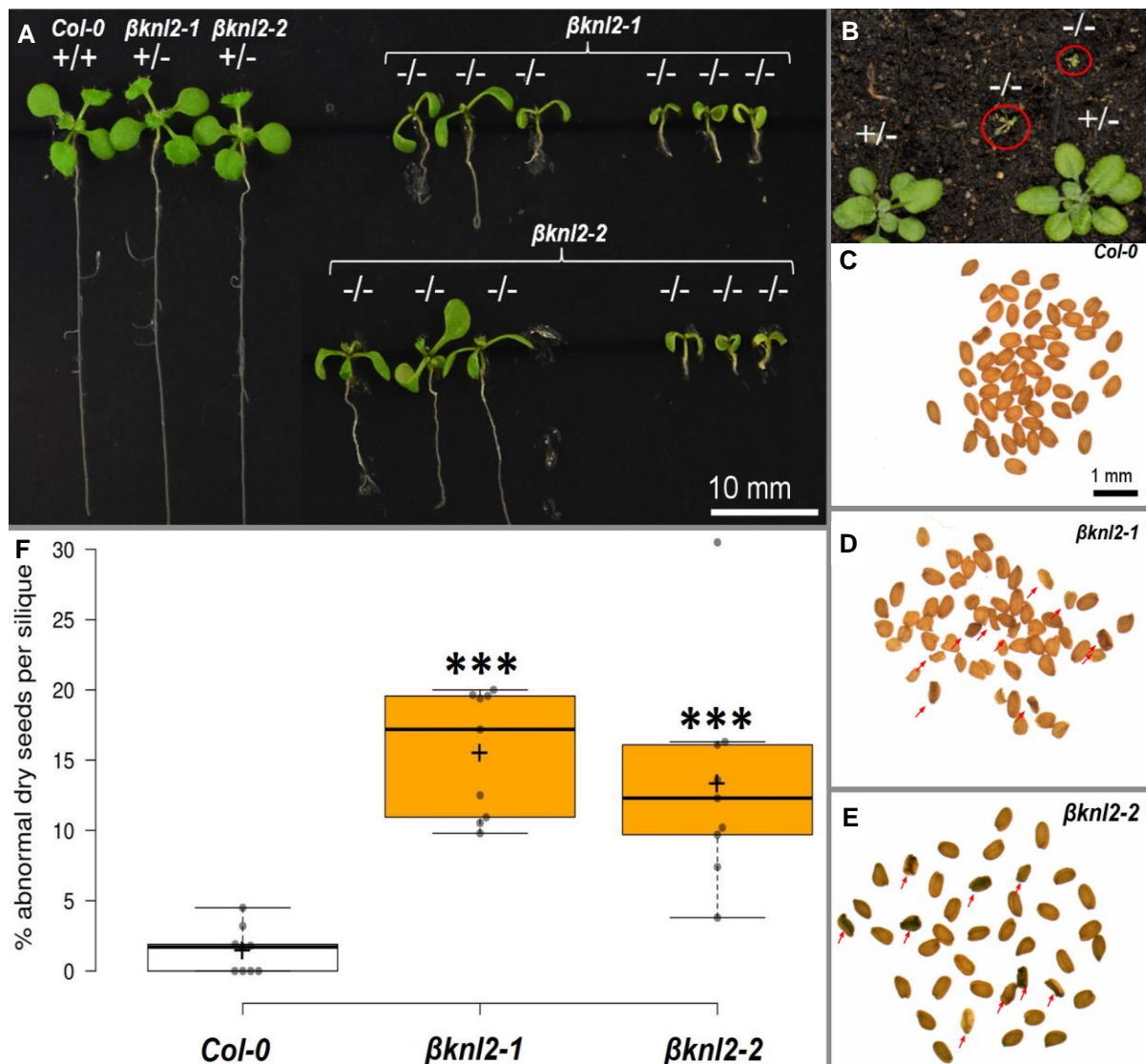


Figure 10. Homozygous mutation of $\beta kn12$ causes semi-lethal phenotype in *Arabidopsis thaliana*. (A) Two-week-old *in-vitro* germinated seedlings from WT, $\beta kn12-1$, and $\beta kn12-2$ heterozygous (+/-) and homozygous (-/-) mutants. The homozygous mutants exhibit stunted growth and yellowing compared to the WT and heterozygous plants. Scale bar: 10 mm. (B) $\beta kn12$ homozygous (-/-) and heterozygous (+/-) mutants grown on soil. The homozygous mutants, indicated within red circles, show signs of yellowing and reduced viability. (C–E) Representative dry seeds from WT (C), $\beta kn12-1$ (D), and $\beta kn12-2$ (E) plants. Red arrowheads point to the abnormal seeds observed in the $\beta kn12-1$ and $\beta kn12-2$ mutants, which appear smaller and misshapen compared to the WT seeds. Scale bar: 1 mm (F) Boxplot illustrating the significant increase in the percentage of abnormal dry seeds per silique in heterozygous $\beta kn12-1$ and $\beta kn12-2$ mutants compared to the WT control. (* $P \leq 0.05$, ** $P \leq 0.01$ *** $P \leq 0.001$).

Interestingly, the heterozygous mutants' siliques yielded less than 25% abnormal seeds, deviating from expected Mendelian ratios (Fig. 9C). To ensure accuracy in seed phenotyping, dry seed phenotypes from individual siliques were subsequently re-examined (Fig. 10C-E). This examination showed that heterozygous mutants, unlike WT, produced small, dark-colored, and shriveled seeds (Fig. 10D-E), correlating with the frequency of whitish, glossy seeds in fresh siliques (Fig. 10F). Thus, it can be assumed that a large part of the whitish seeds with a glossy surface became dark and small or shriveled on drying.

Additionally, germination rate from single siliques was analyzed to underscore the impact of the *βknl2* mutation (Fig. 11A). Heterozygous mutants exhibited significantly decreased germination rate ($P \leq 0.01$) (Fig. 11B) and increased number of abnormal seedlings per single silique ($P \leq 0.01$) (Fig. 11A & C) compared to WT. Genotyping of individual siliques revealed that the homozygous mutation in *βknl2-1* constituted approximately 16% and in *βknl2-2* about 25% per silique (Appendix Table 4). The variation between the two mutants may be due to seed quality and germination efficiency.

To determine if these abnormal seedlings (reduced seedling size and reduced root length) lacked functional *βKNL2*, RT-PCR analysis was conducted using gene-specific primers on pooled RNA from 3-5 seedlings. The results showed an absence of full-length *βKNL2* transcripts in both *βknl2-1* and *βknl2-2* mutants (Fig. 11D). Further selection of homozygous seedlings could be effectively based on their phenotypic abnormalities, eliminating the need for additional genotyping.

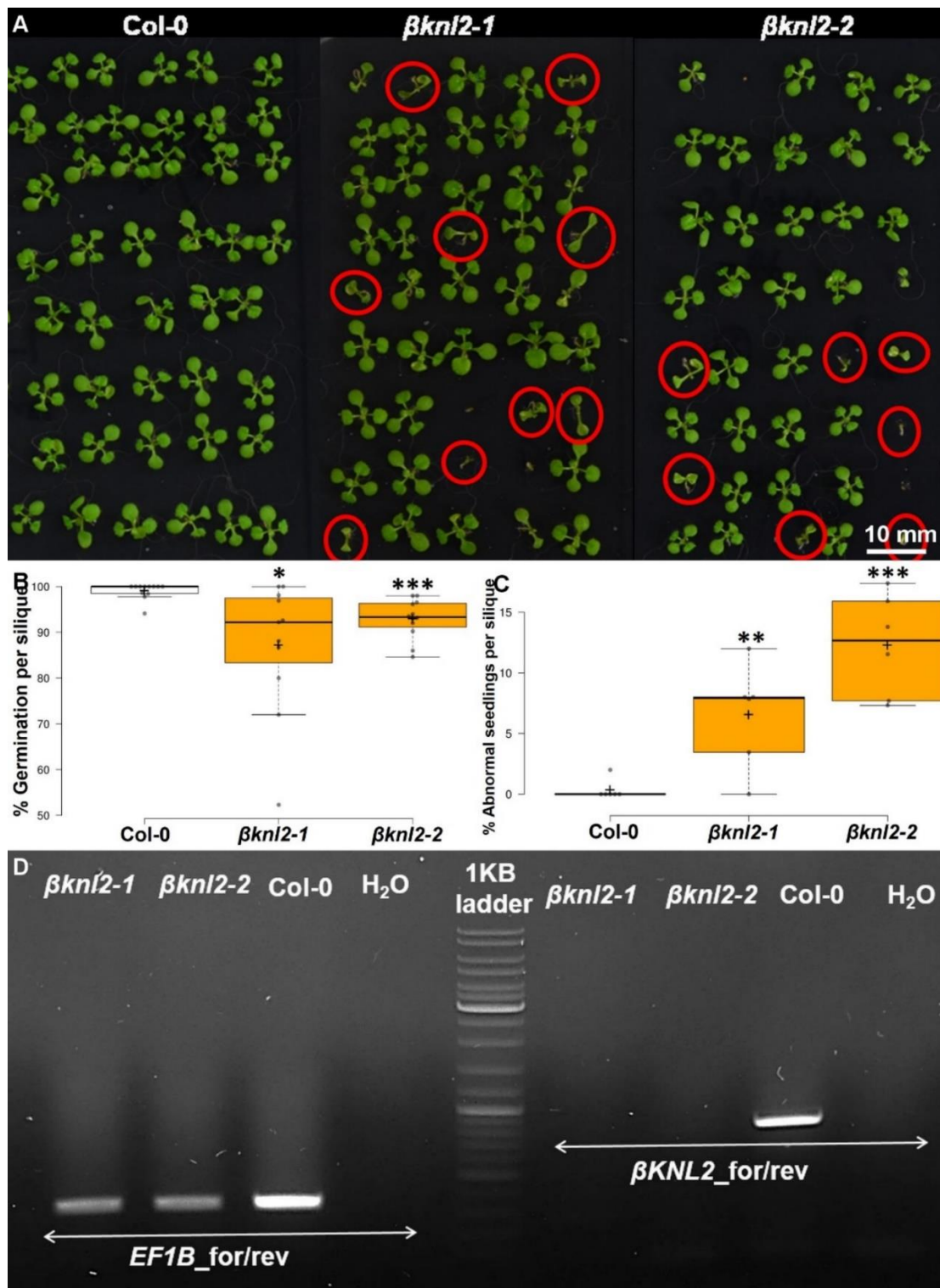


Figure 11. Analysis of single siliques for seeds germination and presence of abnormal seedlings. (A) Two-week-old *in-vitro* germinated seeds collected from single siliques of WT as control and heterozygous self-pollinated $\beta knl2-1$ and $\beta knl2-2$ plants. $\beta knl2$ homozygous seedlings are indicated by red circles. Scale bar: 10 mm. (B) Boxplot depicting the significant decrease of germination percentage per silique of heterozygous $\beta knl2-1$ and $\beta knl2-2$ compared with WT as control. (C) Boxplot depicting the significant increase of abnormal seedlings (red color circled seedlings in (A)) germinated from single silique seeds of heterozygous $\beta knl2-1$ and $\beta knl2-2$ compared with WT as control. (D) RT-PCR amplification of $\beta KNL2$ from $\beta knl2-1$ and $\beta knl2-2$ homozygous null mutants and WT as the positive control with $\beta KNL2$ (EMB1674) gene-specific primers and *EF1B* primers as housekeeping gene. (* $P \leq 0.05$, ** $P \leq 0.01$ *** $P \leq 0.001$).

4.5 *Arabidopsis* β KNL2 is essential for correct somatic cell division

To compare the morphology of homozygous *β knl2* mutant seedlings with WT, scanning electron microscopy (SEM) and histological analyses were performed on roots, hypocotyls, and shoot apical meristems (SAM) (Fig. 12). SEM analysis revealed that the roots of *β knl2* mutant seedlings exhibited a reduced meristematic zone, predominantly displaying an elongation zone compared to WT roots. Histological examination of longitudinal root sections confirmed these observations, showing that the actively dividing cells in *β knl2* mutants were significantly reduced, with the meristematic zone confined to the very tip of the root (Fig. 12A). In both *β knl2* mutants, the stele was present but displayed disorganized cellular architecture and irregular cell shapes in both the meristematic and elongation zones.

The hypocotyl consists of the outermost epidermis, beneath which lies the cortex, composed of parenchyma cells. The endodermis, a single layer between the cortex and vascular tissues, contains the Casparian strip, regulating water and solute movement into the stele. The pericycle, located around the vascular tissues, plays a critical role in lateral root initiation. At the core of the hypocotyl, the stele houses the vascular bundle, which includes the xylem and the phloem. Histological analysis of *β knl2* mutant's hypocotyl sections also revealed abnormal cellular organization in cortex, pericycle and stele. Irregular cell shapes and divisions were evident compared to WT seedlings, which exhibited highly organized cellular arrays (Fig. 12B).

Furthermore, most *β knl2* mutant seedlings failed to develop beyond the first pair of true leaves, with many producing no leaves at all. Transverse sections of homozygous *β knl2* mutant seedlings revealed significant abnormalities in the structure of the SAM (Fig. 12C) compared to WT seedlings. The SAM in WT is a small, dome-shaped structure at the apex, characterized by distinct cellular zones. The central zone (CZ), containing slowly dividing stem cells (SCs) surrounding an organizing center (OC), giving rise to daughter stem cells (DSCs), which in turn supply cells to the peripheral zone (PZ) and rib zone (RZ). These outer zones contain rapidly dividing cells that contribute to the development of new organs. In *β knl2* mutants, SAM zones were randomly organized, deviating from the ordered dome structure of WT, leading to impaired true leaf development.

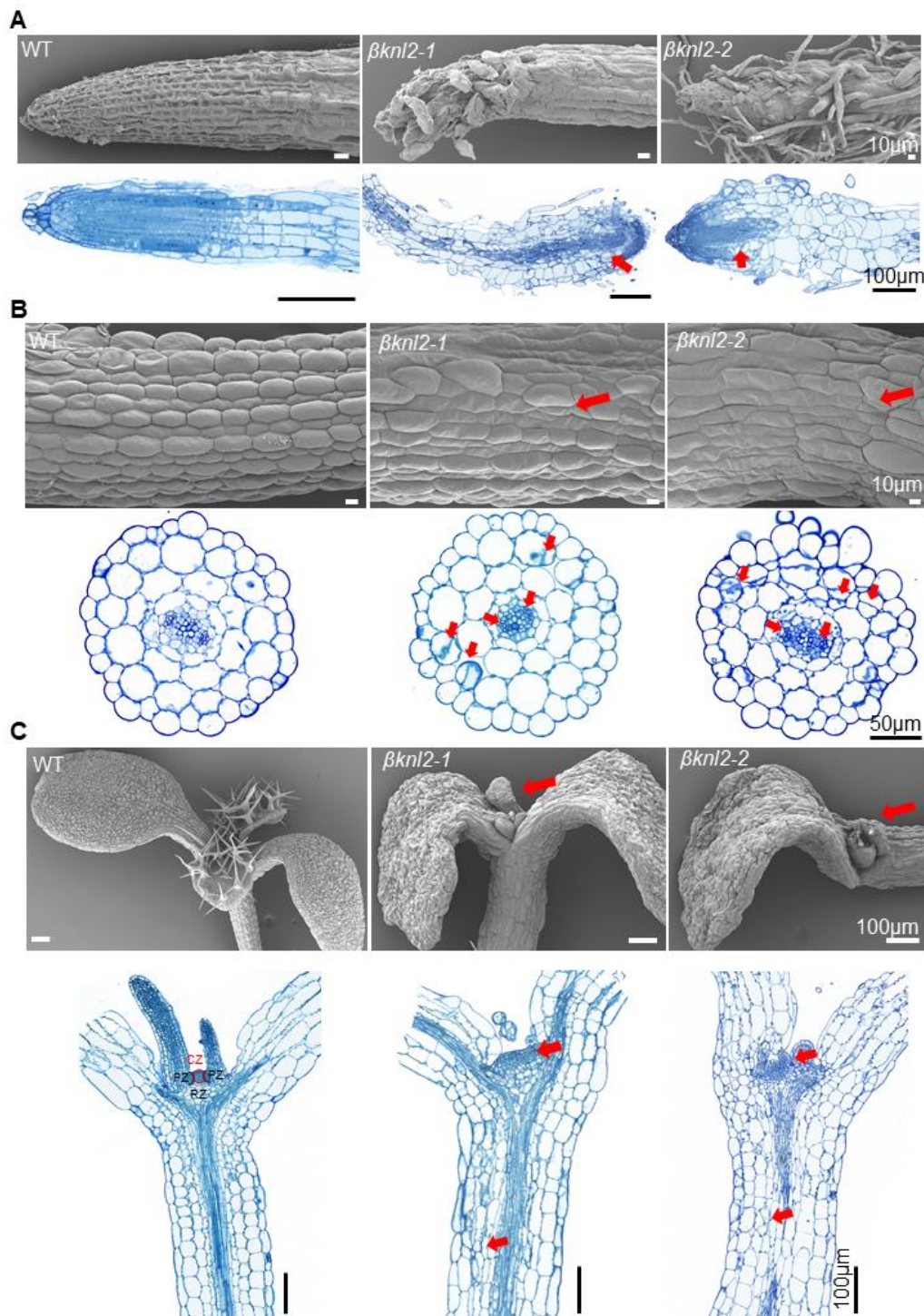


Figure 12. *βknl2* homozygous mutant seedlings exhibit disrupted cellular organization.

(A) SEM and histological analysis of roots in WT and *βknl2* mutant seedlings. Mutants (*βknl2-1* and *βknl2-2*) show significantly reduced meristematic zones compared to WT controls. Red arrows highlight developmental anomalies, including disorganized and enlarged cells in the meristematic zone. (B) SEM and histological analysis of hypocotyls in WT and *βknl2* mutant seedlings. WT hypocotyls exhibit systematically organized cell layers, while *βknl2* mutants show disorganized cell layers, enlarged cells, and abnormal hypocotyl morphology. Histological analysis confirms these anomalies, particularly in the cortex, pericycle, and stele. Red arrows indicate disorganized and enlarged cells in various cell layers and the stele. (C) SEM and histological analysis of SAM in WT and *βknl2* mutants. WT seedlings display a regular dome-shaped SAM with densely packed, organized cell layers and normal cell divisions. In contrast, *βknl2* mutants exhibit irregular SAM shapes, disrupted cell layers, and a shortened meristem structure. Developmental anomalies are marked with red arrows.

Examination of transverse and longitudinal sections of WT seedlings confirmed that cell divisions in roots, hypocotyls, and SAMs were highly systematic, forming distinct and organized cellular layers (Fig. 12A-C, left panels). WT seedlings displayed elongated root meristems with densely packed, actively dividing cells and orderly cellular arrays in the shoot. These seedlings also developed two cotyledons and healthy true leaves, indicative of robust developmental processes. In contrast, *βknl2* mutants exhibited disrupted cellular organization and impaired development, underscoring the critical role of β KNL2 in somatic cell division and meristem functionality.

Transverse and longitudinal sections showed that WT seedlings display orderly and well-organized cell divisions throughout all tissues, contributing to robust development. Whereas *βknl2* mutants showed disrupted cellular organization and impaired growth. These observations underscore the pivotal role of β KNL2 in maintaining cell division integrity, meristem functionality and proper ploidy levels during plant development.

4.6 Loss of β KNL2 impacted nuclear divisions and development of both embryo and endosperm in *Arabidopsis*

Initial reciprocal crosses between heterozygous *βknl2* mutants and WT plants did not reveal any observable abnormalities in seed development (section 4.3). Based on this, we hypothesized that the loss of β KNL2 does not affect gametophyte development.

To further investigate, pollen viability was assessed using FDA (fluorescein diacetate) staining (Fig. 13A), which showed no significant differences between the mutants and WT in terms of pollen viability (Table 5; Fig. 13B). Additionally, female gametophyte development was analyzed through Hoyer's clearing technique (Fig. 13C), revealing no deviations from normal development (Table 6). These findings suggest that the loss of β KNL2 primarily affects post-fertilization development rather than gametophyte formation.

Table 5. Analysis of pollen viability by FDA staining

Genotype	Total analyzed	Viable pollen
WT	689	599 (87%)
<i>βknl2-1</i>	792	726 (91.7%)
<i>βknl2-2</i>	690	656 (95.2%)

Table 6. Analysis of female gametophyte development

Genotype	Total analyzed	Normal ovules
<i>βknl2-1</i>	62	62 (100%)
<i>βknl2-2</i>	38	38 (100%)

In order to understand the role of β KNL2 in cell division and early development, the progression of embryo and endosperm development in $\beta knl2$ mutants was examined. The analysis of abnormal whitish and green seeds from $\beta knl2$ heterozygous mutants and WT plants revealed that mutant embryos were arrested at various stages of development, in contrast to the fully developed embryos observed in the green seeds of control plants (Fig. 14A).

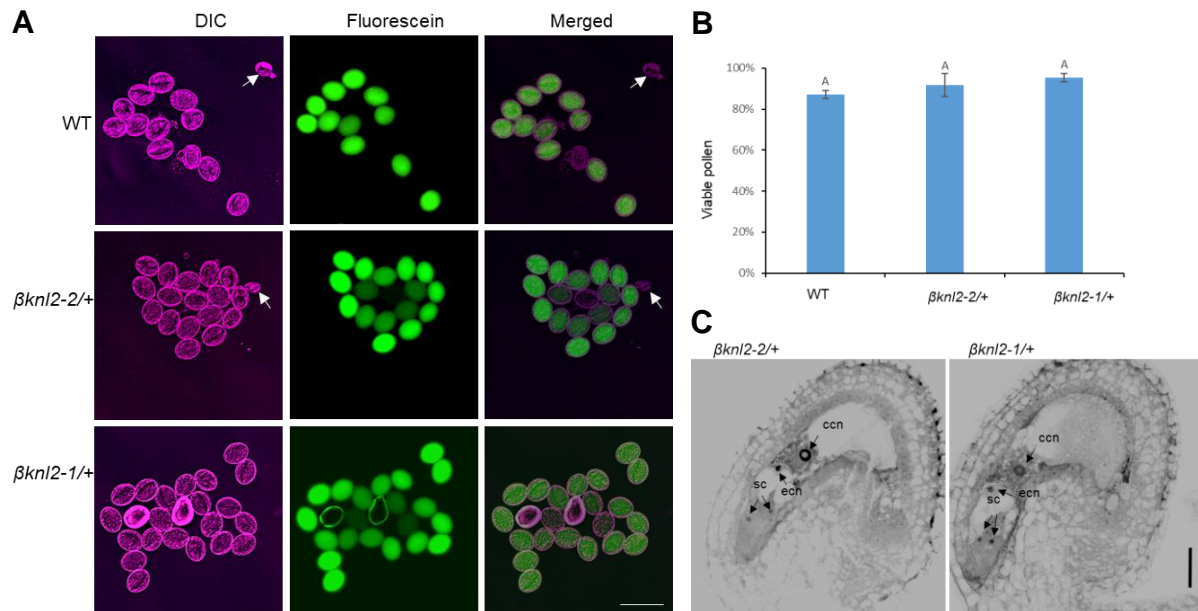


Figure 13. Analysis of pollen viability and ovule development in $\beta knl2$ mutants.

(A) Representative images of pollen from WT and $\beta knl2$ mutant lines ($\beta knl2-1$ and $\beta knl2-2$) after staining with FDA stain. The left column shows DIC images (pseudocolored in magenta), the middle column shows fluorescein signals (pseudocolored in green), and the right column shows the merged images. Green fluorescence indicates viable pollen, while the absence of fluorescence indicates non-viable pollen. Aborted microspores are indicated by arrows. Scale bar: 50 μ m. (B) Bar chart showing the frequencies of viable pollen in WT and $\beta knl2$ mutants. Error bars represent the standard deviation from three biological replicates. Values marked with the same letter do not differ significantly according to one-way ANOVA followed by Tukey's test. (C) Confocal fluorescence micrographs of ovules from $\beta knl2-1/+$ and $\beta knl2-2/+$ plants. The images depict embryo sacs with two synergid cells (sc), one egg cell nucleus (ecn), and one central cell nucleus (ccn). Scale bar: 20 μ m. (* $P \leq 0.05$, ** $P \leq 0.01$ *** $P \leq 0.001$).

To investigate further, manual self-pollinations were performed on both $\beta knl2$ mutants and WT plants. Three plants per genotype were analyzed. Three days after pollination, siliques were collected and subjected to SCRI Renaissance 2200 (SR2200) staining (Fig. 14B-C). Results indicated that abnormal cell division events in $\beta knl2$ mutants commenced as early as the four-celled embryo stage, distinctly diverging from the orderly progression observed in controls (Fig. 14B). Notably, about 15% of early-stage embryos demonstrated abnormal cell divisions with 3 to 5 nuclei instead of normal 4 nuclei (Table 7; Fig. 14B-C). The observed abnormalities are lower than the expected 25% based on Mendelian inheritance, suggesting some embryos may correct or bypass the initial abnormal divisions. Indeed, around 10% of embryos continued

normal cell division processes during early development, potentially explaining the recovery of abnormal homozygous mutants on sterile media.

Table 7. Frequency of abnormal cell divisions in $\beta knl2$ mutant embryos.

Analysis of cell division abnormalities in $\beta knl2$ embryos compared to WT. The numbers in parentheses represent three biological replicates. The percentage of abnormal embryos was calculated based on the total number of embryos analyzed per genotype.

Genotype	Abnormal embryo	Normal embryo	Percentage of abnormality
WT	2(1,0,1)	50(8,8,34)	4%
$\beta knl2-1$	5(5,0,0)	35(18,9,8)	14.3%
$\beta knl2-2$	11(2,8,1)	72(20,29,23)	15.3%

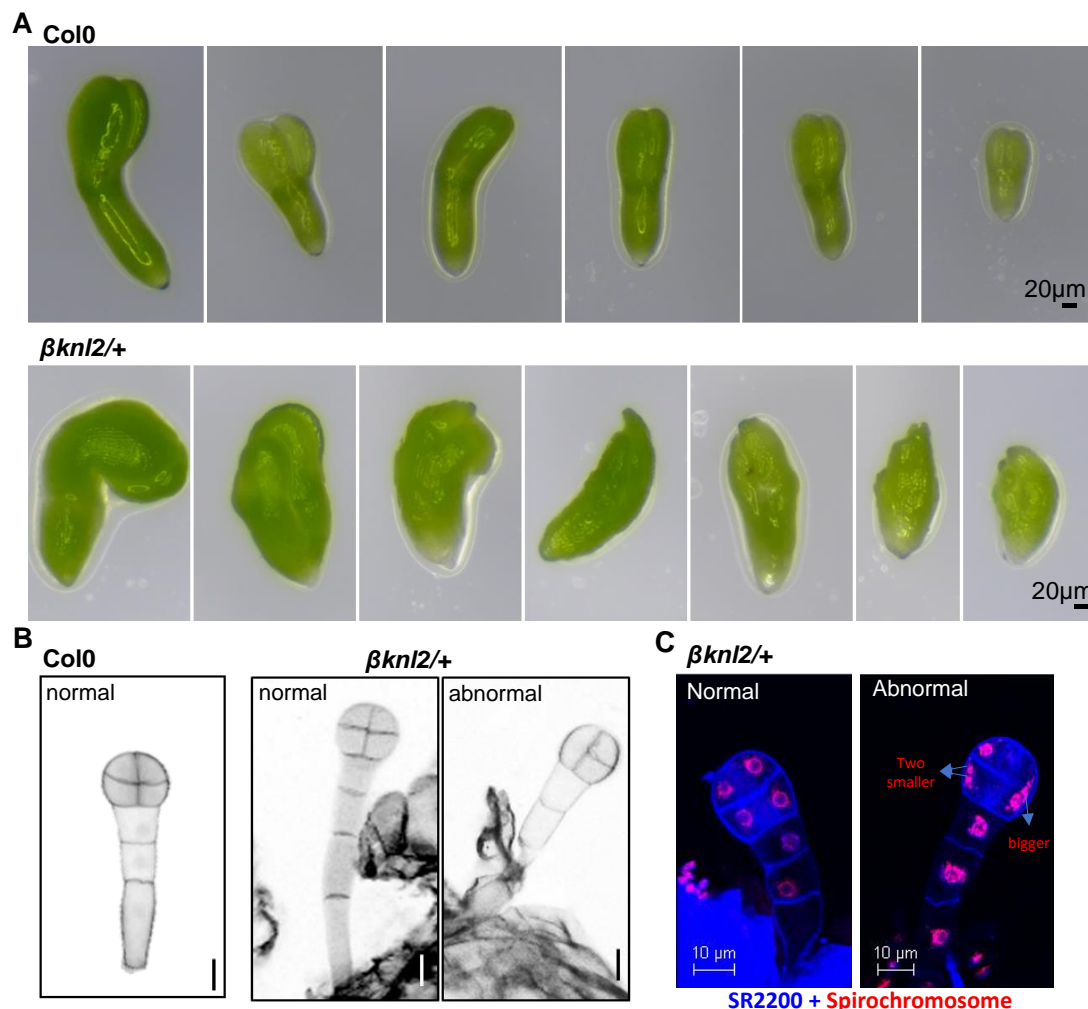


Figure 14. Loss of $\beta KNL2$ resulted in abnormal cell divisions in early embryo development causing EMB phenotype in *Arabidopsis*.

(A) Representative images of embryos from WT and $\beta knl2/+$ heterozygous plants at various stages of development. The $\beta knl2/+$ embryos show a range of abnormal morphologies compared to the uniformly shaped WT embryos. Scale bar: 20 μm (B) Confocal fluorescence micrographs showing the 4-cell stage embryos from WT and $\beta knl2/+$ plants. The images highlight both normal and abnormal embryos in the $\beta knl2-2/+$ background. Scale bar: 10 μm . (C) Confocal fluorescence micrographs of normal 4-cell and abnormal 3-cell stage embryos from $\beta knl2/+$ plants. The cell walls are stained with SR2200, and nuclei are stained using Spirochrome SPY555-DNA. The normal 4-cell embryo contains 4 nuclei, while the abnormal embryos exhibit either 5 or 3 nuclei, indicating disrupted cell division. Scale bar: 10 μm .

4.7 *Arabidopsis* β KNL2 is required for proper CENH3 loading

β KNL2 co-localizes with CENH3 at centromeres (Fig. 8B) and exhibits a localization pattern akin to that of α KNL2 (Lermontova et al., 2013). To explore β KNL2's role in CENH3 loading, immunostaining using anti-CENH3 antibodies was conducted on nuclei from 14-day-old seedlings of WT and *β knl2* mutants.

Immunostaining revealed a reduced number of CENH3 signals in mutant nuclei compared to WT, irrespective of nuclear shape. In total, CENH3 signals were counted in 50 spherical nuclei from WT, *β knl2-1*, and *β knl2-2* mutants. WT nuclei exhibited an average of 8-10 signals, whereas mutant nuclei displayed an average of 4 signals, with some showing no signals at all (Fig. 15A-B). Statistical analysis using Student's t-test confirmed significantly fewer CENH3 signals in mutants compared to WT ($P \leq 0.001$) (Fig. 15B).

Additionally, mean fluorescence intensity (MFI) quantified reduced centromeric CENH3 levels in mutants: 68.98% in *β knl2-1* and 79.47% in *β knl2-2* (Fig. 15C), both significantly lower than in WT ($P \leq 0.01$). In spindle-shaped nuclei, both *β knl2* mutants exhibited dispersed CENH3 signals at chromocenters compared to WT, with some mutant chromocenters entirely lacking signals. This dispersion of CENH3 signals is consistent with our previous findings on increased ploidy levels (Lermontova et al., 2006).

For a detailed examination of chromatin ultrastructure, representative nuclei from the slides were captured using spatial structured illumination super-resolution microscopy (3D-SIM) (Fig. 15D). Despite the reduced CENH3 levels, chromatin structure in the mutants appeared normal, suggesting intact nuclei were selected for analysis. In conclusion, both homozygous *β knl2-1* and *β knl2-2* mutants exhibited decreased CENH3 levels.

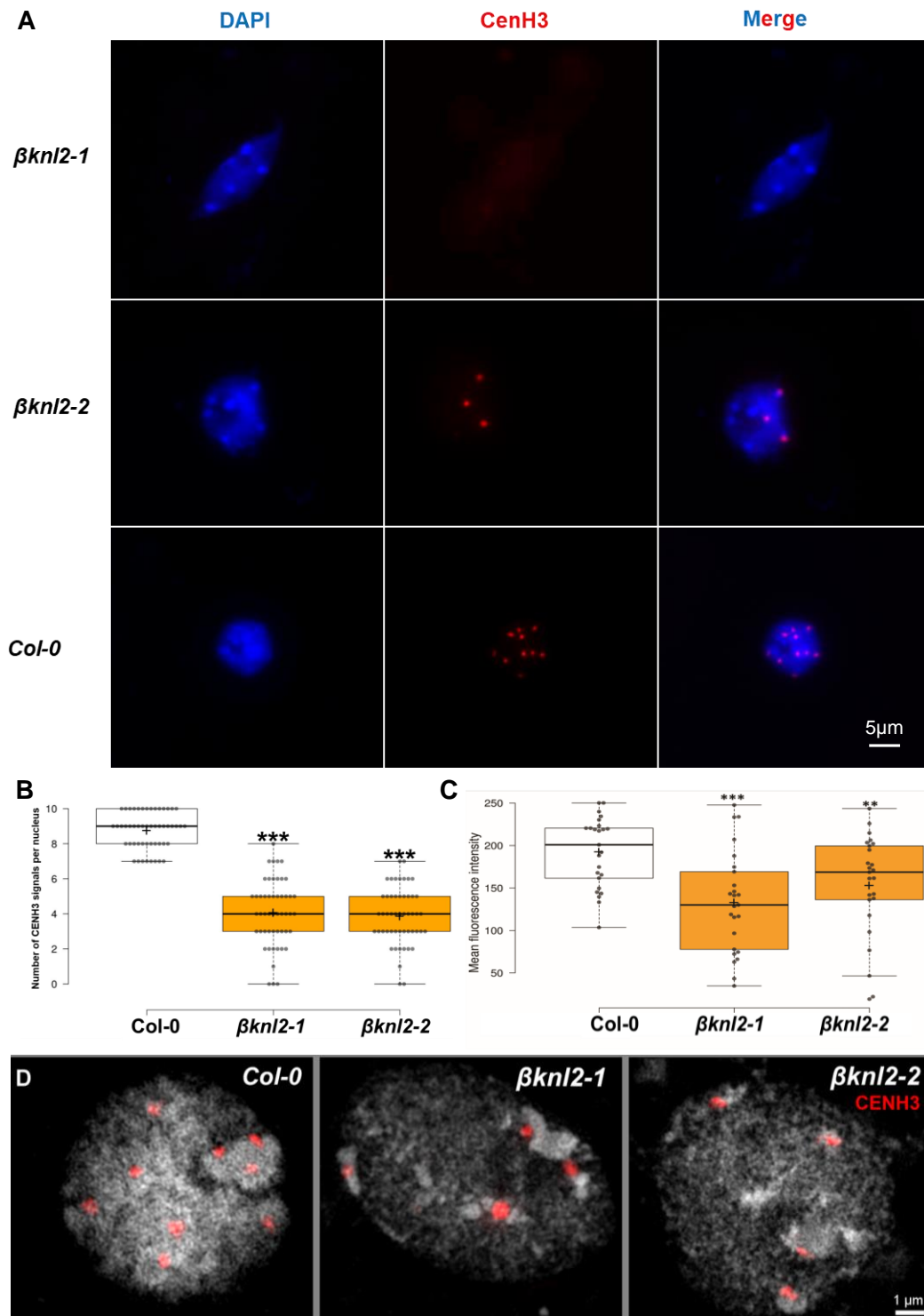


Figure 15. Loss of β KNL2 function disrupts CENH3 localization in *Arabidopsis*.

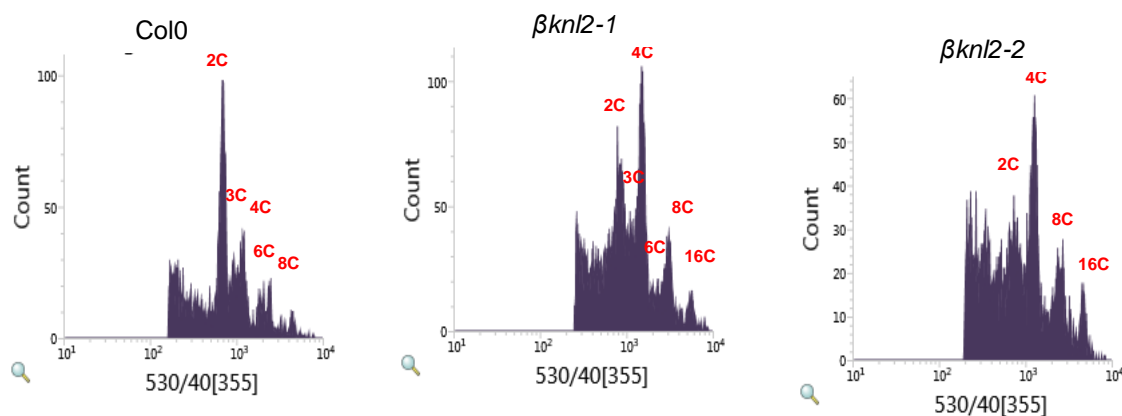
(A) Representative nuclei isolated from *Arabidopsis* WT and *βknl2* mutant seedlings immunostained with anti-CENH3 antibodies. The left panel shows nuclei stained with DAPI, the middle panel shows nuclei immunostained with anti-CENH3 antibodies, and the right panel presents the merged images. (B) Boxplot illustrating a significant decrease in the number of centromeric CENH3 signals in *βknl2-1* and *βknl2-2* mutants compared to the WT control. (C) Mean fluorescence intensity of CENH3 immunosignals in nuclei isolated from *A. thaliana* WT and *βknl2* mutants. The fluorescence intensity per nucleus was measured across 25 nuclei in each variant, demonstrating a marked reduction in CENH3 intensity in *βknl2* mutants. (D) Super-resolution microscopy images of nuclei from WT and *βknl2* null mutants, immunostained with anti-CENH3 antibodies in meristematic cells, revealing reduced CENH3 signals in the *βknl2* mutants. (* $P \leq 0.05$, ** $P \leq 0.01$ *** $P \leq 0.001$).

4.8 Loss of β KNL2 results in cells with high ploidy levels.

To explore the impact of β KNL2 on somatic cell division, flow cytometry (FC) analysis was performed to assess endopolyploidy levels in $\beta knl2$ mutants. This analysis focused on how genome duplication patterns are affected when CENH3 is absent from several chromocenters. First true leaves from $\beta knl2$ mutant seedlings, specifically those with abnormal phenotypes and white seeds were collected for analysis, as endopolyploidy is known to vary across leaf types.

In the heterozygous mutants, green seeds displayed histogram profiles similar to WT, with a pronounced 2C embryo peak (Fig. 16A). In contrast, white seeds from the same plants showed a shift towards increased endopolyploidy levels, with 4C nuclei being predominantly observed (Fig. 16A). Additionally, reduced sharpness peaks were observed, likely due to the presence of aneuploid nuclei. In some instances, it was challenging to distinguish nuclear peaks clearly in mutants.

A



B

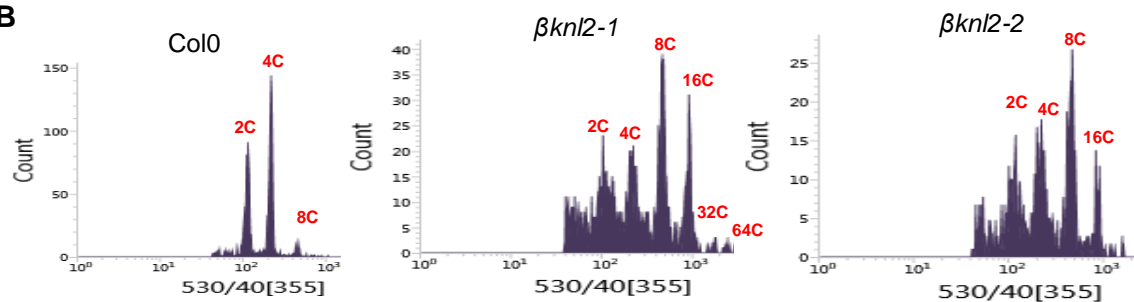


Figure 16. Ploidy analysis reveals elevated ploidy levels in $\beta knl2$ mutants.

(A) Representative flow cytometry histograms of seeds from WT and $\beta knl2$ heterozygous mutants ($\beta knl2-1$ and $\beta knl2-2$). In WT seeds, the histogram prominently displays a 2C peak. In contrast, the white abnormal seeds from the heterozygous $\beta knl2$ mutants show a shift towards increased ploidy levels, with pronounced 4C, 8C, and 16C peaks. These histograms also exhibit reduced peak sharpness, suggesting potential aneuploidy. (B) Flow cytometry histograms of 14-day-old seedling leaves from WT and homozygous $\beta knl2$ mutants ($\beta knl2-1$ and $\beta knl2-2$). While WT seedlings present distinct 2C and 4C peaks, the $\beta knl2$ mutants demonstrate a significant increase in higher ploidy levels, with peaks at 8C, 16C, and even 32C and 64C in the $\beta knl2-1$ mutant.

Ploidy levels were also analyzed in seedlings by chopping a single leaf from six 14-day-old WT and homozygous *βknl2* seedlings (Fig. 16B). Unlike WT leaves, which showed distinct peaks for 2C and 4C nuclei, leaves from *βknl2* mutants predominantly exhibited higher ploidy nuclei, such as 8C and 16C (Fig. 16B). This underscores the crucial role of β KNL2 in maintaining proper ploidy levels during somatic cell division.

4.9 SANTA domain and C-terminus of β KNL2 are required for its efficient centromeric targeting

In plants, contrasting to other organisms, two KNL2 protein variants (α and β KNL2) have been identified. Both KNL2 variants share a conserved SANTA domain. However, both SANTA domains exhibit variant-specific features such as unique conserved regions and different phosphorylation sites (Appendix Fig. 4), this may indicate that they can have some functional differences. Previous studies have demonstrated that the SANTA domain of α KNL2 is not required for its centromeric targeting (Lermontova et al., 2013, Sandmann et al., 2017). However, it remains elusive whether the SANTA domain of β KNL2 plays a role in this process.

To investigate further, various online prediction tools, including PredictProtein (<https://predictprotein.org/>), LambdaPP (<https://lambda.predictprotein.org/>), DNABIND (<https://dnabind.szilab.org/>), and ELM (<http://elm.eu.org/index.html>), were employed for *in silico* analysis of β KNL2. These tools predicted β KNL2 to interact with other proteins and nucleic acids through the SANTA domain and C-terminus (Fig. 17).

Thus, to determine the role of SANTA and other regions of β KNL2 in centromere targeting, three different truncation variants were generated: i) fragment lacking the N-terminal part (β KNL2 Δ N), ii) fragment lacking the SANTA domain (β KNL2 Δ SANTA) and iii) fragment lacking the C-terminal part (β KNL2 Δ C) (Fig. 18A). Each construct was fused to EYFP at the C-terminus and transiently expressed in *Nicotiana benthamiana* leaves (Fig. 18B). As described in chapter 4.2, both N- and C-terminal EYFP fusions showed comparable localization patterns, only the C-terminal fusions were used for subsequent experiments. Upon transient expression, both β KNL2 Δ N and β KNL2 Δ SANTA displayed a dot like localization pattern similar to that of full-length β KNL2. In contrast, β KNL2 Δ C exhibited mis-localization, with signals detected in both the nucleoplasm and cytoplasm.

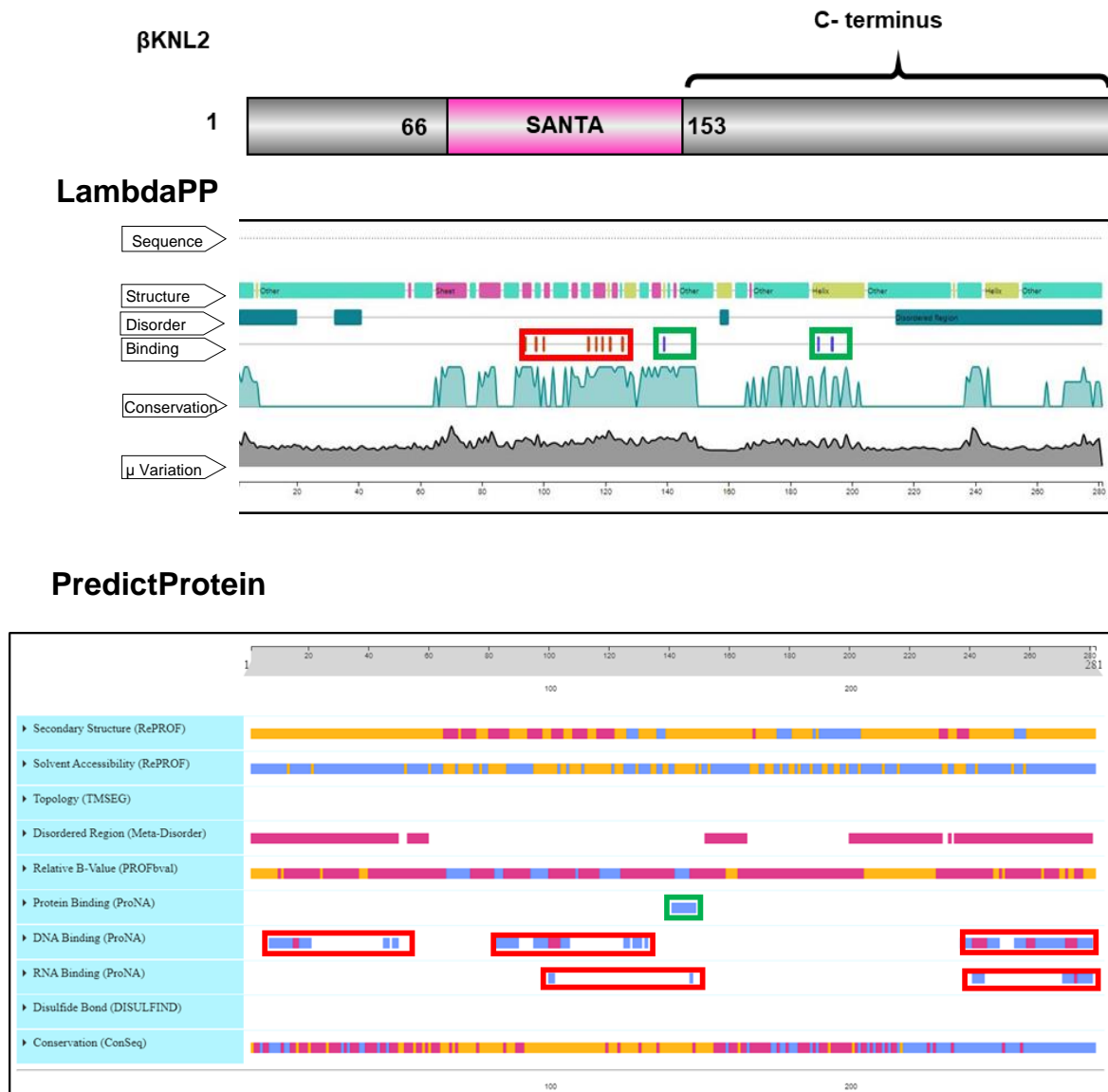


Figure 17. *In silico* prediction of protein-DNA and protein-protein interaction sites of βKNL2.

In silico analysis of the βKNL2 protein, highlighting potential interaction sites for proteins (indicated in green rectangle boxes) and nucleic acids (indicated in red rectangle boxes). Computational predictions using LambdaPP and PredictProtein tools suggest that the SANTA domain and C-terminus of βKNL2 have the potential to interact with other proteins and nucleic acids, respectively. Each color-coded box corresponds to regions within the βKNL2 structure predicted to facilitate these molecular interactions.

To confirm these results, stable *Arabidopsis* transformants were generated expressing all constructs separately (Fig. 18C). The localization pattern was analyzed in the root tips of 7–10 days old seedlings from the T₂ generation. βKNL2ΔN fragment fused with the EYFP showed a typical centromeric dot-like pattern with 7–10 signals (Fig. 18C) similar to control lines with full-length βKNL2. After careful examination of several T₁ and T₂ independent transformants, the βKNL2ΔSANTA transformants showed reduced efficiency of centromeric localization (dispersed or reduced number of signals) compared to the full length (Fig. 18C). Whereas, βKNL2ΔC transformants had strongly reduced centromeric localization and mis-localization to

cytoplasm similar to the transient expression (Fig. 18C). Thus, we confirmed that the efficient centromeric localization of β KNL2 requires the SANTA domain and C-terminus.

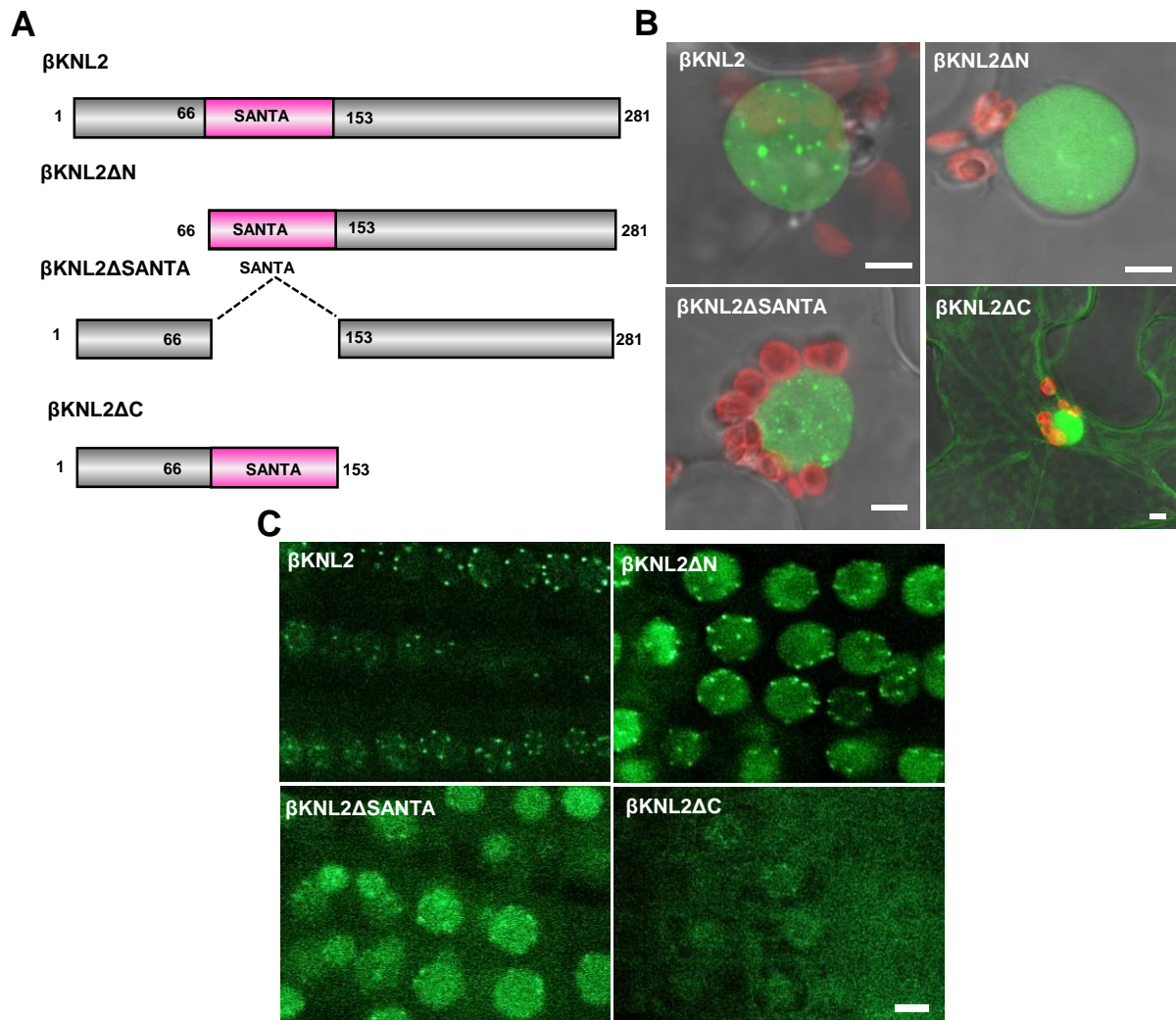


Figure 18. SANTA domain and C-terminus of β KNL2 regulate its centromeric targeting.

(A) Schemata of β KNL2 and β KNL2 truncated variants created by site-directed mutagenesis: β KNL2 Δ N lacks the N-terminus; β KNL2 Δ SANTA lacks the SANTA domain; β KNL2 Δ C lacks the C-terminus. (B) Localization patterns of EYFP-tagged β KNL2 truncated variants (referred in 18A) when transiently expressed in *Nicotiana benthamiana*. (C) Localization patterns of EYFP-tagged β KNL2 truncated variants (referred in 18A) in root tip nuclei of 7-day-old *A. thaliana* seedlings. The deletion of the SANTA domain and C-terminus affect the centromeric localization, underscoring their critical roles in targeting β KNL2 to the centromere. Scale bar: 5 μ m

4.10 C- terminal motif-III of β KNL2 is required for its nuclear localization

Various domains have been identified in KNL2 across different species for its localization and functioning. In *Xenopus*: the SANTA domain, along with the CENP-A nucleosome binding domain; in chicken and *Arabidopsis*, another conserved motif, CENPC-like motif, has been reported for centromeric targeting. However, in humans and some mammals, no such motif has been identified to date and the newly identified β KNL2 also lack CENPC-like motif.

To investigate whether there is another unknown motif or domain responsible for β KNL2 targeting, a search was conducted for the presence of other conserved motifs using ~100 monocot and dicot KNL2 variants without CENPC-like motif (Fig. 19A).

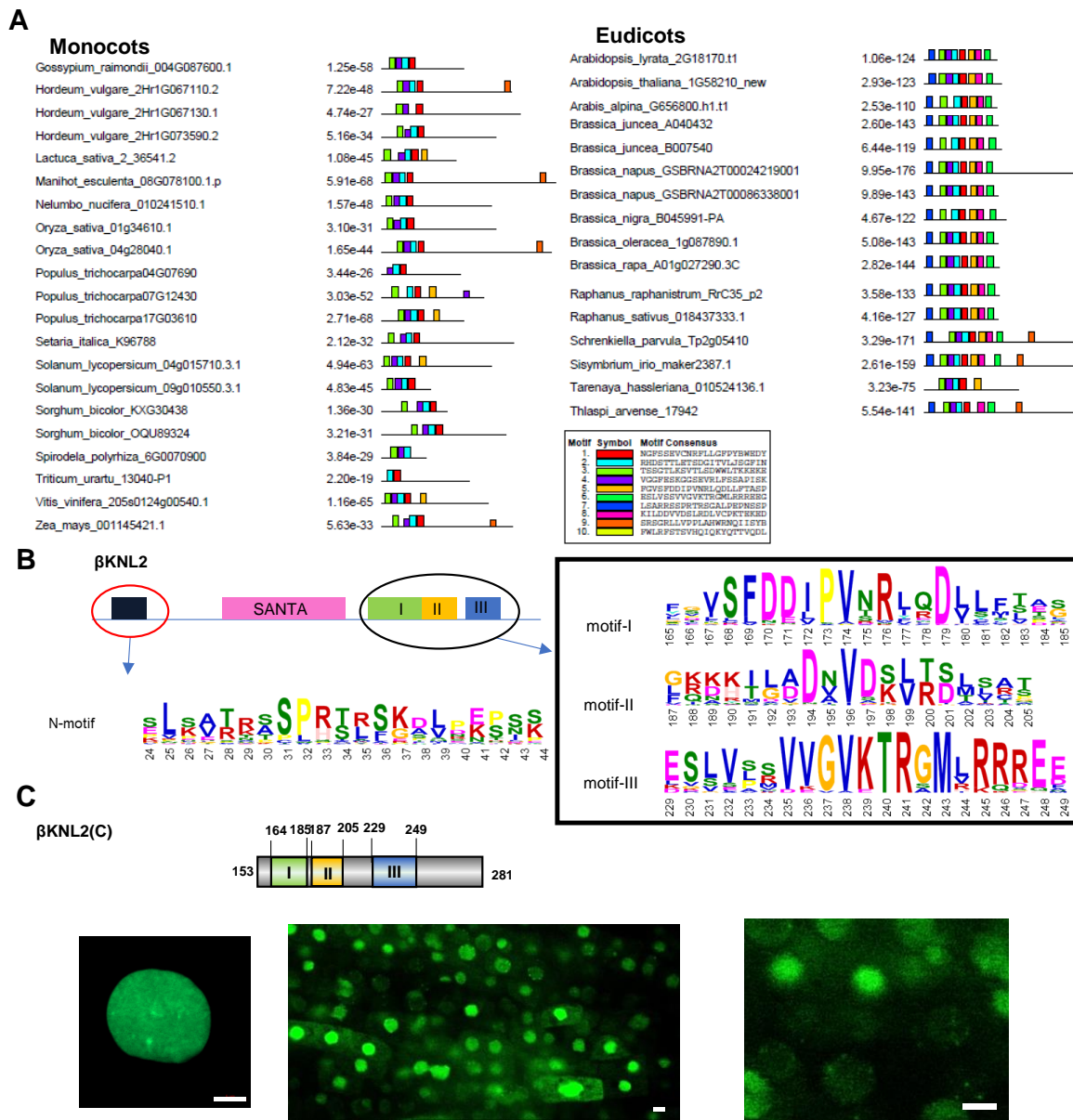


Figure 19. Conserved motifs identified in β KNL2 homologs across monocot and eudicot species. (A) Analysis of conserved motif evolution in KNL2 homologs without CENPC-k motif across various species from monocots to eudicots. Unaligned AA sequences from KNL2 homologs were analyzed using the MEME suite v5.1.0 to identify additional conserved motifs. The conserved motifs identified across different species are represented as colored bars along the length of the protein sequence; only representative species structures are shown. (B) Schematic representation of the β KNL2 protein structure, highlighting the newly identified conserved motifs located at the N- and C-termini. These conserved regions are detailed with WebLogo alignments, illustrating conserved AA sequences across dicots. (C) Truncated construct of β KNL2 used to explore the functional roles of the C-terminal. The β KNL2(C) variant retains only the C-terminal region. Left Panel shows, Localization pattern of β KNL2(C) variant transiently expressed in tobacco leaves. Center, representative images of root tip from 7-day-old *Arabidopsis* seedling showing stable expression of β KNL2(C) within the root tip nuclei. Right, Zoomed-in views of root tip, emphasizing the subcellular localization pattern. Scale bars: 5 μ m.

Our analysis revealed that, β KNL2 consistently exhibits four variant-specific conserved motifs distinct from the SANTA domain (Fig. 19B). Each motif spans approximately 20 AA, and these motifs were further refined by considering their conservation, position and structural relevance. The first motif (AA 24-44) is located at the N-terminal part of β KNL2 upstream of the SANTA domain. The other three motifs, defined as motif-I (AA 164-185), motif-II (AA 186-205), and motif-III (AA 229-249), are located in C-terminus, directly downstream of the SANTA domain (Fig. 19B).

To explore whether the C-terminus containing highly conserved motifs, alone capable to localize to the centromere, we generated a truncated construct containing solely the C-terminal part (β KNL2(C)) (Fig. 19C). EYFP fused β KNL2(C) showed a low centromere targeting efficiency in root tips of stably transformed *Arabidopsis* (Fig. 19C). This confirms our assumption that efficient centromeric targeting of β KNL2 requires the C-terminal part and SANTA domain.

All three C-terminus motifs were deleted in different constructs to determine whether any of these predicted motifs have an effect on the localization of β KNL2 (Fig. 20A). Resulted constructs were fused to EYFP and transiently expressed in tobacco (Fig. 20B, left panels) and later stably expressed in *Arabidopsis*. The localization pattern was confirmed in root tips of 7-10-days-old T₂ seedlings (Fig. 20B, right panels). The lines expressing β KNL2 Δ motif-I and β KNL2 Δ motif-II constructs have centromeric signal pattern and nucleoplasm fluorescence (Fig. 20B). Whereas, β KNL2 Δ motif-III expressing lines exhibited mis-localization of fluorescence to the cytoplasm similar to tobacco transient expression. These data led us to conclude that the C-terminal motif-III plays a crucial role in nuclear localization, thus centromeric targeting of β KNL2.

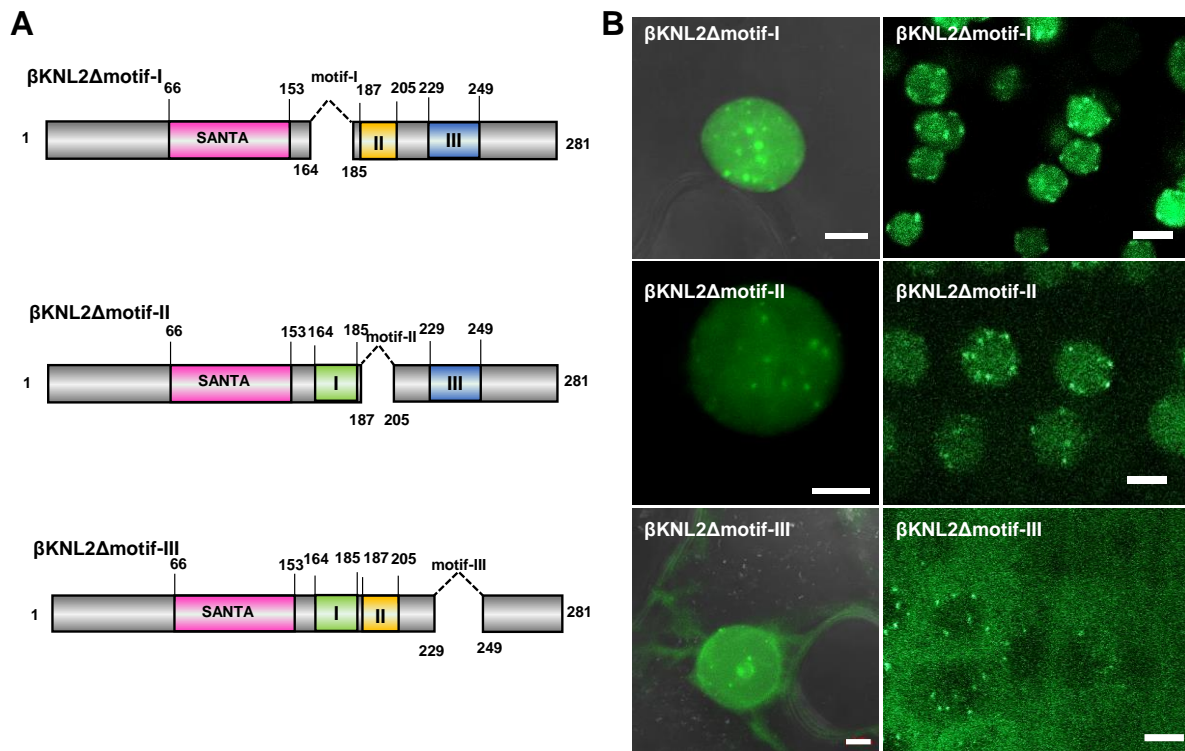


Figure 20. βKNL2 nuclear localization is regulated by conserved C-terminal motif-III.

(A) Truncated constructs of βKNL2 to elucidate the functional role of the C-terminus motifs. The βKNL2Δmotif-I, βKNL2Δmotif-II and βKNL2Δmotif-III variants omit one of the three corresponding motifs. (B) Localization patterns of EYFP-Tagged βKNL2 truncated protein variants (referred in 20A) in *Nicotiana benthamiana* (left panels) and *Arabidopsis* root tip nuclei (right panel). Left Panel: Localization patterns of the respective truncated βKNL2 variants transiently expressed in *Nicotiana benthamiana* leaves, showing initial expression and targeting. Right Panel: Zoomed-in view of the nuclei in *Arabidopsis* root tip cells to highlight the precise subcellular localization of each variant. βKNL2Δmotif-I and βKNL2Δmotif-II fragments displayed normal nuclear and centromeric signals, whereas βKNL2Δmotif-III exhibited mislocalization to the cytoplasm, indicating the critical role of motif-III in nuclear targeting. Scale bars: 5 μm.

BLASTP analysis using "motif-III" as the query revealed numerous hits across eukaryotes and prokaryotes, particularly associated with transcription factors and nucleic acid binding proteins. This motivated us to analyze motif-III in more depth to gain further insights into its function. Using online prediction tools (ELM, GPS-biocuckoo), we identified a putative SUMOylation site within motif-III (AA 229 to 231) (Fig. 21A). Subsequently, we designed a new truncated construct containing the predicted SUMOylation region while excluding other conserved regions of motif-III (Fig. 21B). This construct, termed βKNL2Δmotif-III new, was fused to EYFP and introduced into *Arabidopsis*. Interestingly, we observed a partially restored nucleoplasm localization compared to βKNL2Δmotif-III (Fig. 21B). These findings led us to hypothesize that βKNL2 may undergo SUMOylation, with deleted region of motif III playing a crucial role in its proper localization and influencing centromere targeting. The SUMOylation region may thus be essential for the proper centromeric localization of βKNL2.

A

ELM prediction of SUMO sites					
FPLAVIT	52-58 [A]	-	Motif for the parallel beta augmentation mode of non-covalent binding to SUMO protein.		
RVVTVS	265-270 [A]	-			
DDDDDDDKSL	221-231 [A]	-	Inverted version of SUMOylation motif recognized for modification by SUMO-1		
DDDDDDDKSL	222-231 [A]	-			
DDDDDDDKSL	223-231 [A]	-			
DDDDDKSL	224-231 [A]	-			
DDDDKSL	225-231 [A]	-			
DDDKSL	226-231 [A]	-			
GPS-SUMO 2.0 prediction of SUMO sites					
266-270	ATMSGKR RVTVS KKKNRRR	0.8959	0.5	SUMO interaction	Pred.

B

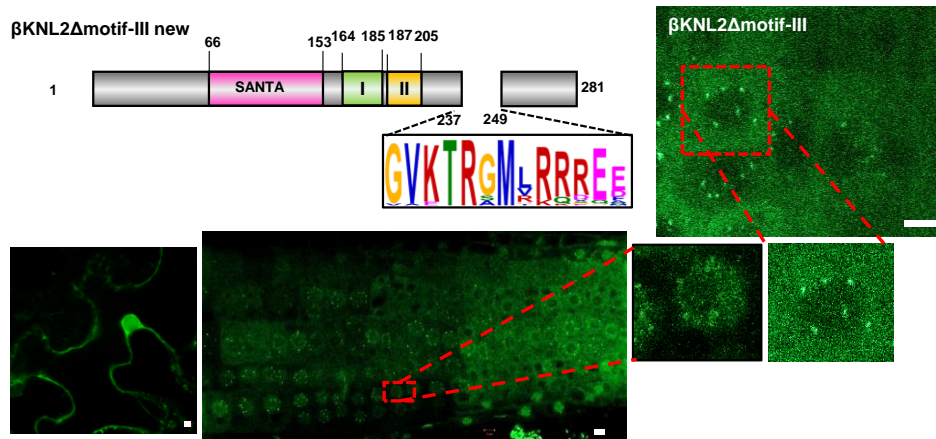


Figure 21. Predicted SUMOylation sites overlap with motif-III of β KNL2.

(A) ELM and GPS-SUMO 2.0 bioinformatics tools predict putative SUMOylation sites in a region of β KNL2 spanning residues 221-231. This region overlaps with motif-III, which extends from residues 229 to 249. In addition, both ELM and GPS-SUMO 2.0 identified a SUMO interaction motif spanning residues 266 to 270. (B) β KNL2 Δ motif-III new, truncated variant excluding highly conserved AA of motif-III, but including the predicted SUMOylation site accompanied by WebLogo alignment. In contrast to the β KNL2 Δ motif-III fragment, this variant showed partially recovered nuclear localization as demonstrated in right panel. Scale bar 5 μ m

4.11 β KNL2 demonstrates *in vitro* binding to centromeric DNA

Different inner kinetochore proteins associate with centromeric nucleosomes via their direct interaction with CENH3, other histones or an interaction with the centromeric DNA (Yamagishi et al., 2014, Cheeseman, 2014, Musacchio and Desai, 2017, Jiang et al., 2022). For example, α KNL2 associates with the centromeric repeat *pAL1* *in-vivo* and has the ability to bind DNA in a sequence-independent manner *in-vitro* (Sandmann et al., 2017, Yalagapati et al., 2024). As it is mentioned above, β KNL2 predicted to be capable to bind or interact with nucleic acids and the DNA/RNA binding regions predicted by different tools are graphically shown in Figure. 22A. To validate the DNA binding ability of β KNL2, we performed Electrophoretic Mobility Shift Assay (EMSA). To perform EMSA, FLAG- β KNL2 was *in-vitro* expressed and confirmed using anti-FLAG tag antibodies on Western blot (Fig. 22B). IRD700-*pAL1* amplified from *Arabidopsis* genomic-DNA, so it contained monomeric and multimeric repeats of *pAL1* (Fig. 22B). *In-vitro* expressed FLAG- α KNL2(C) was used as a positive control and EMSA

experiment was performed using protocol described by Eysholdt-Derzsó et al. (2023) with small adaptations. We observed clear upward shift in the lane of IRD700 labelled *pAL1* incubated with FLAG- β KNL2, similar to positive control (Fig. 22C). However, when unlabeled *pAL1* used as a competitor along with labelled probes, a reduced shift was observed, indicating successful competition.

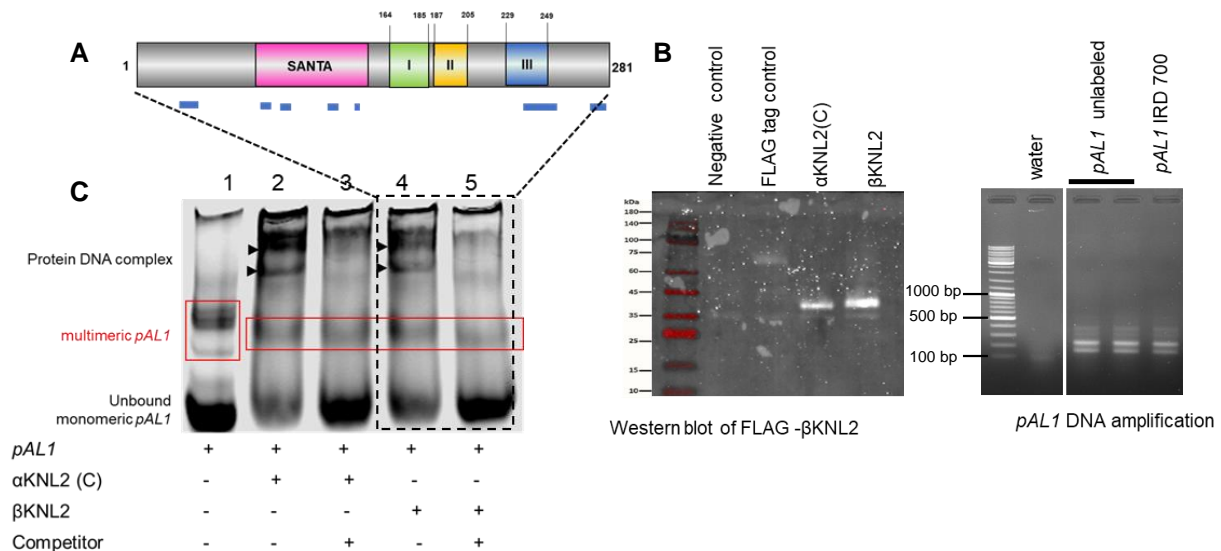


Figure 22. β KNL2 binds to centromeric DNA repeat *pAL1*.

(A) Schematic representation of the β KNL2 protein with predicted DNA-binding regions marked by blue bars below. **(B)** Left: Western blot analysis confirming the expression of FLAG-tagged α KNL2(C) (26.36 kDa) and β KNL2 (31.56 kDa) proteins in TNT SP6 High Yield Wheat Germ system (Promega) using anti-FLAG antibodies. Right: The PCR amplification of the *pAL1* centromeric repeat from *Arabidopsis* genomic DNA. **(C)** EMSA on native gel showing FLAG- β KNL2 binding to centromeric *pAL1* DNA. IRD700-labeled *pAL1* monomer and multimeric repeats probes were amplified from *Arabidopsis* genomic DNA (lane 1). IRD700-*pAL1* probes shifted upwards indicating binding by in vitro expressed FLAG- α KNL2(C) as a positive control (lane 2) and FLAG- β KNL2 (lane 4). Competition with an excess of unlabeled *pAL1* DNA reduced the shifts confirming specific binding of FLAG- α KNL2 (lane 3) and FLAG- β KNL2 (lane 5) to *pAL1* DNA.

4.12 Centromeric recruitment of β KNL2 depends on CENPC-k motif containing α KNL2

Previous studies have shown that the M18BP1/KNL2 requires the CENPC-like motif for centromeric localization and association with nucleosomes (Sandmann et al., 2017, Hori et al., 2017, Smith and Maddox, 2017, Jiang et al., 2022). Interestingly, β KNL2 exhibits centromeric localization even without this motif, suggesting a distinctive mechanism for centromere targeting. We hypothesize that β KNL2 might rely on CENPC-like motif containing proteins (α KNL2 or CENP-C) for its centromere targeting.

To test this hypothesis, we introduced a β KNL2:: β KNL2-EYFP genomic construct into both *aknl2* and *βknl2* mutants. Assuming that α KNL2 is required for centromeric localization of

β KNL2, we would expect a significant reduction or complete absence of β KNL2-EYFP at the centromere in the *aknl2* mutant compared to *β knl2*.

As we previously demonstrated that *KNL2* genes transcription is high in meristematic tissues like floral organs (section 4.2). Thus, firstly we examined the floral tissues of both *aknl2* and *β knl2* transformants. In the *β knl2* mutant background, we observed that the β KNL2-EYFP protein localizes to the centromeres and nucleoplasm of generative and vegetative nuclei in developing pollen (bi-nucleate), and to the sperm nuclei in mature pollen (tri-nucleate) (Fig. 23A). However, in mature pollen, the vegetative nuclei displayed fluorescent signals exclusively in the nucleoplasm. In contrast, in the *aknl2* mutant background, there were no clear centromeric signals in the nuclei of bi- and tri-nucleate pollen (Fig. 23B). Instead, the β KNL2-EYFP fluorescence was distributed throughout the nucleoplasm and nucleoli in bi-nucleate pollen, and solely in the nucleoplasm of sperm nuclei. This disturbed localization of β KNL2 in *aknl2* null mutant transformants supports our hypothesis that the centromeric localization of β KNL2 may depend on α KNL2.

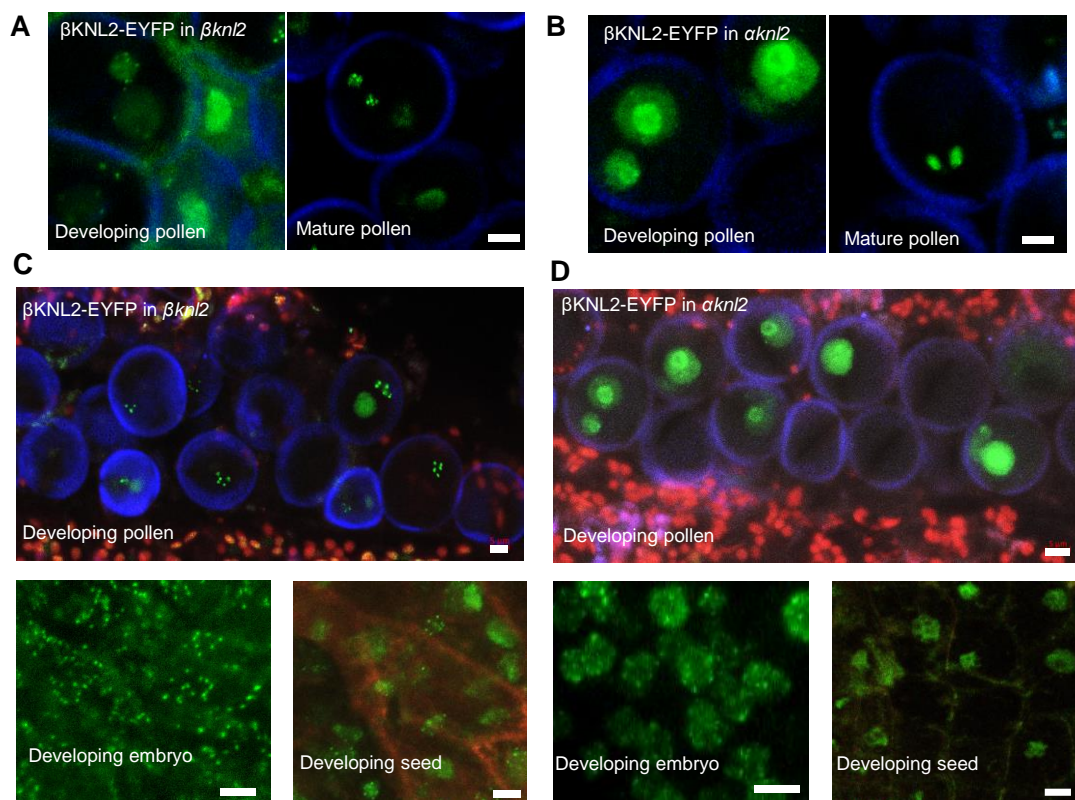


Figure 23. Centromeric recruitment of β KNL2 depends on α KNL2 in pollen nuclei.

(A-B) Disturbed centromeric localization of β KNL2-EYFP in *aknl2* compared to *β knl2* mutant pollen nuclei, indicating centromeric recruitment of β KNL2 is dependent on α KNL2 (C) *Arabidopsis* *β knl2* transformants expressing β KNL2:: β KNL2-EYFP serving as controls showed β KNL2-EYFP signals localized in both the centromeres and nucleoplasm within the nuclei of developing pollen, embryos, and seeds. (D) In *aknl2* mutant transformants, β KNL2-EYFP was primarily observed in the nucleoplasm of developing pollen and seeds. Notably, in developing embryos, β KNL2-EYFP targeted to the centromeres, similar to *β knl2* mutant transformants. Scale bar: 5 μ m.

Next, we examined meristematic tissues, including developing seeds with embryos, in both *aknl2* and *βknl2* transformants. However, embryos of both *aknl2* and *βknl2* transformants showed similar centromeric localization patterns (Fig. 23C-D). Notably, other tissues in the developing seeds displayed disrupted centromeric localization similar to that observed in pollen nuclei.

Based on these results, we infer that the centromeric localization of β KNL2 is not solely dependent on α KNL2. The CENP-C protein, which possesses a CENPC motif, may also be involved in this process. Thus, we conclude that centromeric localization of β KNL2 depends on α KNL2 in a tissue-specific manner.

4.13 β KNL2 form homodimer and heterodimer with α KNL2

Across various organisms, kinetochore components tend to form homodimers and oligomers, which play crucial roles in centromeric targeting, centromere assembly, and kinetochore function. In vertebrates, the Mis18 complex is formed by a M18BP1/KNL2 homodimer and a hetero-oligomer of Mis18 α and Mis18 β (Stellfox et al., 2016, Subramanian et al., 2016, Pan et al., 2017). In contrast to vertebrates, plants lack the Mis18 α and Mis18 β components of the Mis18 complex. Notably, they possess two variants of M18BP1/KNL2. Thus, we addressed the question of whether β KNL2 can form homodimers and potential heteromers similar to Mis18 components. Using AlphaFold2, we predicted the possible formation of β KNL2 monomeric state, homodimers as well as heterodimers and oligomers of β KNL2 with α KNL2 in various combinations.

AlphaFold2 predicted the monomeric state of β KNL2, revealing structured regions in the SANTA domain and in the C-terminus, while the rest of the protein was predicted to be disordered (Fig. 24). Several prolines present at the N-terminal part of β KNL2 support its intrinsic disorder as they prevent the formation of helices and sheets (Fig. 24). The SANTA domain is formed by a β -roll connected to a region of small α -helices and short loops, while the C-terminus contained three motifs predicted to form three stretches of α -helices (Fig. 24). The structural prediction of β KNL2 leaves some positively charged and other hydrophobic surfaces exposed (Fig. 24), which convey its involvement in DNA binding and protein-protein interactions, respectively. These predictions and experimental validations for DNA binding align with its presumed functions in centromere targeting and kinetochore assembly.

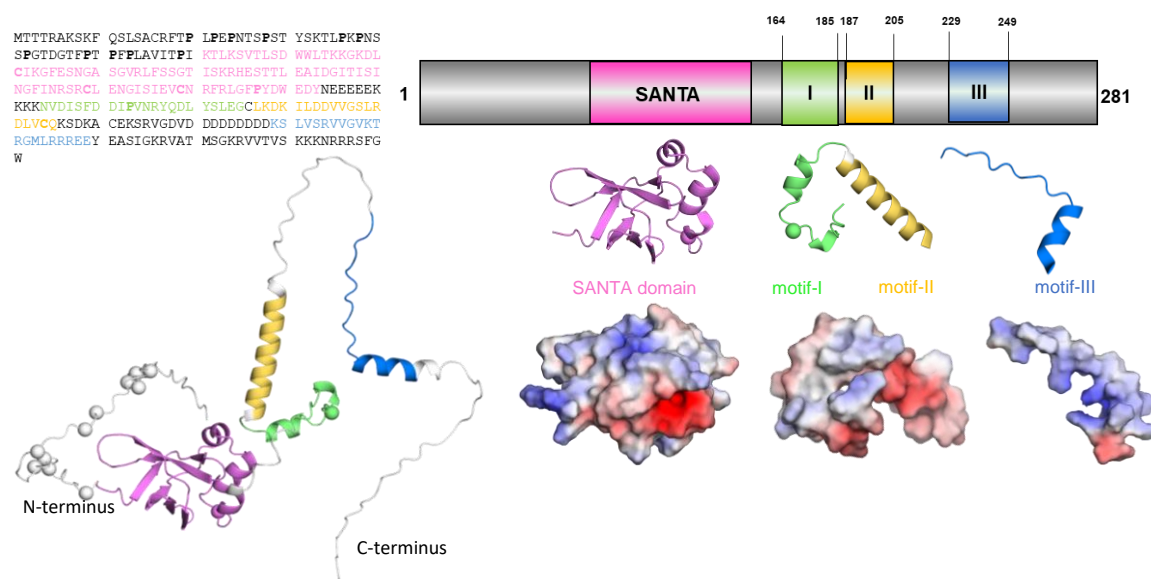


Figure 24. Structural prediction of β KNL2 monomeric state

Structural prediction of β KNL2 by AlphaFold2: The β KNL2 protein is illustrated with its key structural domains highlighted: the SANTA domain (pink), motif I (green), motif II (yellow), and motif III (blue). The surface charge distribution of β KNL2 is depicted, with the SANTA domain and motif III exhibiting predominantly positive charges, suggesting potential roles in electrostatic interactions, possibly with DNA or RNA. The structural elements are visualized in both cartoon and surface modes, emphasizing the spatial organization and electrostatic properties critical for protein interactions.

AlphaFold2 predicted β KNL2 homodimer to be a symmetrical complex, conveying stability of interaction interfaces (Fig. 25A). The homodimerization is mediated through the SANTA domain and C-terminus conserved motifs. The heterodimer of α KNL2 and β KNL2 consistently appears interacting through the same interface in different predictions, with their SANTA domains one in front of the other similarly to the β KNL2 homodimer (Fig. 25B). We also tested other possible combinations of β KNL2: α KNL2 heterotrimers (Fig. 25C-D). Notably, the N-terminal tails of both α KNL2 and β KNL2 are predicted to form an intermonomeric β -sheet (Fig. 25B) through the SANTA domains and their pre-SANTA conserved AA (S₁₄F₁₅Q₁₆ in α KNL2 & T₅₈P₅₉V/I₆₀K₆₁ in β KNL2 Appendix Fig. 5). The conserved TPV/IK motif predicted to be a phospho-dependent CDK motif and the same was experimentally proven in other vertebrates (Pan et al., 2017, French and Straight, 2019, Watanabe et al., 2019). We are convinced that α KNL2 and β KNL2 can thus bind to each other.

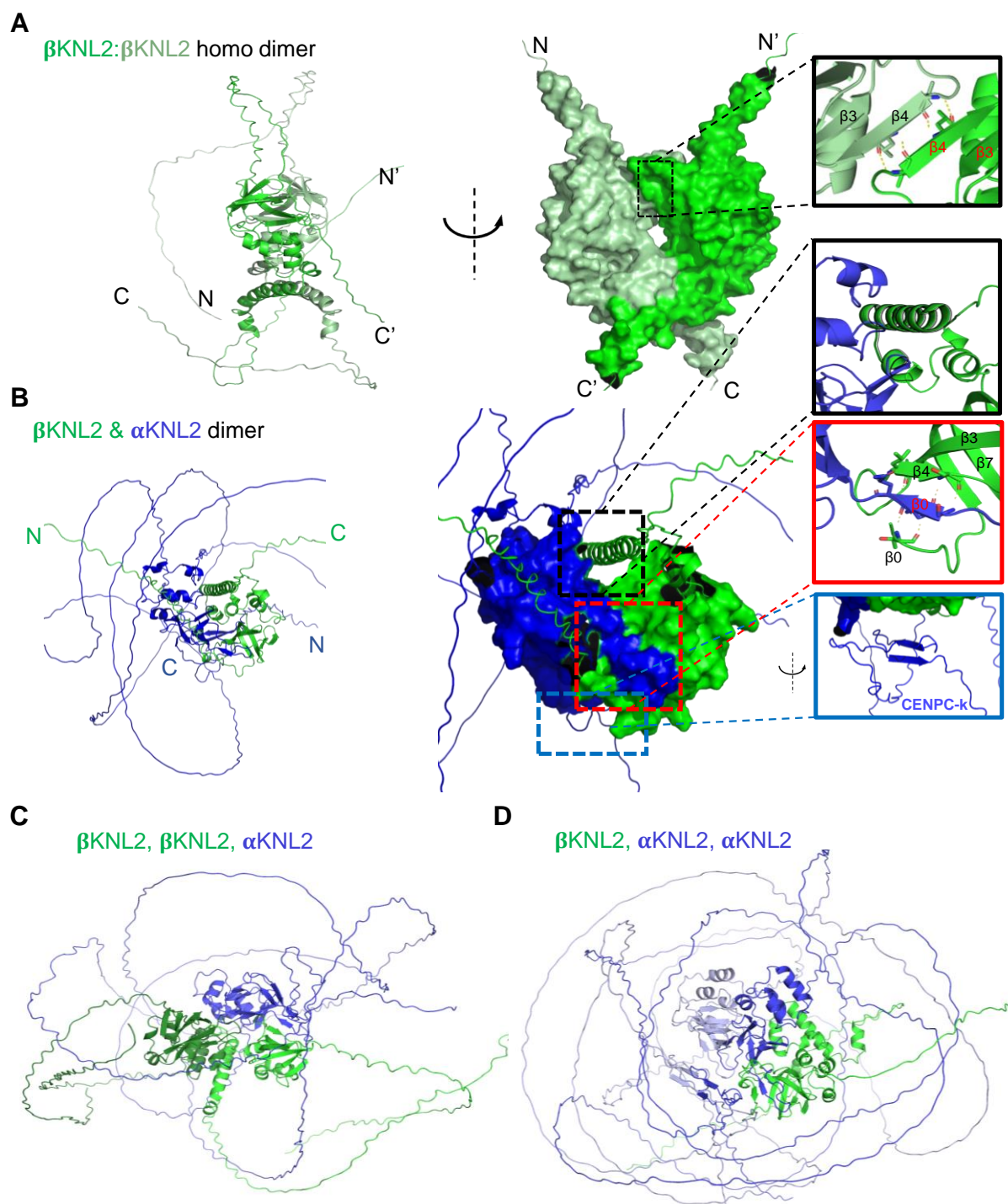


Figure 25. β KNL2 forms homo- and heterodimers.

AlphaFold2-predicted structures of β KNL2 homo- and heterodimers: **(A)** β KNL2 homodimer: The left panel shows the homodimer in secondary structure (cartoon mode), while the right panel presents the surface representation, with each monomer colored differently. A zoomed-in view highlights the interaction between the $\beta 4$ strands of the SANTA domain, along with additional predicted contacts in the C-terminal motifs. **(B)** β KNL2 & α KNL2 heterodimer: Similar to the homodimer, this panel shows the dimeric interaction between β KNL2 and α KNL2, with structural and surface representations. The inset provides a detailed view of the interaction interface predicted by AlphaFold2. **(C)** β KNL2: α KNL2 heterotrimer (2 β KNL2:1 α KNL2): AlphaFold2-predicted structure depicting a heterotrimeric complex consisting of two β KNL2 molecules and one α KNL2 molecule. **(D)** β KNL2: α KNL2 heterotrimer (1 β KNL2:2 α KNL2): This panel shows the heterotrimeric configuration with one β KNL2 molecule and two α KNL2 molecules.

Using these structures, we performed DSSP analysis and observed structural changes in all three C-terminal motifs of β KNL2 when it was in dimeric or trimeric form (Fig. 26A). This suggests that these motifs are not only essential for centromeric targeting but also flexibly adapt based on the interaction partner.

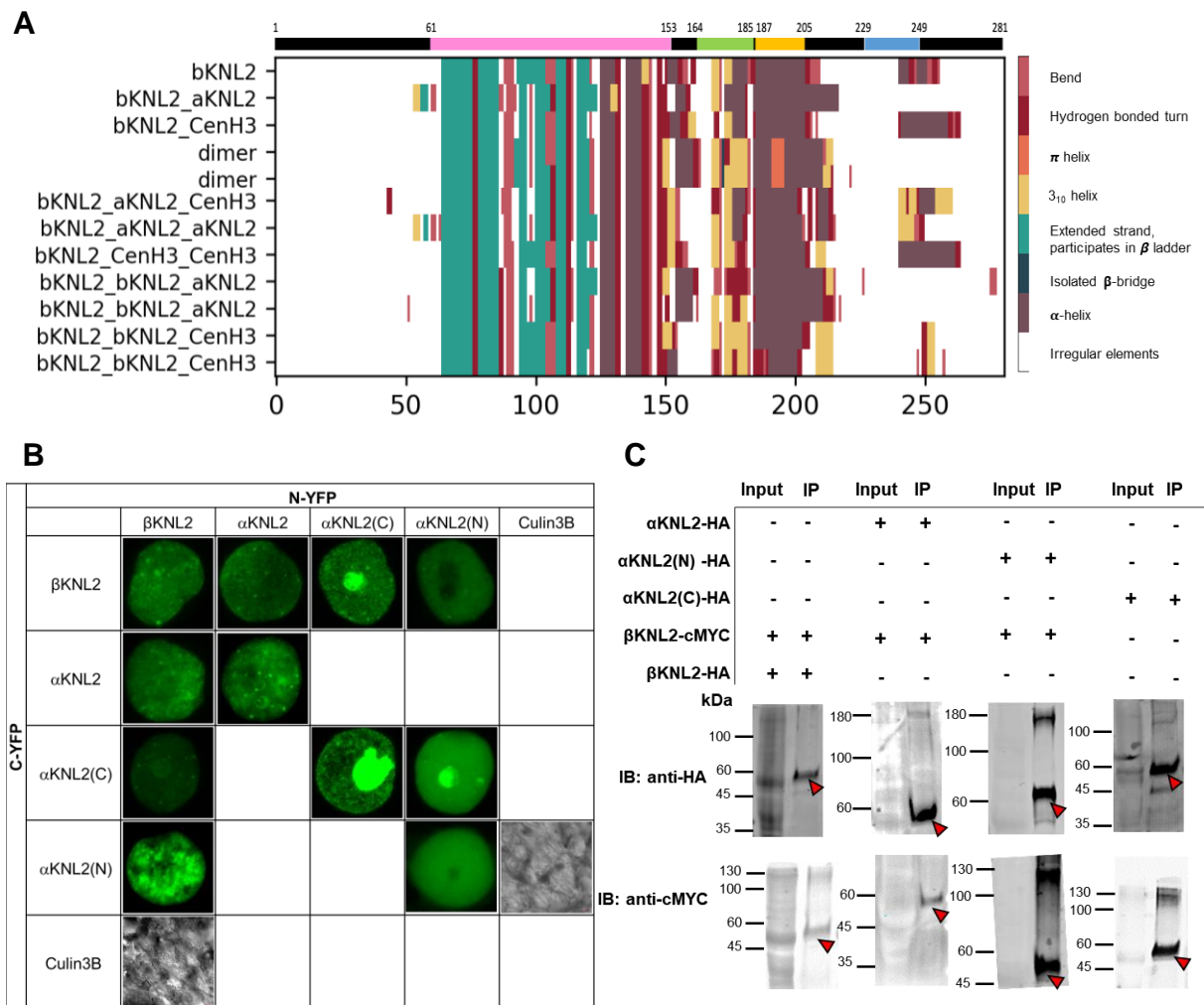


Figure 26. DSSP analysis and β KNL2 interactions with kinetochore protein α KNL2.

(A) DSSP analysis illustrating the structural adaptability of β KNL2's C-terminal motifs when interacting with itself and kinetochore proteins α KNL2 and CENH3. The analysis is based on models generated by AlphaFold2. the structural changes can be observed when β KNL2 forms heterodimers and oligomers with α KNL2. When β KNL2 combines with CENH3, the most significant modifications occur in motif-III. (B) BiFC assays in *Nicotiana benthamiana* confirm the formation of homo- and heterodimers involving β KNL2. β KNL2 interacts with itself and α KNL2, α KNL2(N) and α KNL2(C). (C) Western blots with anti-HA and anti-cMYC tag antibodies display monomeric size bands (red arrow heads) from co-IP performed in *Nicotiana benthamiana* with anti-HA trap.

To validate homo- and heterodimer formation, BiFC assays were conducted in *Nicotiana benthamiana*. β KNL2 and α KNL2 were fused to the N-terminal (VN) and C-terminal (VC) fragments of the Venus fluorescent protein in both orientations. To overcome the challenge of

overexpressing α KNL2 due to its proteasomal regulation (Lermontova et al., 2013), we employed the proteasomal inhibitor bortezomib.

Fluorescence signals were observed when β KNL2-VN/ β KNL2-VC and α KNL2-VN/ α KNL2-VC were co-infiltrated, confirming the ability of β KNL2 to form homodimers and heterodimers with α KNL2 (Fig. 26B). Additionally, BiFC assays were performed using truncated α KNL2 constructs: α KNL2(N) (residues 1–362, containing the SANTA domain) and α KNL2(C) (residues 363–598, containing the CENPC-k motif). Interestingly, both α KNL2(N) and α KNL2(C) interacted with β KNL2 in both VN and VC fusion orientations, as evidenced by fluorescence signals (Fig. 26B). As noted earlier, the use of the proteasomal inhibitor bortezomib was necessary to visualize fluorescence for constructs containing α KNL2 and α KNL2(N), suggesting that their regulation is tightly linked to proteasomal degradation.

Further to validate these results, we performed Co-IP with anti-HA trap trap by transiently expressing β KNL2-MYC-VN, β KNL2-HA-VC and α KNL2(C)-HA-VC in combinations in *Nicotiana benthamiana*. Monomer-sized bands were detected (between 45kDa–60kDa) higher than the predicted 43.42kDa for β KNL2-HA-VC (Fig. 26C, left) and 38.21 kDa for α KNL2(C)-HA-VC (Fig. 26C, right) from precipitated elutes. This could be due to post-translational modifications. A similar migration pattern was observed for β KNL2 and α KNL2(C) when expressed *in-vitro* using a wheat germ expression system (Fig. 22B). These results substantiate the structural predictions and support the formation of β KNL2 homo and heterodimers.

4.14 β KNL2 is highly dynamic and loosely bound to centromeric nucleosome through its SANTA domain and C-terminal conserved motifs

We performed FLIP (Fluorescence Loss in Photobleaching) and FRAP (Fluorescence Recovery After Photobleaching) experiments to track the dynamics of β KNL2-EYFP within *Arabidopsis* elongated nuclei. These nuclei were selected from non-meristematic regions because they are structurally stable and less active, which reduces variability and improves the clarity of our observations. Their stability also prevents them from moving out of focus during the experiment. FLIP showed that β KNL2-EYFP has high mobility, as indicated by rapid fluorescence reduction followed by swift movement (Fig. 27A). This observation was supported by FRAP, which revealed that rapid recovery of fluorescence with a short half-time ($t_{1/2}$) of approximately 0.7 seconds (Fig. 27B). These findings provide valuable insights into the dynamic behavior of β KNL2, emphasizing its continuous mobility within the nucleus and its potential significance for centromere function. Similar turnover rates and mobility were also

observed for EYFP- α KNL2 as well (Lermontova et al., 2013), indicating that both KNL2 proteins bind flexibly to nucleosomes.

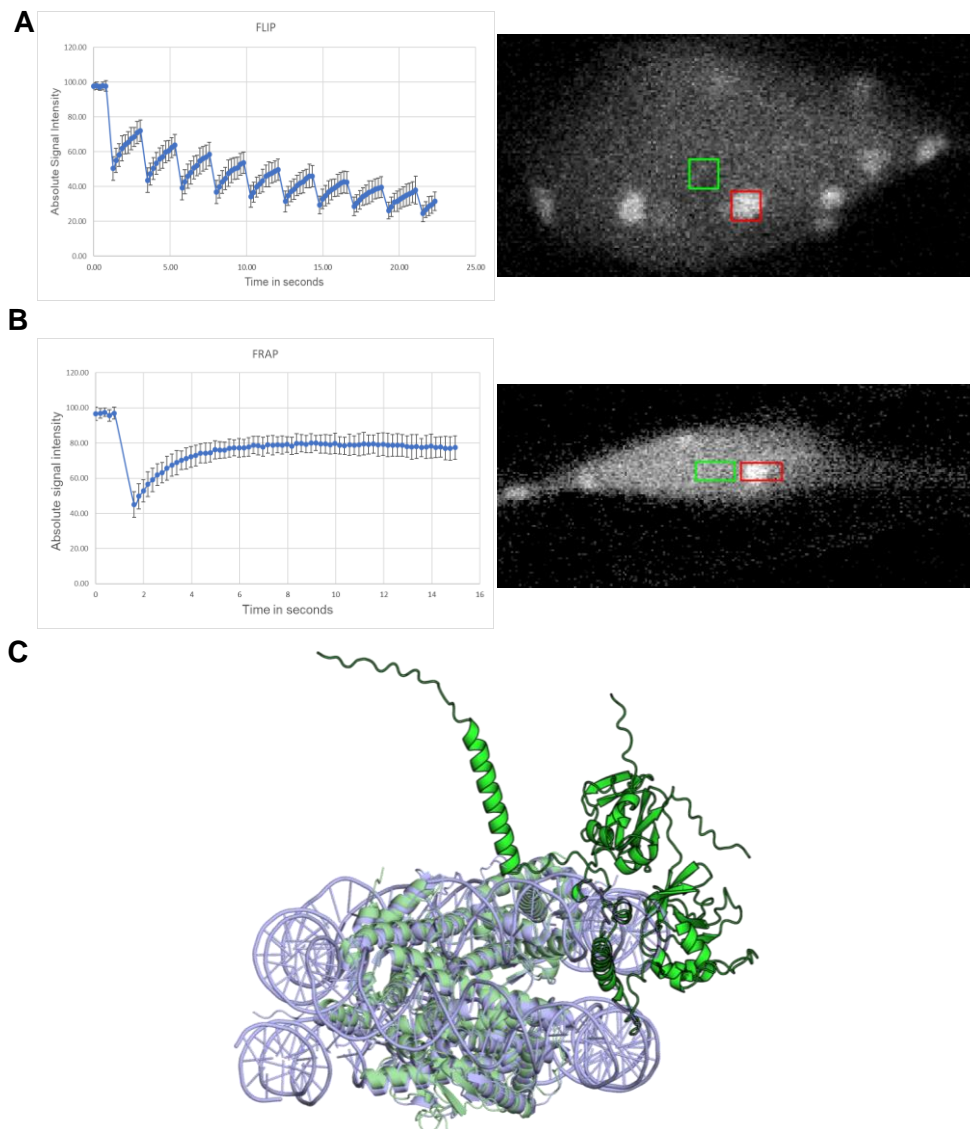


Figure 27. FLIP and FRAP experiments unveil the dynamic nature of β KNL2-EYFP.

(A) For both FLIP and FRAP, individual nuclei were first scanned three times with a 488 nm laser line (2.5% laser power, scan speed 6 without averaging). Following this, FLIP was performed with repeated bleaching of a region of interest within the nucleus measuring $1.4 \mu\text{m}^2$, using 100% laser power and 4 iterations alternated by single recordings. (B) For FRAP, a region of interest measuring $1.4 \mu\text{m}^2$ was bleached by more than 50% and followed by 40 additional scans. Each experiment was run over the time scale of 40 sec, repeated 20–25 times and results averaged. In case of β KNL2 fluorescence intensity at chromocenters recovers to about 80% within 6 sec. For both FLIP and FRAP experiments fluorescence intensity was measured in the area of bleaching (red colour box) as well as in adjacent regions. The x axis represents the time scale of the experiment in second, the y axis corresponds to fluorescence intensity (arbitrary units). (C) The predicted model of β KNL2 and α KNL2 with the octameric histones (green) superposed with *Arabidopsis* euchromatic nucleosome (blue) (PDB code 7ux9 (Lee et al., 2023)). The predicted β KNL2 and α KNL2 are highlighted with stronger green color and black contour, evincing its clash with the DNA.

To investigate how KNL2 proteins bind to centromeric nucleosomes, we generated structural models using AlphaFold2. However, these models failed to accurately position β KNL2 and

α KNL2 relative to the nucleosome (Fig. 27C), necessitating the construction of a chimeric model. Consequently, we constructed a chimeric model of β KNL2 and α KNL2 bound to centromeric nucleosomes using different structural predictions from AlphaFold2 and molecular dynamics simulations were repeated twice independently to assess its stability (methods).

In this chimeric model (Fig. 28), The SANTA domains of β KNL2 and α KNL2 closely interacted with each other on the upper side of the nucleosome, contacting all histones and DNA. Residues from motif-III (230 to 237) were predicted to be positioned above the DNA and exposed to the solvent (Fig. 28A), making it an accessible region for SUMOylation. Furthermore, the C-terminus of β KNL2, starting from motif-III, formed a long stretch of positively charged interface, with the extended α -helix embracing the DNA (Fig. 28B). The CENPC-k motif of α KNL2 was placed similar to the experimentally solved structure of the chicken CENH3 nucleosome (Fig. 28C) (Jiang et al., 2022). This extended α -helix is predicted to interact with phosphate groups, although it does not have specific interactions with DNA bases. This placement allowed β KNL2's charge distribution to complement other regions of the nucleosome. The results including the dynamics of β KNL2-EYFP and other findings from our study support our proposed model.

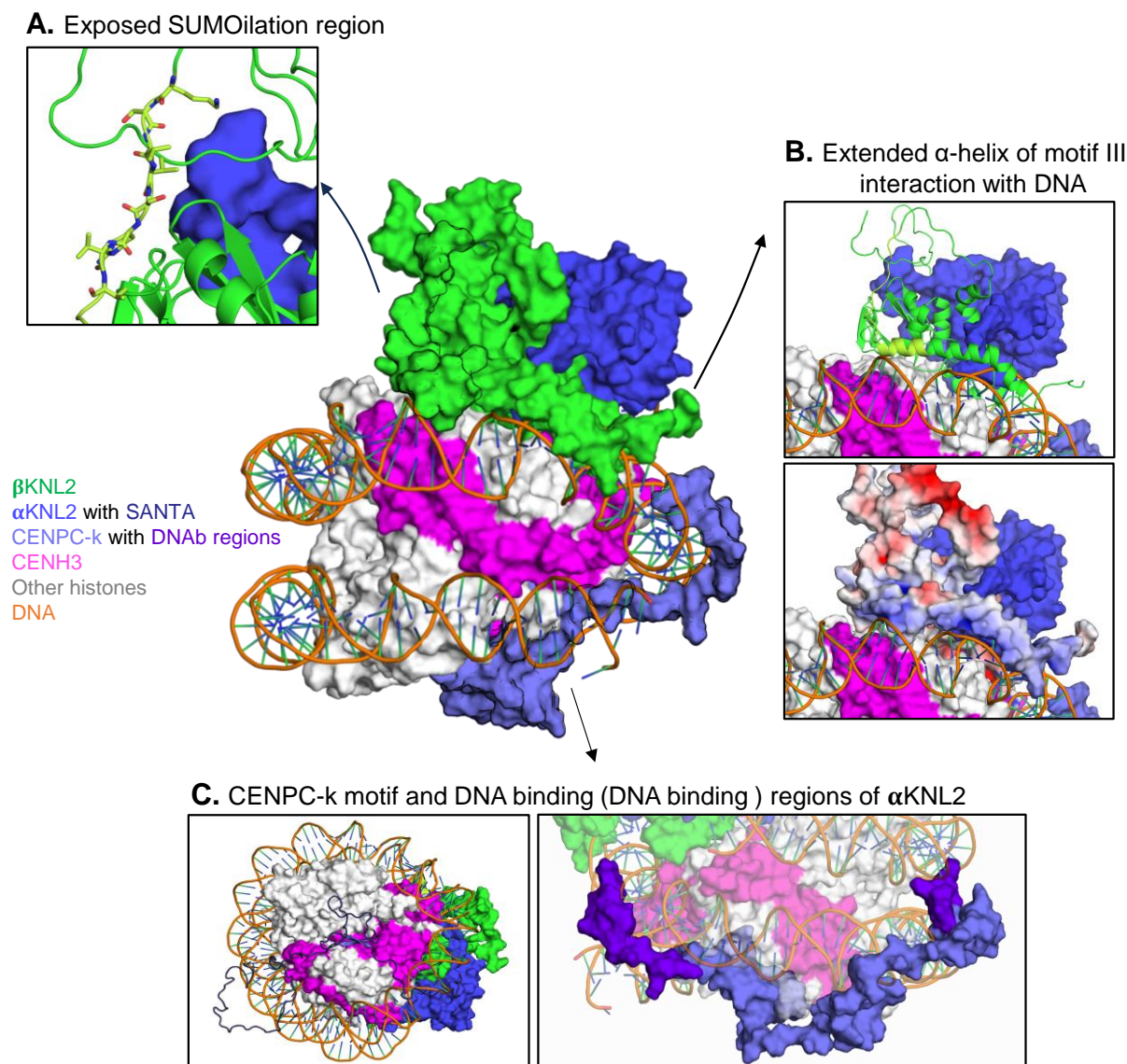


Figure 28. Proposed model of plant-specific inner kinetochore assembly involving β KNL2, α KNL2, and the centromeric nucleosome.

The primary visualization highlights the protein surfaces of β KNL2 (green), α KNL2 (blue), and CENP-A/CENH3 (pink) as they interact with the double helix of DNA. These color codes are consistent throughout all detailed views. (A) The surface exposure of conserved residues at a potential SUMOylation site, as described in the results of this study and illustrated in figure 2D, highlights their accessibility to solvent. (B) Motif-III of β KNL2, with its positively charged surface, wraps around the DNA. Top inset shows ribbon view and bottom shows charged surface mode. Emphasizing its interaction with phosphate groups, which facilitates secure attachment to the nucleosome. (C) Left: The CENPC-k motif (blue) is positioned on the underside of the nucleosome, close to the lower monomer of CENP-A/CENH3. This was similar to the ggKNL2-nucleosome interaction detailed by Jiang et al. (2022). Right: A purple overlay marks DNA-binding regions on α KNL2, as identified by Yalagapati et al. (2024).

Chapter 5: Discussion

5.1 Duplication of *KNL2*

Most metazoan genomes have only one *KNL2* gene with the SANTA domain, except for the allotetraploid *Xenopus laevis*, where two *KNL2* genes were identified; both with identical CENPC-k motifs, nearly identical SANTA and Myb (SANT) domains, and 74% sequence similarity (Moree et al., 2011, French et al., 2017). In contrast, two genes containing the SANTA domain were identified in water ferns, eudicots and grasses, whereas only one *KNL2* copy was found in bryophytes and gymnosperms (Appendix Table 1). Though Brassicaceae species experienced multiple whole genome duplication (WGD) events such as the *At-α* and *At-β* WGDs (Edger et al., 2018), most species exhibit two *KNL2* gene copies, α KNL2 and β KNL2, except for a few neopolyploid species which have experienced an extra recent WGD event(s).

We found strong conservation of the SANTA domain of *KNL2*, notably in the VxLxDW motif at the N-terminus of the SANTA domain and the GFxxxxxxx**F**xxGFPxx**W** motif at the C-terminus (Appendix Fig. 4), where the bolded residues impaired CENP-C binding when mutated in *Xenopus* M18BP (French and Straight, 2019), suggesting that plant *KNL2* variants may also bind CENP-C through the SANTA domain. In addition, analysis of α KNL2 and β KNL2 protein sequences identified numerous paralog-specific motifs, suggesting that the paralogs might be sub-functionalized. A study in *Drosophila* has shown that Cid (CENH3) paralogs evolved new motifs following Cid duplication (Kursel and Malik, 2017). Loss of ancestral motifs in *Drosophila* Cids was proposed as direct evidence of sub-functionalization (Kursel and Malik, 2017, Kursel et al., 2020).

We identified positive selection in and near the SANTA domain of *KNL2* in the analyzed Brassicaceae species, similar to what has been previously reported for CENH3 (Talbert et al., 2002) and CENP-C (Talbert et al., 2004). Thus, *KNL2* might be responding to centromere drive through interaction with rapidly evolving CENH3 and CENH3 chaperone NASP^{SIM3}, which recently was identified in *Arabidopsis* (Le Goff et al., 2020), or with CENP-C. However, the mechanisms of adaptively evolving regions remain to be elucidated.

5.2 The function of β KNL2 in plants

Although *KNL2* protein homologues have been identified in different organisms as components of the CENH3 loading machinery, they differ considerably in the composition of their functional domains, interacting partners, and localization timing in the mitotic cell cycle. The

mammalian M18BP1, composed of the conserved N-terminal (Mis18 α -binding) region, SANTA domain, CENP-C-binding domain, SANT (Myb-like) domain and the C-terminus, is lacking the CENPC-k motif. The N-terminal (Mis18 α -binding) region and the CENP-C-binding domain are required for centromere targeting (Stellfox et al., 2016). Deletion of the SANTA domain in mammalian and chicken M18BP1/KNL2 does not abolish its centromeric localization (Stellfox et al., 2016, Hori et al., 2017). In contrast, mutation of the SANTA domain in *Xenopus* reduced centromeric localization of M18BP1/KNL2 by 90% (French et al., 2017). Later, the same authors demonstrated that the SANTA domain is required for the interaction of M18BP1/KNL2 with CENP-C during metaphase (French and Straight, 2019).

We showed previously that in *Arabidopsis* the centromeric localization of α KNL2 depends on the CENPC-k motif (Sandmann et al., 2017), while it was not abolished in the complete absence of the N-terminal part of KNL2 containing the SANTA domain (Lermontova et al., 2013). The C-terminal half of *Arabidopsis* KNL2 also sufficient for DNA interaction (Sandmann et al., 2017). In the present study, we demonstrated that β KNL2 co-localizes with CENH3 at centromeres, despite lacking a CENPC-k motif. In general, both variants of *Arabidopsis* KNL2 showed a similar localization pattern during interphase. However, in contrast to α KNL2, β KNL2 can be detected on chromosomes during metaphase and early anaphase (Fig. 8B). The centromeric location of β KNL2 suggests that β KNL2 may partially compensate for the loss of α KNL2 in the corresponding *Arabidopsis* mutant which showed only reduced, but not completely abolished CENH3 loading which would be lethal (Lermontova et al., 2013).

Homozygous T-DNA insertions for β KNL2 resulted in plant death at the seedling stage, likely caused by abnormal cell divisions and impaired root development. However, the T-DNA insertion in the α KNL2 mutants is after the SANTA domain coding region, whereas in the case of β KNL2 mutants, one T-DNA was inserted before and the other directly in the SANTA domain. Therefore, it cannot be excluded that truncated α KNL2 with the full SANTA domain may retain some function in the mutant. Taken together, our results suggest that the *KNL2* gene in eudicots underwent an early duplication with the core function of CENH3 deposition.

Although in the SANTA domain of β KNL2 three putative Aurora kinase phosphorylation sites can be identified, there is only one in α KNL2 (Appendix Fig. 4A). This fact might suggest that both KNL2 variants are involved in the formation of different protein complexes. We also could not rule out the possibility that β KNL2 assembles with a Mis18 complex to ensure centromeric localization and subsequent CENH3 deposition. So far, Mis18 α and β proteins have not been identified and characterized in *Arabidopsis*. However, *in-silico* analysis

(<https://bioinformatics.psb.ugent.be/plaza/>) revealed a family of seven genes (*AT2G40110*, *AT3G08990*, *AT3G11230*, *AT3G55890*, *AT4G27740*, *AT4G27745*, *AT5G53940*) encoding proteins with the Yippee-Mis18 domain-specific to Mis18 proteins (Stellfox et al., 2016). Recently it was demonstrated that the direct binding of *Schizosaccharomyces pombe* Mis18 to nucleosomal DNA is important for the recruitment of *sp*Mis18 and Cnp1 (CENH3) to the centromere in fission yeast (Zhang et al., 2021). We demonstrate that β KNL2 exhibits independent DNA-binding ability, which is likely crucial for its interaction with centromeric nucleosomes and the subsequent recruitment of additional components necessary for CENH3 loading.

5.3 Loss of β KNL2 resulted in abnormal cell divisions

Reciprocal crosses between *βknl2* mutants and WT plants resulted in normal seed development in both directions, leading us to hypothesize that β KNL2 null mutations do not impact gametes or fertilization but rather affect postzygotic cell divisions. Supporting this hypothesis, pollen FDA staining and Hoyer's clearing of ovules in *βknl2* heterozygous mutants showed normal development. Our analysis of T-DNA insertion mutants, *βknl2-1* and *βknl2-2*, further underscores the critical role of the β KNL2 protein in maintaining proper cell division and development in *Arabidopsis*. Homozygous knockout lines were found to be lethal, unable to progress beyond the seedling stage, highlighting the essential role of β KNL2 in early plant development, particularly in seed formation and embryogenesis. The absence of homozygous mutants in soil-grown plants and the reduced viability of seedlings grown *in-vitro* emphasize the fundamental importance of β KNL2 in these developmental processes.

Impaired mitotic divisions in mutant seedlings can be explained by the reduced levels of CENH3 on the centromeres of both mutants (Fig. 16). Thus, our data strongly suggest the involvement of β KNL2 protein in CENH3 loading. The ability of cells in homozygous seedlings to undergo some mitotic divisions can be explained by residual amounts of CENH3 from parental plants, and when CENH3 levels are highly diluted, cells switch from mitotic cycle to endoreplications or endomitosis. We observed that the development of homozygous seedlings is inhibited at various stages (Fig. 10A), likely due to the abnormal embryo development detected in the *βknl2-2/+* heterozygous plants stuck at different stages of embryo development (Fig. 14).

FC ploidy analysis of young seedlings revealed that in contrast to the WT with distinct 2C and 4C peaks, homozygous mutants showed a shift towards endopolyploidisation (Fig. 15),

potentially a consequence of disrupted cell divisions. Further analysis showed that *βknl2* mutants exhibit significant disruptions in cell division, including reduced meristematic zones and abnormal leaf development. These defects suggest that β KNL2 is vital for maintaining proper cell division and genomic stability. One possible mechanism is that the loss of β KNL2 disrupts the reloading of CENH3 at centromeres, leading to DNA replication without proper cell division leading to endomitosis. Additionally, β KNL2 may be involved in coordinating the assembly of the mitotic spindle during cytokinesis. Understanding the precise functions of β KNL2, including its role in CENH3 reloading and tubulin interaction, could provide valuable insights.

5.4 Distinct conserved motifs regulate proper localization of β KNL2

In the intricate world of cellular processes, the kinetochore stands out as a critical site essential for the distribution of genetic material during cell division. The establishment and regulation of this kinetochore rely on key regulators like CENH3, M18BP1/KNL2 and CENP-C. While metazoans typically possess a single version of M18BP1/KNL2, plants have evolved a distinct variant. In our investigation, we identified this new variant as β KNL2, exclusive to plants. β KNL2 can be distinguished from its counterpart α KNL2/M18BP1 with the presence of a centromere-targeting CENPC-like motif. Despite lacking the CENPC-like CENPC-k motif, β KNL2 localizes to centromeres. The mechanism behind this phenomenon remained elusive. M18BP1/KNL2 proteins across different species exhibit significant variations in length, sequence, and the presence of conserved motifs and domains. However, amidst this diversity, the SANTA domain stands out as a highly conserved feature among KNL2 proteins (Stellfox et al., 2013). The SANTA domain has been implicated in various functions, including chromatin remodeling, protein-protein interactions (PPI), and nucleic acid binding (Zhang et al., 2006), yet experimental evidence supporting these functions remains limited.

In our study, we demonstrated that deletion of the SANTA domain led to reduced centromeric targeting of β KNL2. Additionally, we identified four distinct conserved motifs specific to β KNL2. The N-terminal part of β KNL2 contains proline-rich sites, and its deletion does not affect centromeric localization, suggesting it may play a role in promoting or stabilizing oligomerization and complex formation. Moreover, conserved N-terminal AA in the motif predicted to undergo phosphorylation by proline-directed kinases. In vertebrates, Cyclin-dependent kinase (CDK) regulate M18BP1/KNL2 centromere localization through oligomerization (French and Straight, 2019, Pan et al., 2017). It is plausible that β KNL2 is

phosphorylated by CDK at these proline-directed phosphorylation sites similar to vertebrate M18BP1/KNL2.

Further investigation revealed that motif-III overlaps with a SUMO site (221-231 AA) and can undergo SUMOylation. Deletion of this motif-III resulted in mis-localization of β KNL2 to the cytoplasm. However, deleting the highly conserved region of motif-III (237-249 AA) while retaining the predicted SUMOylation region led to partial restoration of nucleoplasm localization. This demonstrates the crucial role of the entire motif-III in targeting the β KNL2 protein to the nucleus and centromeres. The role of SUMOylation in β KNL2 localization remains to be fully elucidated. However, it is known that SUMOylation plays an important role in the correct localization and function of kinetochore proteins. For instance, loss of the SUMO protease SENP6 in human cells results in the mislocalization of essential kinetochore proteins CENP-C, CENP-I (Mitra et al., 2020), M18BP1/KNL2, and other kinetochore proteins (Liebelt et al., 2019).

Moreover, deletion of Motif-I and Motif-II did not disrupt centromeric localization. Structural changes were observed in these motifs (Fig. 26A), when predicted to interact with different proteins. Suggesting that these motifs might involve in protein-protein interactions with other kinetochore proteins. In summary, our findings underscore the essential role of the SANTA domain and the C-terminus in the efficient centromeric localization of β KNL2, independent of the N-terminal region.

5.5 β KNL2 is an inner kinetochore protein recruited by CENPC-like motif containing proteins like α KNL2

The kinetochore, a multilayered protein complex, is categorized into inner kinetochore, consisting of structural and DNA-binding proteins forming on chromatin, and an outer kinetochore, comprising the KMN network that forms the platform for microtubule binding (Yamagishi et al., 2014, Cheeseman, 2014, Musacchio and Desai, 2017, Dong and Li, 2022). Inner kinetochore proteins typically bind to centromeres consistently, while outer kinetochore proteins assemble during mitosis.

In many organisms, including plants, M18BP1/KNL2 is associated with centromeres throughout the cell cycle, although in plants it is absent during metaphase to mid-anaphase (French et al., 2017, Hori et al., 2017, Lermontova et al., 2013). In contrast, mammals exhibit a more restricted localization, with M18BP1/KNL2 being present at centromeres only during telophase and early G1, coinciding with the period before CENH3 loading (Fujita et al., 2007,

Maddox et al., 2007). Previously, we demonstrated that *Arabidopsis* α KNL2 binds to centromeric DNA via a distinct region separate from the centromere-targeting CENPC-k motif (Sandmann et al., 2017, Ramakrishnan Chandra et al., 2023, Yalagapati et al., 2024). The newly identified β KNL2 localizes at centromeres throughout the cell cycle, except for reduced levels in early prophase. Online functional prediction tools like PredictProtein, DNA pred, DNA Bind suggested that β KNL2 has potential to bind nucleic acids. Independently, through AlphaFold2 predictions and molecular dynamics, we also observed that conserved motif-III of β KNL2 contacts the chromatin DNA (Fig. 28). To address the question of β KNL2 ability to bind to DNA, we conducted EMSA and showed FLAG- β KNL2 was able to bind *pAL1* centromeric DNA. Which supports that the β KNL2's DNA binding ability is independent of α KNL2 and its involvement in inner kinetochore dynamics and chromatin interactions.

β KNL2 localizes to centromeres without the centromere targeting CENPC-k motif. We hypothesized that β KNL2 might interact with CENPC-like motif containing proteins - α KNL2 and/or CENP-C to achieve centromeric targeting. AlphaFold2 prediction also shows α and β KNL2 bound together to contact nucleosome complex. In the complex of β KNL2, α KNL2 and nucleosome, CENPC-k motif may contact CENH3 and the heterodimer of β KNL2 and α KNL2 formed via their SANTA domains may interact with the nucleosome. Furthermore, *aknl2* null mutants showing abolished centromere targeting of β KNL2 in sperm nuclei confirmed our hypothesis that the α KNL2 recruits β KNL2 to the centromeres. We observed dispersed signals in tissues like anthers and developing seeds compared to the control rather than complete mis-localization. This diverse tissue-specific localization pattern of β KNL2 in *aknl2* mutants suggests that α KNL2 may not be the sole recruiter of β KNL2 to the centromere.

5.6 β KNL2 dimerize to facilitate or support centromere assembly and kinetochore platform

In animals and yeast, M18BP1/KNL2 establish homodimers and hetero-oligomers to guide the CENP-A recruitment and kinetochore assembly. This dimerization and oligomerization are required for its function and are regulated by CDK phosphorylation (Pan et al., 2017, French and Straight, 2019). Even the Mis18 proteins oligomerize with Yippee/Med1Y and a C-terminal α -helix (Subramanian et al., 2016, Nardi et al., 2016, Spiller et al., 2017). Interestingly, plants possess two KNL2 variants (α KNL2 and β KNL2) and lacks Mis18 α & β . In plants, this extra SANTA-containing KNL2 tends to interact with other kinetochore proteins. With help of structural predictions and experimental evidences we showed that β KNL2 can interact with α KNL2 and also form homodimers.

In our proposed models, the dimerization of β KNL2 is mediated by the SANTA domain, which is similar to *Xenopus* KNL2 (French and Straight, 2019). Additionally, α KNL2 and β KNL2 are predicted to form an intermonomeric β -sheet through the SANTA domains and their pre-SANTA conserved TPV/IK. Apart from predictions BiFC validates the direct interaction between SANTA-containing α KNL2(N) and β KNL2. Deletion of SANTA domain resulted in reduced centromere targeting and moreover we have proven that β KNL2 depends on α KNL2 for centromere targeting. These results highlight the role of β SANTA in centromere targeting and dimerization with α KNL2.

In different organisms it was shown that M18BP1/KNL2 and CENP-C take over some common roles in different cell cycles stages like CENP-A loading and kinetochore assembly. CENP-C cupin domain, a feature absent in plants oligomerizes to create a platform for kinetochore proteins to assemble (Hara et al., 2023). Previous studies have also indicated the AtCENP-C protein absence at the centromeres in non-meristematic nuclei (Lermontova et al., 2011). Highlighting these unique features of plants with two KNL2 variants and their ability to dimerization raises the question about their adaptation to a different kinetochore assembly platform. Here we propose β KNL2 together with α KNL2 and/or CENP-C, facilitate or support the kinetochore assembly platform (Fig. 29). Evidences such as the consistent presence of β KNL2 at centromeres throughout the cell cycle, abolished or reduced CENH3 loading onto centromeres when disrupted β KNL2 expression and its interaction with α KNL2 and CENH3, all support its role in the kinetochore assembly platform.

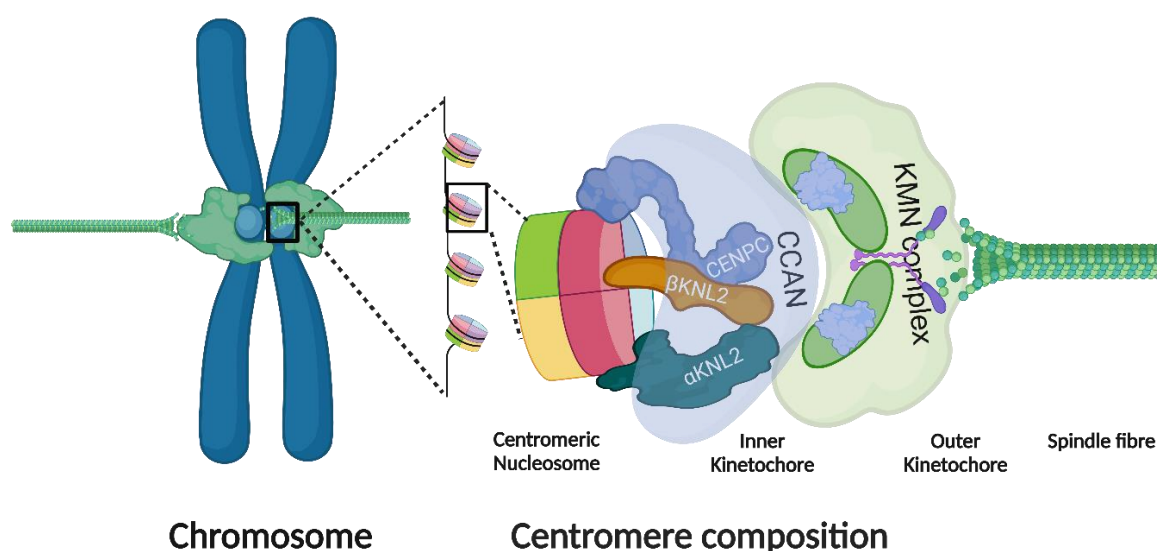


Figure 29. Graphical model of β KNL2 supporting centromere assembly and kinetochore platform. This graphical representation illustrates how β KNL2 possibly dimerizes to facilitate or support the assembly and function of the centromere and kinetochore structures together with α KNL2.

Chapter 6: Outlook

The KNL2 protein plays an essential role in plant development by facilitating the loading of CENH3 onto centromeres. Our research revealed that the *KNL2* gene in plants has undergone three independent duplications in ferns, monocots, and eudicots. In eudicots, two variants of the KNL2 protein have been identified: α KNL2 (previously characterized) and β KNL2 (newly identified). While both proteins contain a SANTA domain, only α KNL2 possesses a centromere-targeting CENPC-k motif, similar to the CENP-C protein. Additionally, several motifs specific to either the α KNL2 or β KNL2 protein variants have been identified.

Disruption of β KNL2 expression results in decreased CENH3 levels at centromeres, leading to abnormal cell divisions and ultimately impairing embryo development, with outcomes ranging from developmental arrest at various stages to embryo lethality. To gain a deeper understanding of the role of β KNL2 in kinetochore assembly, plant growth, and development, several critical questions must be addressed:

1. What is the role of SUMOylation and the different domains of β KNL2 in its centromere and kinetochore functions?
2. Does CENP-C recruit β KNL2 to the centromeres during embryogenesis?
3. How does β KNL2 interact with other kinetochore proteins?
4. What is the protein-protein interaction network of kinetochore proteins, with a particular focus on β KNL2?
5. What is the 3D structure of the KNL2 (both α KNL2 and β KNL2)-centromeric nucleosome complex?

Our future research will focus on these aspects to address the aforementioned questions and provide a comprehensive understanding of KNL2's role in plant-specific kinetochore assembly and its broader implications for plant development.

6.1 Functional roles of β KNL2 domains and SUMOylation beyond centromere targeting

β KNL2, a plant-specific variant of KNL2, stands out due to its unique structure, containing only the conserved SANTA domain without the additional motifs or domains found in other KNL2 variants. Despite its smaller size, β KNL2 is essential for plant survival, highlighting its critical role in plant-specific kinetochore assembly and evolution. The severe developmental defects

observed in β KNL2 mutant phenotypes further underscore the importance of this protein and the necessity of understanding its fundamental functions.

Our findings demonstrate that both the SANTA domain and the C-terminal regions of β KNL2 are vital for its centromeric localization. However, it is essential to explore the functional roles of these regions and the conserved motifs within them beyond mere localization. To achieve this, generating and transforming different truncated constructs of the genomic fragment β KNL2:: β KNL2-EYFP into *βknl2* mutants is needed. Evaluating these transformants for their ability to rescue abnormal seed and embryo development will provide valuable insights into the functional significance of β KNL2's conserved domains. Additionally, the identification of potential SUMOylation sites suggests a possible regulatory role of SUMOylation in β KNL2's function. Exploring this aspect by mutagenizing the predicted SUMOylation sites will be crucial to understanding the impact of SUMOylation on β KNL2's functionality.

These research directions are vital for advancing our understanding of β KNL2's role in plant growth and development. This study will illuminate the complex processes that control cell division and chromosomal stability in plants.

6.2 Tissue dependent centromeric recruitment of β KNL2 governed by CENPC-like motif containing proteins

In section 4.12, we demonstrated that the centromeric localization of *A. thaliana* β KNL2 typically depends on α KNL2, which contains the CENPC-k motif. However, our findings also revealed that in the absence of α KNL2, β KNL2 can still localize to centromeres in embryos, indicating that α KNL2 is not the sole recruiter of β KNL2. This suggests that the recruitment process of β KNL2 is tissue-specific and involves additional factors.

One potential candidate for this alternative recruitment is the CENP-C protein, which also contains the CENPC motif. Given its structural similarity, CENP-C may play a role in the localization of β KNL2 in tissues where α KNL2 is absent or involved in formation of other protein complexes. To further investigate this possibility, it is necessary to generate *cenp-c* mutants, as complete loss-of-function mutants are not viable, by introducing targeted mutations in the promoter or non-conserved regions, or by developing RNAi lines in *Arabidopsis*. This approach will enable the assessment of β KNL2 localization specifically in meristematic tissues, such as root tips and embryos.

By elucidating the roles of CENP-C and other potential recruiters, we can gain deeper insights into the tissue-specific regulation of β KNL2 and its broader implications for plant development and genome stability.

6.3 Bridging the gap: mapping the interaction network of plant kinetochore proteins and their role in chromosome stability

While over 50 kinetochore proteins have been identified and extensively studied in animals, the plant kingdom remains relatively underexplored in this area. The intricate composition of the animal kinetochore has provided significant insights into chromosome segregation, centromere function, and cell division. Despite the critical importance of these processes in plants, only a limited number of plant kinetochore proteins have been identified and characterized to date.

This gap in our understanding of plant kinetochores presents both a challenge and an opportunity for further research. Unraveling the unique kinetochore components in plants is essential for understanding how they have adapted the conserved mechanisms of chromosome segregation to accommodate their distinct cellular structures and life cycles.

A promising approach to identifying novel kinetochore proteins in plants lies in the investigation of β KNL2's interactions. β KNL2 is plant-specific variant and is present throughout most of the cell cycle, making it a perfect candidate. By employing a combination of PPI identification methods, we can identify proteins that interact with β KNL2, particularly those involved in centromere assembly, cell division, and chromatin remodeling. Integrating this data with known KNL2 and kinetochore protein interaction networks could lead to the identification of a more comprehensive set of plant kinetochore proteins.

Constructing a detailed interaction network and performing Gene Ontology (GO) analysis will help classify and understand the molecular functions of these identified proteins. This approach will enable the identification of key players in the kinetochore complex, particularly those involved in plant-specific pathways related to embryo development and growth.

Following the identification of potential interactors, validating these interactions using multiple techniques will confirm their direct involvement in kinetochore function. This will provide a deeper understanding of the roles these proteins play in plant development and chromosome stability.

Overall, this could bridge the knowledge gap in plant kinetochore biology, offering new insights into the unique mechanism plants use to maintain chromosomal stability and ensure proper cell

division. Identifying and characterizing these novel kinetochore proteins will not only enhance our understanding of plant biology but also open up new avenues for crop improvement through targeted manipulation of these critical cellular processes.

Future research should focus on employing advanced techniques such as proteomics, high-resolution microscopy, and comparative genomics to identify and characterize kinetochore proteins in plants. Additionally, functional studies using gene editing technologies like CRISPR/Cas9 will be essential for determining the roles of these proteins in kinetochore assembly, chromosome segregation, and overall plant development.

In conclusion, expanding our knowledge of plant kinetochore proteins is fundamental to understanding plant biology and holds the potential to unlock new opportunities for agricultural innovation. By bridging the knowledge gap between animal and plant kinetochores, we can achieve a more comprehensive understanding of chromosome dynamics across all life forms.

6.4 Structural determination of the *Arabidopsis* CENH3 nucleosome complex with α KNL2 and β KNL2

Understanding the structural and functional dynamics of the CENH3 nucleosome complex bound by *Arabidopsis* KNL2 proteins (α KNL2 and β KNL2) is crucial for identifying critical interaction sites that could be targeted for generating mutants, particularly for haploid induction strategies. Detailed structural insights into the inner kinetochore are essential for this purpose. A key step in this process is the *in-vitro* reconstitution of the CENH3 nucleosome complex using *Arabidopsis*-derived α KNL2 and β KNL2 proteins.

By employing cryo-electron microscopy (cryo-EM) single-particle analysis on the reconstituted CENH3 nucleosome complex, it is possible to obtain high-resolution structural data that will provide insights into the assembly, spatial organization of this complex. This approach would greatly enhance our understanding of how these KNL2 proteins interact with centromeric chromatin, laying the groundwork for further exploration of kinetochore assembly and chromosome segregation in plants. Additionally, incorporating other kinetochore proteins into this analysis could further refine our knowledge of kinetochore assembly in plants.

6.5 KNL2 manipulation: A gateway to efficient haploid production

Understanding the function and network of kinetochore proteins, such as KNL2, is crucial for deepening our knowledge of genome stability and maintenance in plants. This insight not only

advances our fundamental understanding of plant biology but also opens new avenues for manipulating kinetochore function to induce haploids and improve crop varieties.

Previous studies have demonstrated that manipulating α KNL2 can facilitate the production of haploids and, subsequently, double haploids in *Arabidopsis* (Ahmadli et al., 2022a, Lermontova, 2017). The production of double haploids significantly accelerates plant breeding by enabling the creation of true-breeding lines in a single generation, compared to the 7-9 generations required for conventional selection methods (Britt and Kuppu, 2016, Kalinowska et al., 2019). In our research, we have identified that *KNL2* genes exist in two variants within eudicots (α , β *KNL2*) and monocots (γ , δ *KNL2*). The conserved gene structure and expression patterns of α/γ *KNL2* in both eudicots and monocots suggest that mutations in these genes could be harnessed to develop *in-vivo* haploid induction systems in various crop plants.

Similarly, the newly identified β KNL2 presents an exciting opportunity for manipulation to induce haploids in *Arabidopsis* and other crops. Given that homozygous β *knl2* mutants are lethal at the seedling stage, it is plausible that heterozygous mutant plants might also induce haploids, similar to what has been observed in heterozygous *cenh3* mutants of maize and wheat (Lv et al., 2020, Wang et al., 2021). Additionally, partially complemented β *knl2* mutants, generated using truncation constructs, could potentially recover viable homozygous mutants, offering further opportunities for haploid production.

Chapter 7: Summary

The kinetochore is a crucial protein complex responsible for ensuring accurate chromosome segregation during cell division. The assembly of the kinetochore is initiated by the incorporation of CENP-A/CENH3. KINETOCHORE NULL2 (KNL2) plays a pivotal role in recognizing centromeres and facilitating the deposition of new CENH3. To better understand the origin and diversification of the *KNL2* gene, we reconstructed its evolutionary history within the plant kingdom. Our findings indicate that the *KNL2* gene in plants underwent three independent ancient duplications in ferns, grasses, and eudicots. Furthermore, we identified previously unclassified *KNL2* genes, which can be categorized into two clades: α *KNL2* and β *KNL2* in eudicots, and γ *KNL2* and δ *KNL2* in grasses.

All *KNL2* variants encode the conserved SANTA domain; however, only the α *KNL2* and γ *KNL2* groups also encode the CENPC-k motif. The confirmed centromeric localization of β *KNL2*, along with mutant analysis, suggests that it plays a role in the deposition of new CENH3, similar to α *KNL2*. A high rate of seed abortion was observed in heterozygous β *knl2* plants, and germinated homozygous mutants failed to develop beyond the seedling stage.

While both *KNL2* variants in eudicots possess the conserved SANTA domain, only α *KNL2* contains the centromere-targeting CENPC-k motif. Despite lacking this motif, the plant-specific β *KNL2* still localizes to centromeres and aids in CENP-A/CENH3 loading. We found that efficient centromeric targeting of β *KNL2* requires both the SANTA domain and the C-terminal region, with nuclear targeting depending on a conserved C-terminal motif-III. Structural predictions and experimental validations reveal that β *KNL2* forms homodimers and interacts with centromeric DNA and α *KNL2*. Additionally, we confirm that the centromeric targeting of β *KNL2* is dependent on α *KNL2* in a tissue-specific manner.

In conclusion, our study provides new insights into the evolutionary diversification of the plant kinetochore assembly gene *KNL2*, highlighting the distinct roles of duplicated *KNL2* genes in centromere recognition and kinetochore assembly. This research underscores the importance of these plant-specific *KNL2* variants in maintaining genome stability through their involvement in the precise loading of CENH3 and the overall organization of the kinetochore complex. Our findings further shed light on β *KNL2* centromeric targeting mechanism and its essential role in plant-specific kinetochore assembly.

Chapter 8: Zusammenfassung

Das Kinetochor ist ein entscheidender Proteinkomplex, der für die genaue Trennung der Chromosomen während der Zellteilung verantwortlich ist. Die Assemblierung des Kinetochors wird durch die Integration von CENP-A/CENH3 eingeleitet. KINETOCHORE NULL2 (KNL2) spielt eine zentrale Rolle bei der Erkennung von Centromeren und der Ablagerung von neuem CENH3. Um die Herkunft und Diversifizierung des *KNL2*-Gens besser zu verstehen, haben wir dessen evolutionäre Geschichte im Pflanzenreich rekonstruiert. Unsere Ergebnisse zeigen, dass das *KNL2*-Gen in Pflanzen drei unabhängige, uralte Duplikationen in Farnen, Gräsern und Eudikotylen durchlaufen hat. Darüber hinaus haben wir bisher nicht klassifizierte *KNL2*-Gene identifiziert, die in zwei Kladen unterteilt werden können: α *KNL2* und β *KNL2* in Eudikotylen sowie γ *KNL2* und δ *KNL2* in Gräsern.

Alle *KNL2*-Varianten kodieren für die konservierte SANTA-Domäne; jedoch kodieren nur die Gruppen α *KNL2* und γ *KNL2* auch für das CENPC-k-Motiv. Die bestätigte centromerische Lokalisierung von β *KNL2*, zusammen mit Mutantenanalysen, deutet darauf hin, dass es eine Rolle bei der Ablagerung von neuem CENH3 spielt, ähnlich wie α *KNL2*. In heterozygoten β *KNL2*-Pflanzen wurde eine hohe Rate an Samenaborten beobachtet, und gekeimte homozygote Mutanten entwickelten sich nicht über das Keimlingsstadium hinaus.

Obwohl beide *KNL2*-Varianten in Eudikotylen die konservierte SANTA-Domäne besitzen, enthält nur α *KNL2* das Centromer-gerichtete CENPC-k-Motiv. Trotz des Fehlens dieses Motivs lokalisiert sich das pflanzenspezifische β *KNL2* dennoch an den Centromeren und unterstützt die Beladung von CENP-A/CENH3. Wir haben festgestellt, dass eine effiziente centromerische Zielsteuerung von β *KNL2* sowohl die SANTA-Domäne als auch die C-terminale Region erfordert, wobei die nukleäre Zielsteuerung von einem konservierten C-terminalen Motiv-III abhängt. Strukturelle Vorhersagen und experimentelle Validierungen zeigen, dass β *KNL2* Homodimere bildet und mit centromerischer DNA sowie α *KNL2* interagiert. Darüber hinaus bestätigen wir, dass die centromerische Zielsteuerung von β *KNL2* in gewebeabhängiger Weise von α *KNL2* abhängt.

Zusammenfassend bietet unsere Studie neue Einblicke in die evolutionäre Diversifizierung des pflanzlichen Kinetochor-Assemblierungsgens *KNL2* und hebt die unterschiedlichen Rollen der duplizierten *KNL2*-Gene bei der Centromer-Erkennung und Kinetochor-Assemblierung hervor. Diese Forschung unterstreicht die Bedeutung dieser pflanzenspezifischen *KNL2*-Varianten für die Erhaltung der Genomstabilität durch ihre Beteiligung an der präzisen Beladung von CENH3

und der Gesamtorganisation des Kinetochorkomplexes. Unsere Ergebnisse werfen zudem neues Licht auf den Mechanismus der centromerischen Zielsteuerung von β KNL2 und seine wesentliche Rolle bei der pflanzenspezifischen Kinetochor-Assemblierung.

Chapter 9: References

- Abraham, A.** 1939. Chromosome Structure and the Mechanics of Mitosis and Meiosis: I. Mitosis in *Lilium*. *Annals of Botany*, 3, 545-568.
- Abraham, M. J., Murtola, T., Schulz, R., Páll, S., Smith, J. C., Hess, B. & Lindahl, E.** 2015. GROMACS: High performance molecular simulations through multi-level parallelism from laptops to supercomputers. *SoftwareX*, 1-2, 19-25.
- Adams, S., Vinkenoog, R., Spielman, M., Dickinson, H. G. & Scott, R. J.** 2000. Parent-of-origin effects on seed development in *Arabidopsis thaliana* require DNA methylation. *Development*, 127, 2493-2502.
- Ahmadli, U., Kalidass, M., Khaitova, L. C., Fuchs, J., Cuacos, M., Demidov, D., Zuo, S., Pecinkova, J., Mascher, M., Ingouff, M., . . . Lermontova, I.** 2022a. High temperature increases centromere-mediated genome elimination frequency and enhances haploid induction in *Arabidopsis*. *Plant Communications*, 100507.
- Ahmadli, U., Sandmann, M., Fuchs, J. & Lermontova, I.** 2022b. Immunolabeling of nuclei/chromosomes in *Arabidopsis thaliana*. *Plant Cell Division: Methods and Protocols*, 19-28.
- Armenta-Medina, A., Gillmor, C. S., Gao, P., Mora-Macias, J., Kochian, L. V., Xiang, D. & Datla, R.** 2021. Developmental and genomic architecture of plant embryogenesis: from model plant to crops. *Plant Communications*, 2.
- Bailey, T. L., Boden, M., Buske, F. A., Frith, M., Grant, C. E., Clementi, L., Ren, J., Li, W. W. & Noble, W. S.** 2009. MEME SUITE: tools for motif discovery and searching. *Nucleic acids research*, 37, W202-W208.
- Bailey, T. L. & Gribskov, M.** 1998. Combining evidence using p-values: application to sequence homology searches. *Bioinformatics (Oxford, England)*, 14, 48-54.
- Barnhart-Dailey, M. C. & Foltz, D. R.** 2014. Centromere Licensing: Mis18 Is Required to Polo-ver. *Current Biology*, 24, R808-R810.
- Barra, V. & Fachinetti, D.** 2018. The dark side of centromeres: types, causes and consequences of structural abnormalities implicating centromeric DNA. *Nature Communications*, 9, 4340.
- Beaudouin, J., Gerlich, D., Daigle, N., Eils, R. & Ellenberg, J.** 2002. Nuclear envelope breakdown proceeds by microtubule-induced tearing of the lamina. *Cell*, 108, 83-96.
- Bellutti, L., Macaisne, N., El Mossadeq, L., Ganeswaran, T., Canman, J. C. & Dumont, J.** 2024. Regulation of outer kinetochore assembly during meiosis I and II by CENP-A and KNL-2/M18BP1 in *C. elegans* oocytes. *Current Biology*.
- Berger, F. & Twell, D.** 2011. Germline specification and function in plants. *Annual review of plant biology*, 62, 461-484.
- Best, C., Mizrahi, R., Edris, R., Tang, H., Zer, H., Colas Des Francs-Small, C., Finkel, O. M., Zhu, H., Small, I. D. & Ostersetzer-Biran, O.** 2023. MSP1 encodes an essential RNA-binding pentatricopeptide repeat factor required for nad1 maturation and complex I biogenesis in *Arabidopsis* mitochondria. *New Phytologist*, 238, 2375-2392.
- Black, B. E. & Cleveland, D. W.** 2011. Epigenetic centromere propagation and the nature of CENP-a nucleosomes. *Cell*, 144, 471-479.
- Bleckmann, A., Alter, S. & Dresselhaus, T.** 2014. The beginning of a seed: regulatory mechanisms of double fertilization. *Frontiers in plant science*, 5, 452.
- Blower, M. D., Sullivan, B. A. & Karpen, G. H.** 2002. Conserved organization of centromeric chromatin in flies and humans. *Developmental cell*, 2, 319-330.
- Bobkov, G. O., Huang, A., Van Den Berg, S. J., Mitra, S., Anselm, E., Lazou, V., Schunter, S., Feederle, R., Imhof, A. & Lusser, A.** 2020. Spt6 is a maintenance factor for centromeric CENP-A. *Nature Communications*, 11, 2919.
- Boisnard-Lorig, C., Colon-Carmona, A., Bauch, M., Hodge, S., Doerner, P., Bancharel, E., Dumas, C., Haseloff, J. & Berger, F.** 2001. Dynamic analyses of the expression of the HISTONE::YFP fusion protein in *Arabidopsis* show that syncytial endosperm is divided in mitotic domains. *The Plant Cell*, 13, 495-509.
- Bouck, G. B. & Brown, D. L.** 1973. Microtubule biogenesis and cell shape in *Ochromonas*: I. the distribution of cytoplasmic and mitotic microtubules. *The Journal of cell biology*, 56, 340-359.

- Boudichevskaia, A., Houben, A., Fiebig, A., Prochazkova, K., Pecinka, A. & Lermontova, I.** 2019. Depletion of KNL2 results in altered expression of genes involved in regulation of the cell cycle, transcription, and development in Arabidopsis. *International Journal of Molecular Sciences*, 20, 5726.
- Boyer, L. A., Latek, R. R. & Peterson, C. L.** 2004. The SANT domain: a unique histone-tail-binding module? *Nature reviews Molecular cell biology*, 5, 158-163.
- Britt, A. B. & Kuppu, S.** 2016. CenH3: an emerging player in haploid induction technology. *Frontiers in plant science*, 7, 357.
- Brown, J. R., Douady, C. J., Italia, M. J., Marshall, W. E. & Stanhope, M. J.** 2001. Universal trees based on large combined protein sequence data sets. *Nature Genetics*, 28, 281-285.
- Brown, R. C. & Lemmon, B. E.** 2007. The pleiomorphic plant MTOC: an evolutionary perspective. *Journal of Integrative Plant Biology*, 49, 1142-1153.
- Bush, M. S., Crowe, N., Zheng, T. & Doonan, J. H.** 2015. The RNA helicase, eIF4A-1, is required for ovule development and cell size homeostasis in Arabidopsis. *The Plant Journal*, 84, 989-1004.
- Cámara, A. S., Kubalová, I. & Schubert, V.** 2024. Helical chromonema coiling is conserved in eukaryotes. *The Plant Journal*, 118, 1284-1300.
- Caryl, A. P., Jones, G. H. & Franklin, F. C. H.** 2003. Dissecting plant meiosis using Arabidopsis thaliana mutants. *Journal of Experimental Botany*, 54, 25-38.
- Cebolla, A., Vinardell, J. M., Kiss, E., Olah, B., Roudier, F., Kondorosi, A. & Kondorosi, E.** 1999. The mitotic inhibitor ccs52 is required for endoreduplication and ploidy-dependent cell enlargement in plants. *The EMBO journal*.
- Chaudhury, A. M., Ming, L., Miller, C., Craig, S., Dennis, E. S. & Peacock, W. J.** 1997. Fertilization-independent seed development in Arabidopsis thaliana. *Proceedings of the National Academy of Sciences*, 94, 4223-4228.
- Cheeseman, I. M.** 2014. The Kinetochore. *Cold Spring Harbor Perspectives in Biology*, 6, a015826.
- Cheeseman, I. M. & Desai, A.** 2008. Molecular architecture of the kinetochore-microtubule interface. *Nature Reviews Molecular Cell Biology*, 9, 33-46.
- Cimini, D.** 2007. Detection and correction of merotelic kinetochore orientation by Aurora B and its partners. *Cell cycle*, 6, 1558-1564.
- Cimini, D., Wan, X., Hirel, C. B. & Salmon, E.** 2006. Aurora kinase promotes turnover of kinetochore microtubules to reduce chromosome segregation errors. *Current Biology*, 16, 1711-1718.
- Clough, S. J. & Bent, A. F.** 1998. Floral dip: a simplified method for Agrobacterium-mediated transformation of Arabidopsis thaliana. *Plant J*, 16, 735-43.
- Darwin, C.** 1859. On The Origin of Species.
- Dawe, R., Richardson, E. & Zhang, X.** 2005. The simple ultrastructure of the maize kinetochore fits a two-domain model. *Cytogenetic and genome research*, 109, 128-133.
- De Groot, C., Houston, J., Davis, B., Gerson-Gurwitz, A., Monen, J., Lara-Gonzalez, P., Oegema, K., Shiau, A. K. & Desai, A.** 2021. The N-terminal tail of C. elegans CENP-A interacts with KNL-2 and is essential for centromeric chromatin assembly. *Molecular Biology of the Cell*, 32, 1193-1201.
- De Nooijer, S., Wellink, J., Mulder, B. & Bisseling, T.** 2009. Non-specific interactions are sufficient to explain the position of heterochromatic chromocenters and nucleoli in interphase nuclei. *Nucleic acids research*, 37, 3558-3568.
- De Rop, V., Padeganeh, A. & Maddox, P. S.** 2012. CENP-A: the key player behind centromere identity, propagation, and kinetochore assembly. *Chromosoma*, 121, 527-538.
- Deatherage, F. E. & Deatherage, F. E.** 1975. Cells, the Fundamental Biological Units. *Food for Life*, 11-30.
- Delisle, R. G.** 2021. Natural Selection as a Mere Auxiliary Hypothesis (Sensu Stricto I. Lakatos) in Charles Darwin's Origin of Species. In: DELISLE, R. G. (ed.) *Natural Selection: Revisiting its Explanatory Role in Evolutionary Biology*. Cham: Springer International Publishing.
- Deluca, J. G., Gall, W. E., Ciferri, C., Cimini, D., Musacchio, A. & Salmon, E.** 2006. Kinetochore microtubule dynamics and attachment stability are regulated by Hec1. *Cell*, 127, 969-982.
- Demidov, D., Heckmann, S., Weiss, O., Rutten, T., Dvorak Tomastikova, E., Kuhlmann, M., Scholl, P., Municio, C. M., Lermontova, I. & Houben, A.** 2019. Deregulated Phosphorylation

- of CENH3 at Ser65 Affects the Development of Floral Meristems in *Arabidopsis thaliana*. *Front Plant Sci*, 10, 928.
- Demidov, D., Lermontova, I., Weiss, O., Fuchs, J., Rutten, T., Kumke, K., Sharbel, T. F., Van Damme, D., De Storme, N. & Geelen, D.** 2014. Altered expression of Aurora kinases in *Arabidopsis* results in aneuploidy and polyploidization. *The Plant Journal*, 80, 449-461.
- Deng, X., He, Y., Tang, X., Liu, X., Lee, Y.-R. J., Liu, B. & Lin, H.** 2024. A coadapted KNL1 and spindle assembly checkpoint axis orchestrates precise mitosis in *Arabidopsis*. *Proceedings of the National Academy of Sciences*, 121, e2316583121.
- Dimario, P. J.** 2004. Cell and molecular biology of nucleolar assembly and disassembly. *Int Rev Cytol*, 239, 99-178.
- Dittmer, T. A., Stacey, N. J., Sugimoto-Shirasu, K. & Richards, E. J.** 2007. LITTLE NUCLEI genes affecting nuclear morphology in *Arabidopsis thaliana*. *The Plant Cell*, 19, 2793-2803.
- Dixon, J. R., Selvaraj, S., Yue, F., Kim, A., Li, Y., Shen, Y., Hu, M., Liu, J. S. & Ren, B.** 2012. Topological domains in mammalian genomes identified by analysis of chromatin interactions. *Nature*, 485, 376-380.
- Dolinsky, T. J., Nielsen, J. E., Mccammon, J. A. & Baker, N. A.** 2004. PDB2PQR: an automated pipeline for the setup of Poisson-Boltzmann electrostatics calculations. *Nucleic Acids Res*, 32, W665-7.
- Dong, Q. & Li, F.** 2022. Cell cycle control of kinetochore assembly. *Nucleus*, 13, 208-220.
- Dorée, M. & Galas, S.** 1994. The cyclin-dependent protein kinases and the control of cell division. *The FASEB journal*, 8, 1114-1121.
- Doronina, T. V., Ashapkin, V. V. & Lazareva, E. M.** 2022. Wheat Antipodal Cells with Polytene Chromosomes in the Embryo Sac Are Key to Understanding the Formation of Grain in Cereals. *Biology*, 11, 1340.
- Dpooležel, J., Binarová, P. & Lcretti, S.** 1989. Analysis of nuclear DNA content in plant cells by flow cytometry. *Biologia plantarum*, 31, 113-120.
- Drews, G. N. & Koltunow, A. M.** 2011. The female gametophyte. *The Arabidopsis book/American Society of Plant Biologists*, 9.
- Earnshaw, W. C. & Rothfield, N.** 1985. Identification of a family of human centromere proteins using autoimmune sera from patients with scleroderma. *Chromosoma*, 91, 313-321.
- Edger, P. P., Hall, J. C., Harkess, A., Tang, M., Coombs, J., Mohammadin, S., Schranz, M. E., Xiong, Z., Leebens-Mack, J. & Meyers, B. C.** 2018. Brassicales phylogeny inferred from 72 plastid genes: a reanalysis of the phylogenetic localization of two paleopolyploid events and origin of novel chemical defenses. *American journal of botany*, 105, 463-469.
- Edwards, K., Johnstone, C. & Thompson, C.** 1991. A simple and rapid method for the preparation of plant genomic DNA for PCR analysis. *Nucleic Acids Research*, 19, 1349-1349.
- Embley, T. M., Van Der Giezen, M., Horner, D. S., Dyal, P. L. & Foster, P.** 2003. Mitochondria and hydrogenosomes are two forms of the same fundamental organelle. *Philosophical Transactions of the Royal Society of London. Series B, Biological Sciences*, 358, 191-201; discussion 201-202.
- Eysholdt-Derzsó, E., Renziehausen, T., Frings, S., Frohn, S., Von Bongartz, K., Igisch, C. P., Mann, J., Häger, L., Macholl, J., Leisse, D., . . . Schmidt-Schippers, R. R.** 2023. Endoplasmic reticulum-bound ANAC013 factor is cleaved by RHOMBOID-LIKE 2 during the initial response to hypoxia in *Arabidopsis thaliana*. *Proceedings of the National Academy of Sciences*, 120, e2221308120.
- Fachinetti, D., Diego Folco, H., Nechemia-Arbely, Y., Valente, L. P., Nguyen, K., Wong, A. J., Zhu, Q., Holland, A. J., Desai, A., Jansen, L. E. T., . . . Cleveland, D. W.** 2013. A two-step mechanism for epigenetic specification of centromere identity and function. *Nature Cell Biology*, 15, 1056-1066.
- Ferreira, L. T. & Maiato, H.** Prometaphase. *Seminars in Cell & Developmental Biology*, 2021. Elsevier, 52-61.
- Fiserova, J. & Goldberg, M. W.** 2010. Relationships at the nuclear envelope: lamins and nuclear pore complexes in animals and plants. *Biochemical Society Transactions*, 38, 829-831.
- Foley, E. A. & Kapoor, T. M.** 2013. Microtubule attachment and spindle assembly checkpoint signalling at the kinetochore. *Nature reviews Molecular cell biology*, 14, 25-37.

- Foltz, D. R., Jansen, L. E., Black, B. E., Bailey, A. O., Yates III, J. R. & Cleveland, D. W.** 2006. The human CENP-A centromeric nucleosome-associated complex. *Nature cell biology*, 8, 458-469.
- Franklin, A. E. & Cande, W. Z.** 1999. Nuclear organization and chromosome segregation. *The Plant Cell*, 11, 523-534.
- French, B. T. & Straight, A. F.** 2019. CDK phosphorylation of *Xenopus laevis* M18BP1 promotes its metaphase centromere localization. *The EMBO journal*, 38, e100093.
- French, B. T., Westhorpe, F. G., Limouse, C. & Straight, A. F.** 2017. *Xenopus laevis* M18BP1 Directly Binds Existing CENP-A Nucleosomes to Promote Centromeric Chromatin Assembly. *Developmental Cell*, 42, 190-199.e10.
- Friis, E. M., Pedersen, K. R. & Crane, P. R.** 2016. The emergence of core eudicots: new floral evidence from the earliest Late Cretaceous. *Proceedings of the Royal Society B: Biological Sciences*, 283, 20161325.
- Fujita, Y., Hayashi, T., Kiyomitsu, T., Toyoda, Y., Kokubu, A., Obuse, C. & Yanagida, M.** 2007. Priming of Centromere for CENP-A Recruitment by Human hMis18 α , hMis18 β , and M18BP1. *Developmental Cell*, 12, 17-30.
- Gehring, M.** 2013. Genomic imprinting: insights from plants. *Annual review of genetics*, 47, 187-208.
- Genschik, P., Marrocco, K., Bach, L., Noir, S. & Criqui, M.-C.** 2014. Selective protein degradation: a rheostat to modulate cell-cycle phase transitions. *Journal of Experimental Botany*, 65, 2603-2615.
- Grafi, G. & Larkins, B. A.** 1995. Endoreduplication in maize endosperm: involvement of M phase—promoting factor inhibition and induction of S phase—related kinases. *Science*, 269, 1262-1264.
- Halbritter, H., Ulrich, S., Grímsson, F., Weber, M., Zetter, R., Hesse, M., Buchner, R., Svojtka, M., Frosch-Radivo, A. & Halbritter, H.** 2018. Pollen development. *Illustrated Pollen Terminology*, 23-35.
- Hamamura, Y., Saito, C., Awai, C., Kurihara, D., Miyawaki, A., Nakagawa, T., Kanaoka, M. M., Sasaki, N., Nakano, A. & Berger, F.** 2011. Live-cell imaging reveals the dynamics of two sperm cells during double fertilization in *Arabidopsis thaliana*. *Current Biology*, 21, 497-502.
- Hara, M., Ariyoshi, M., Sano, T., Nozawa, R.-S., Shinkai, S., Onami, S., Jansen, I., Hirota, T. & Fukagawa, T.** 2023. Centromere/kinetochore is assembled through CENP-C oligomerization. *Molecular Cell*, 83, 2188-2205.e13.
- Hartley, J. L., Temple, G. F. & Brasch, M. A.** 2000. DNA cloning using in vitro site-specific recombination. *Genome research*, 10, 1788-1795.
- Hayashi, T., Fujita, Y., Iwasaki, O., Adachi, Y., Takahashi, K. & Yanagida, M.** 2004. Mis16 and Mis18 are required for CENP-A loading and histone deacetylation at centromeres. *Cell*, 118, 715-729.
- Hehenberger, E., Kradolfer, D. & Köhler, C.** 2012. Endosperm cellularization defines an important developmental transition for embryo development. *Development*, 139, 2031-2039.
- Hendzel, M. J., Wei, Y., Mancini, M. A., Van Hooser, A., Ranalli, T., Brinkley, B., Bazett-Jones, D. P. & Allis, C. D.** 1997. Mitosis-specific phosphorylation of histone H3 initiates primarily within pericentromeric heterochromatin during G2 and spreads in an ordered fashion coincident with mitotic chromosome condensation. *Chromosoma*, 106, 348-360.
- Henikoff, S., Ahmad, K. & Malik, H. S.** 2001. The centromere paradox: stable inheritance with rapidly evolving DNA. *Science*, 293, 1098-1102.
- Higashiyama, T.** 2002. The synergid cell: attractor and acceptor of the pollen tube for double fertilization. *Journal of plant research*, 115, 0149-0160.
- Higgins, J. D., Sanchez-Moran, E., Armstrong, S. J., Jones, G. H. & Franklin, F. C. H.** 2005. The *Arabidopsis* synaptonemal complex protein ZYP1 is required for chromosome synapsis and normal fidelity of crossing over. *Genes & development*, 19, 2488-2500.
- Hirai, H., Shogaki, Y. & Sato, M.** 2022. The Mis6 inner kinetochore subcomplex maintains CENP-A nucleosomes against centromeric non-coding transcription during mitosis. *Communications Biology*, 5, 818.
- Hiraoka, Y., Agard, D. A. & Sedat, J. W.** 1990. Temporal and spatial coordination of chromosome movement, spindle formation, and nuclear envelope breakdown during prometaphase in *Drosophila melanogaster* embryos. *The Journal of cell biology*, 111, 2815-2828.

- Ho, K.-H., Tsuchiya, D., Oliger, A. C. & Lacefield, S. 2014. Localization and function of budding yeast CENP-A depends upon kinetochore protein interactions and is independent of canonical centromere sequence. *Cell reports*, 9, 2027-2033.
- Hoffmann, S., Dumont, M., Barra, V., Ly, P., Nechemia-Arbely, Y., McMahon, M. A., Hervé, S., Cleveland, D. W. & Fachinetti, D. 2016. CENP-A is dispensable for mitotic centromere function after initial centromere/kinetochore assembly. *Cell reports*, 17, 2394-2404.
- Holder, J., Mohammed, S. & Barr, F. A. 2020. Ordered dephosphorylation initiated by the selective proteolysis of cyclin B drives mitotic exit. *Elife*, 9, e59885.
- Hori, T., Shang, W.-H., Hara, M., Ariyoshi, M., Arimura, Y., Fujita, R., Kurumizaka, H. & Fukagawa, T. 2017. Association of M18BP1/KNL2 with CENP-A Nucleosome Is Essential for Centromere Formation in Non-mammalian Vertebrates. *Developmental Cell*, 42, 181-189.e3.
- Howard, A. & Pelc, S. 1953. Heredity. *Suppl*, 6, 261.
- Huang, H., Strømme, C. B., Saredi, G., Hödl, M., Strandsby, A., González-Aguilera, C., Chen, S., Groth, A. & Patel, D. J. 2015. A unique binding mode enables MCM2 to chaperone histones H3-H4 at replication forks. *Nature structural & molecular biology*, 22, 618-626.
- Huang, J., Rauscher, S., Nawrocki, G., Ran, T., Feig, M., De Groot, B. L., Grubmüller, H. & Mackerell, A. D., Jr. 2017. CHARMM36m: an improved force field for folded and intrinsically disordered proteins. *Nat Methods*, 14, 71-73.
- Imai, K. K., Ohashi, Y., Tsuge, T., Yoshizumi, T., Matsui, M., Oka, A. & Aoyama, T. 2006. The A-type cyclin CYCA2; 3 is a key regulator of ploidy levels in Arabidopsis endoreduplication. *The Plant Cell*, 18, 382-396.
- Izawa, D. & Pines, J. 2011. How APC/C-Cdc20 changes its substrate specificity in mitosis. *Nature cell biology*, 13, 223-233.
- Jacob, S. M. 1839. Beiträge zur Phytogenesis. *Archiv für Anatomie, Physiologie und wissenschaftliche Medizin*, 1838, 137-176.
- Jaške, K., Mokroš, P., Mozgová, I., Fojtová, M. & Fajkus, J. 2013. A telomerase-independent component of telomere loss in chromatin assembly factor 1 mutants of Arabidopsis thaliana. *Chromosoma*, 122, 285-293.
- Jiang, H., Ariyoshi, M., Watanabe, R., Makino, F., Namba, K. & Fukagawa, T. 2022. The cryo-EM structure of the CENP-A nucleosome in complex with ggKNL2. *Biochemistry*.
- Johri, B. & Ambegaokar, K. 1984. Embryology: then and now. *Embryology of angiosperms*. Springer.
- Jozefkiewicz, C., Bottero, E., Pascuan, C., Pagano, E., Ayub, N. D. & Soto, G. 2016. Minimizing the time and cost of production of transgenic alfalfa libraries using the highly efficient completely sequenced vector pPZP200BAR. *Plant cell reports*, 35, 1987-1990.
- Kabsch, W. & Sander, C. 1983. Dictionary of protein secondary structure: pattern recognition of hydrogen-bonded and geometrical features. *Biopolymers*, 22, 2577-637.
- Kalinowska, K., Chamas, S., Unkel, K., Demidov, D., Lermontova, I., Dresselhaus, T., Kumlehn, J., Dunemann, F. & Houben, A. 2019. State-of-the-art and novel developments of in vivo haploid technologies. *Theoretical and Applied Genetics*, 132, 593-605.
- Kamenz, J. & Hauf, S. 2014. Slow checkpoint activation kinetics as a safety device in anaphase. *Current Biology*, 24, 646-651.
- Klepikova, A. V., Kasianov, A. S., Gerasimov, E. S., Logacheva, M. D. & Penin, A. A. 2016. A high resolution map of the Arabidopsis thaliana developmental transcriptome based on RNA-seq profiling. *The Plant Journal*, 88, 1058-1070.
- Kops, G. J. & Gassmann, R. 2020. Crowning the kinetochore: the fibrous corona in chromosome segregation. *Trends in cell biology*, 30, 653-667.
- Kubalová, I., Němečková, A., Weissart, K., Hřibová, E. & Schubert, V. 2021. Comparing Super-Resolution Microscopy Techniques to Analyze Chromosomes. *International Journal of Molecular Sciences*, 22, 1903.
- Kursel, L. E. & Malik, H. S. 2017. Recurrent gene duplication leads to diverse repertoires of centromeric histones in Drosophila species. *Molecular biology and evolution*, 34, 1445-1462.
- Kursel, L. E., Welsh, F. C. & Malik, H. S. 2020. Ancient corentention of paralogs of Cid centromeric histones and Cal1 chaperones in mosquito species. *Molecular Biology and Evolution*, 37, 1949-1963.

- Le Goff, S., Keçeli, B. N., Jeřábková, H., Heckmann, S., Rutten, T., Cotterell, S., Schubert, V., Roitinger, E., Mechtler, K. & Franklin, F. C. H. 2020. The H3 histone chaperone NASPSIM3 escorts CenH3 in Arabidopsis. *The Plant Journal*, 101, 71-86.
- Lechner, J. & Carbon, J. 1991. A 240 kd multisubunit protein complex, CBF3, is a major component of the budding yeast centromere. *Cell*, 64, 717-725.
- Lee, H. O., Davidson, J. M. & Duronio, R. J. 2009. Endoreplication: polyploidy with purpose. *Genes Dev*, 23, 2461-77.
- Lee, S. C., Adams, D. W., Ipsaro, J. J., Cahn, J., Lynn, J., Kim, H.-S., Berube, B., Major, V., Calarco, J. P., Leblanc, C., . . . Martienssen, R. A. 2023. Chromatin remodeling of histone H3 variants underlies epigenetic inheritance of DNA methylation. *bioRxiv*, 2023.07.11.548598.
- Leiva-Neto, J. T., Grafi, G., Sabelli, P. A., Dante, R. A., Woo, Y.-M., Maddock, S., Gordon-Kamm, W. J. & Larkins, B. A. 2004. A dominant negative mutant of cyclin-dependent kinase A reduces endoreduplication but not cell size or gene expression in maize endosperm. *The Plant Cell*, 16, 1854-1869.
- Lermontova, I. 2017. *Generation of haploid plants based on knl2*. PCT/EP2016/071559. 2017-04-27.
- Lermontova, I., Fuchs, J., Schubert, V. & Schubert, I. 2007. Loading time of the centromeric histone H3 variant differs between plants and animals. *Chromosoma*, 116, 507-510.
- Lermontova, I., Koroleva, O., Rutten, T., Fuchs, J., Schubert, V., Moraes, I., Koszegi, D. & Schubert, I. 2011. Knockdown of CENH3 in Arabidopsis reduces mitotic divisions and causes sterility by disturbed meiotic chromosome segregation. *The Plant Journal*, 68, 40-50.
- Lermontova, I., Kuhlmann, M., Friedel, S., Rutten, T., Heckmann, S., Sandmann, M., Demidov, D., Schubert, V. & Schubert, I. 2013. Arabidopsis KINETOCHORE NULL2 Is an Upstream Component for Centromeric Histone H3 Variant cenH3 Deposition at Centromeres[W]. *The Plant Cell*, 25, 3389-3404.
- Lermontova, I., Sandmann, M., Mascher, M., Schmit, A.-C. & Chabouté, M.-E. 2015. Centromeric chromatin and its dynamics in plants. *The Plant Journal*, 83, 4-17.
- Lermontova, I., Schubert, V., Fuchs, J., Klatte, S., Macas, J. & Schubert, I. 2006. Loading of Arabidopsis centromeric histone CENH3 occurs mainly during G2 and requires the presence of the histone fold domain. *Plant Cell*, 18, 2443-51.
- Levan, A. & Hauschka, T. S. 1953. Endomitotic reduplication mechanisms in ascites tumors of the mouse. *Journal of the National Cancer Institute*, 14, 1-43.
- Liebelt, F., Jansen, N. S., Kumar, S., Gracheva, E., Claessens, L. A., Verlaan-De Vries, M., Willemstein, E. & Vertegaal, A. C. 2019. The poly-SUMO2/3 protease SENP6 enables assembly of the constitutive centromere-associated network by group deSUMOylation. *Nature Communications*, 10, 3987.
- Lilly, M. A. & Spradling, A. C. 1996. The Drosophila endocycle is controlled by Cyclin E and lacks a checkpoint ensuring S-phase completion. *Genes & development*, 10, 2514-2526.
- Liu, B. & Lee, Y.-R. J. 2022. Spindle assembly and mitosis in plants. *Annual Review of Plant Biology*, 73, 227-254.
- Liu, B. & Palevitz, B. A. 1991. Kinetochore fiber formation in dividing generative cells of Tradescantia kinetochore reorientation associated with the transition between lateral microtubule interactions and end-on kinetochore fibers. *Journal of Cell Science*, 98, 475-482.
- Luger, K., Mäder, A. W., Richmond, R. K., Sargent, D. F. & Richmond, T. J. 1997a. Crystal structure of the nucleosome core particle at 2.8 Å resolution. *Nature*, 389, 251-260.
- Luger, K., Rechsteiner, T. J., Flaus, A. J., Waye, M. M. & Richmond, T. J. 1997b. Characterization of nucleosome core particles containing histone proteins made in bacteria. *Journal of molecular biology*, 272, 301-311.
- Luo, M., Bilodeau, P., Dennis, E. S., Peacock, W. J. & Chaudhury, A. 2000. Expression and parent-of-origin effects for FIS2, MEA, and FIE in the endosperm and embryo of developing Arabidopsis seeds. *Proceedings of the National Academy of Sciences*, 97, 10637-10642.
- Lv, J., Yu, K., Wei, J., Gui, H., Liu, C., Liang, D., Wang, Y., Zhou, H., Carlin, R. & Rich, R. 2020. Generation of paternal haploids in wheat by genome editing of the centromeric histone CENH3. *Nature Biotechnology*, 38, 1397-1401.
- Ma, H. 2005. Molecular genetic analyses of microsporogenesis and microgametogenesis in flowering plants. *Annu. Rev. Plant Biol.*, 56, 393-434.

- Maddox, P. S., Hyndman, F., Monen, J., Oegema, K. & Desai, A. 2007. Functional genomics identifies a Myb domain-containing protein family required for assembly of CENP-A chromatin. *The Journal of Cell Biology*, 176, 757-763.
- Marrocco, K., Thomann, A., Parmentier, Y., Genschik, P. & Criqui, M. C. 2009. The APC/C E3 ligase remains active in most post-mitotic Arabidopsis cells and is required for proper vasculature development and organization.
- Mathieu-Rivet, E., Gévaudant, F., Sicard, A., Salar, S., Do, P. T., Mouras, A., Fernie, A. R., Gibon, Y., Rothan, C. & Chevalier, C. 2010. Functional analysis of the anaphase promoting complex activator CCS52A highlights the crucial role of endo-reduplication for fruit growth in tomato. *The Plant Journal*, 62, 727-741.
- Mazia, D. 1961. Mitosis and the physiology of cell division. *The cell*. Elsevier.
- Mcainsh, A. D. & Kops, G. J. 2023. Principles and dynamics of spindle assembly checkpoint signalling. *Nature Reviews Molecular Cell Biology*, 24, 543-559.
- McGhee, J. D. & Felsenfeld, G. 1980. Nucleosome structure. *Annual review of biochemistry*, 49, 1115-1156.
- Mcintosh, J. R. 1985. Spindle structure and the mechanisms of chromosome movement. *Aneuploidy: etiology and mechanisms*. Springer.
- Mcintosh, J. R. 2016. Mitosis. *Cold Spring Harbor perspectives in biology*, 8, a023218.
- Mckinley, K. L. & Cheeseman, I. M. 2014. Polo-like Kinase 1 Licenses CENP-A Deposition at Centromeres. *Cell*, 158, 397-411.
- Mckinley, K. L. & Cheeseman, I. M. 2016. The molecular basis for centromere identity and function. *Nature Reviews Molecular Cell Biology*, 17, 16-29.
- Meinke, D. W. 2020. Genome-wide identification of EMBRYO-DEFECTIVE (EMB) genes required for growth and development in Arabidopsis. *New Phytologist*, 226, 306-325.
- Mellone, B. G. & Fachinetti, D. 2021. Diverse mechanisms of centromere specification. *Current Biology*, 31, R1491-R1504.
- Meraldi, P., Mcainsh, A. D., Rheinbay, E. & Sorger, P. K. 2006. Phylogenetic and structural analysis of centromeric DNA and kinetochore proteins. *Genome biology*, 7, 1-21.
- Miller, S. L. 1953. A Production of Amino Acids Under Possible Primitive Earth Conditions. *Science*, 117, 528-529.
- Misteli, T. 2020. The self-organizing genome: principles of genome architecture and function. *Cell*, 183, 28-45.
- Mitra, S., Srinivasan, B. & Jansen, L. E. 2020. Stable inheritance of CENP-A chromatin: Inner strength versus dynamic control. *The Journal of Cell Biology*, 219.
- Mo, X., Kowenz-Leutz, E., Laumonier, Y., Xu, H. & Leutz, A. 2005. Histone H3 tail positioning and acetylation by the c-Myb but not the v-Myb DNA-binding SANT domain. *Genes & development*, 19, 2447-2457.
- Moree, B., Meyer, C. B., Fuller, C. J. & Straight, A. F. 2011. CENP-C recruits M18BP1 to centromeres to promote CENP-A chromatin assembly. *Journal of Cell Biology*, 194, 855-871.
- Muralla, R., Lloyd, J. & Meinke, D. 2011. Molecular foundations of reproductive lethality in Arabidopsis thaliana. *PloS one*, 6, e28398.
- Murray, A. W. & Szostak, J. W. 1983. Construction of artificial chromosomes in yeast. *Nature*, 305, 189-193.
- Musacchio, A. & Desai, A. 2017. A Molecular View of Kinetochore Assembly and Function. *Biology*, 6, 5.
- Nagata, Y., Muro, Y. & Todokoro, K. 1997. Thrombopoietin-induced polyploidization of bone marrow megakaryocytes is due to a unique regulatory mechanism in late mitosis. *The Journal of cell biology*, 139, 449-457.
- Nakamura, S., Mano, S., Tanaka, Y., Ohnishi, M., Nakamori, C., Araki, M., Niwa, T., Nishimura, M., Kaminaka, H. & Nakagawa, T. 2010. Gateway binary vectors with the bialaphos resistance gene, bar, as a selection marker for plant transformation. *Bioscience, biotechnology, and biochemistry*, 74, 1315-1319.
- Nardi, I. K., Zasadzińska, E., Stellfox, M. E., Knippler, C. M. & Foltz, D. R. 2016. Licensing of Centromeric Chromatin Assembly through the Mis18 α -Mis18 β Heterotetramer. *Molecular Cell*, 61, 774-787.

- Neumann, P., Oliveira, L., Jang, T.-S., Novák, P., Koblížková, A., Schubert, V., Houben, A. & Macas, J. 2023. Disruption of the standard kinetochore in holocentric *Cuscuta* species. *Proceedings of the National Academy of Sciences*, 120, e2300877120.
- Nishimura, K., Komiya, M., Hori, T., Itoh, T. & Fukagawa, T. 2019. 3D genomic architecture reveals that neocentromeres associate with heterochromatin regions. *The Journal of cell biology*, 218, 134.
- Oegema, K., Desai, A., Rybina, S., Kirkham, M. & Hyman, A. A. 2001. Functional analysis of kinetochore assembly in *Caenorhabditis elegans*. *The Journal of cell biology*, 153, 1209-1226.
- Oliveira, L., Neumann, P., Jang, T.-S., Klemme, S., Schubert, V., Koblížková, A., Houben, A. & Macas, J. 2020. Mitotic spindle attachment to the holocentric chromosomes of *Cuscuta europaea* does not correlate with the distribution of CENH3 chromatin. *Frontiers in Plant Science*, 10, 1799.
- Olsen, O.-A. 2004. Nuclear endosperm development in cereals and *Arabidopsis thaliana*. *The Plant Cell*, 16, S214-S227.
- Owen, H. A. & Makaroff, C. 1995. Ultrastructure of microsporogenesis and microgametogenesis in *Arabidopsis thaliana* (L.) Heynh. ecotype Wassilewskija (Brassicaceae). *Protoplasma*, 185, 7-21.
- Paganelli, L., Caillaud, M. C., Quentin, M., Damiani, I., Govetto, B., Lecomte, P., Karpov, P. A., Abad, P., Chabouté, M. E. & Favery, B. 2015. Retracted: Three BUB 1 and BUBR 1/MAD 3-related spindle assembly checkpoint proteins are required for accurate mitosis in *Arabidopsis*. *New Phytologist*, 205, 202-215.
- Pan, D., Klare, K., Petrovic, A., Take, A., Walstein, K., Singh, P., Rondelet, A., Bird, A. W. & Musacchio, A. 2017. CDK-regulated dimerization of M18BP1 on a Mis18 hexamer is necessary for CENP-A loading. *eLife*, 6, e23352.
- Pasteur, L. & Edelfelt, A. 1886. *Pasteur*, Mr. Deschiens.
- Peris, C. I. L., Rademacher, E. H. & Weijers, D. 2010. Green beginnings—pattern formation in the early plant embryo. *Current topics in developmental biology*, 91, 1-27.
- Petronczki, M., Siomos, M. F. & Nasmyth, K. 2003. Un ménage à quatre: the molecular biology of chromosome segregation in meiosis. *Cell*, 112, 423-440.
- Petryk, N., Dalby, M., Wenger, A., Stromme, C. B., Strandsby, A., Andersson, R. & Groth, A. 2018. MCM2 promotes symmetric inheritance of modified histones during DNA replication. *Science*, 361, 1389-1392.
- Pettkó-Szandtner, A., Magyar, Z. & Komaki, S. 2024. Functional framework of the kinetochore and spindle assembly checkpoint in *Arabidopsis thaliana*. *bioRxiv*, 2024.11. 04.621965.
- Pickett-Heaps, J. & Northcote, D. 1966. Organization of microtubules and endoplasmic reticulum during mitosis and cytokinesis in wheat meristems. *Journal of cell science*, 1, 109-120.
- Pidoux, A. L., Choi, E. S., Abbott, J. K., Liu, X., Kagansky, A., Castillo, A. G., Hamilton, G. L., Richardson, W., Rappsilber, J. & He, X. 2009. Fission yeast Scm3: A CENP-A receptor required for integrity of subkinetochore chromatin. *Molecular cell*, 33, 299-311.
- Polymenis, M. 2022. *Two from one: a short introduction to cell division mechanisms*, John Wiley & Sons.
- Poole, A. M. & Penny, D. 2007. Evaluating hypotheses for the origin of eukaryotes. *BioEssays*, 29, 74-84.
- Probst, A. V., Dunleavy, E. & Almouzni, G. 2009. Epigenetic inheritance during the cell cycle. *Nature reviews Molecular cell biology*, 10, 192-206.
- Prosée, R. F., Wenda, J. M., Özdemir, I., Gabus, C., Delaney, K., Schwager, F., Gotta, M. & Steiner, F. A. 2021. Transgenerational inheritance of centromere identity requires the CENP-A N-terminal tail in the *C. elegans* maternal germ line. *PLoS Biology*, 19, e3000968.
- Ramakrishnan Chandra, J., Kalidass, M., Demidov, D., Dabravolski, S. A. & Lermontova, I. 2023. The role of centromeric repeats and transcripts in kinetochore assembly and function. *The Plant Journal*, n/a.
- Ravi, M., Shibata, F., Ramahi, J. S., Nagaki, K., Chen, C., Murata, M. & Chan, S. W. L. 2011. Meiosis-Specific Loading of the Centromere-Specific Histone CENH3 in *Arabidopsis thaliana*. *PLoS Genetics*, 7, e1002121.

- Renaud-Pageot, C., Quivy, J.-P., Lochhead, M. & Almouzni, G. 2022. CENP-A regulation and cancer. *Frontiers in Cell and Developmental Biology*, 10, 907120.
- Riha, K., Mcknight, T. D., Griffing, L. R. & Shippen, D. E. 2001. Living with genome instability: plant responses to telomere dysfunction. *Science*, 291, 1797-1800.
- Roodbarkelari, F., Bramsiepe, J., Weinl, C., Marquardt, S., Novák, B., Jakoby, M. J., Lechner, E., Genschik, P. & Schnittger, A. 2010. Cullin 4-ring finger-ligase plays a key role in the control of endoreplication cycles in *Arabidopsis* trichomes. *Proceedings of the National Academy of Sciences*, 107, 15275-15280.
- Rosas-Salvans, M., Sutanto, R., Suresh, P. & Dumont, S. 2022. The Astrin-SKAP complex reduces friction at the kinetochore-microtubule interface. *Current Biology*, 32, 2621-2631. e3.
- Safavian, D., Zayed, Y., Indriolo, E., Chapman, L., Ahmed, A. & Goring, D. R. 2015. RNA Silencing of Exocyst Genes in the Stigma Impairs the Acceptance of Compatible Pollen in *Arabidopsis*. *Plant Physiology*, 169, 2526-2538.
- Sakamoto, Y. & Takagi, S. 2013. LITTLE NUCLEI 1 and 4 regulate nuclear morphology in *Arabidopsis thaliana*. *Plant and Cell Physiology*, 54, 622-633.
- Salinas-Luypaert, C. & Fachinetti, D. 2024. Canonical and noncanonical regulators of centromere assembly and maintenance. *Current Opinion in Cell Biology*, 89, 102396.
- Sandmann, M., Talbert, P., Demidov, D., Kuhlmann, M., Rutten, T., Conrad, U. & Lermontova, I. 2017. Targeting of *Arabidopsis* KNL2 to Centromeres Depends on the Conserved CENPC-k Motif in Its C Terminus. *The Plant Cell*, 29, 144-155.
- Sax, K. & O'mara, J. 1941. Mechanism of mitosis in pollen tubes. *Botanical Gazette*, 102, 629-636.
- Schrader, F. 1936. The kinetochore or spindle fibre locus in *Amphiuma tridactylum*. *The Biological Bulletin*, 70, 484-498.
- Schubert, V., Neumann, P., Marques, A., Heckmann, S., Macas, J., Pedrosa-Harand, A., Schubert, I., Jang, T.-S. & Houben, A. 2020. Super-resolution microscopy reveals diversity of plant centromere architecture. *International journal of molecular sciences*, 21, 3488.
- Schwann, T. 1847. *Microscopical researches into the accordance in the structure and growth of animals and plants*, Sydenham society.
- Serralbo, O., Pérez-Pérez, J. M., Heidstra, R. & Scheres, B. 2006. Non-cell-autonomous rescue of anaphase-promoting complex function revealed by mosaic analysis of HOBBIT, an *Arabidopsis* CDC27 homolog. *Proceedings of the National Academy of Sciences*, 103, 13250-13255.
- Sharp, L. W. 1934. *Introduction to cytology*, New York, McGraw-Hill Book Co.
- Shin, J., Jeong, G., Park, J.-Y., Kim, H. & Lee, I. 2018. MUN (MERISTEM UNSTRUCTURED), encoding a SPC24 homolog of NDC80 kinetochore complex, affects development through cell division in *Arabidopsis thaliana*. *The Plant Journal*, 93, 977-991.
- Shu, Z., Row, S. & Deng, W. M. 2018. Endoreplication: The Good, the Bad, and the Ugly. *Trends Cell Biol*, 28, 465-474.
- Silva, M. C. C., Bodor, D. L., Stellfox, M. E., Martins, N. M. C., Hohegger, H., Foltz, D. R. & Jansen, L. E. T. 2012. Cdk activity couples epigenetic centromere inheritance to cell cycle progression. *Developmental Cell*, 22, 52-63.
- Smertenko, A. 2018. Phragmoplast expansion: the four-stroke engine that powers plant cytokinesis. *Current Opinion in Plant Biology*, 46, 130-137.
- Smith, L. & Maddox, P. S. 2017. Reading the Centromere Epigenetic Mark. *Developmental Cell*, 42, 110-112.
- Song, X., Yuan, L. & Sundaresan, V. 2014. Antipodal cells persist through fertilization in the female gametophyte of *Arabidopsis*. *Plant reproduction*, 27, 197-203.
- Spiller, F., Medina-Pritchard, B., Abad, M. A., Wear, M. A., Molina, O., Earnshaw, W. C. & Jeyaprakash, A. A. 2017. Molecular basis for Cdk1-regulated timing of Mis18 complex assembly and CENP-A deposition. *EMBO reports*, 18, 894-905.
- Stellfox, M. E., Bailey, A. O. & Foltz, D. R. 2013. Putting CENP-A in its place. *Cell Mol Life Sci*, 70, 387-406.
- Stellfox, M. E., Nardi, I. K., Knippler, C. M. & Foltz, D. R. 2016. Differential Binding Partners of the Mis18 α/β YIPPEE Domains Regulate Mis18 Complex Recruitment to Centromeres. *Cell Reports*, 15, 2127-2135.

- Stirpe, A. & Heun, P.** The ins and outs of CENP-A: Chromatin dynamics of the centromere-specific histone. *Seminars in Cell & Developmental Biology*, 2023. Elsevier, 24-34.
- Strick, J. E.** 1997. *The British spontaneous generation debates of 1860-1880: medicine, evolution, and laboratory science in the victorian context*, Princeton University.
- Su, X. B., Wang, M., Schaffner, C., Nerusheva, O. O., Clift, D., Spanos, C., Kelly, D. A., Tatham, M., Wallek, A., Wu, Y., . . . Marston, A. L.** 2021. SUMOylation stabilizes sister kinetochore biorientation to allow timely anaphase. *Journal of Cell Biology*, 220, e202005130.
- Su'udi, M., Cha, J.-Y., Jung, M. H., Ermawati, N., Han, C.-D., Kim, M. G., Woo, Y.-M. & Son, D.** 2012. Potential role of the rice OsCCS52A gene in endoreduplication. *Planta*, 235, 387-397.
- Subramanian, L., Medina-Pritchard, B., Barton, R., Spiller, F., Kulasegaran-Shylini, R., Radaviciute, G., Allshire, R. C. & Arockia Jeyaprakash, A.** 2016. Centromere localization and function of Mis18 requires Yippee-like domain-mediated oligomerization. *EMBO reports*, 17, 496-507.
- Talbert, P. B., Bryson, T. D. & Henikoff, S.** 2004. Adaptive evolution of centromere proteins in plants and animals. *Journal of biology*, 3, 1-17.
- Talbert, P. B. & Henikoff, S.** 2018. Transcribing centromeres: noncoding RNAs and kinetochore assembly. *Trends in Genetics*, 34, 587-599.
- Talbert, P. B., Masuelli, R., Tyagi, A. P., Comai, L. & Henikoff, S.** 2002. Centromeric localization and adaptive evolution of an Arabidopsis histone H3 variant. *The Plant Cell*, 14, 1053-1066.
- Tourdot, E., Mauxion, J. P., Gonzalez, N. & Chevalier, C.** 2023. Endoreduplication in plant organogenesis: a means to boost fruit growth. *J Exp Bot*, 74, 6269-6284.
- Umbreit, N. T., Gestaut, D. R., Tien, J. F., Vollmar, B. S., Gonen, T., Asbury, C. L. & Davis, T. N.** 2012. The Ndc80 kinetochore complex directly modulates microtubule dynamics. *Proceedings of the National Academy of Sciences*, 109, 16113-16118.
- Varas, J., Santos, J. L. & Pradillo, M.** 2017. The absence of the Arabidopsis chaperone complex CAF-1 produces mitotic chromosome abnormalities and changes in the expression profiles of genes involved in DNA repair. *Frontiers in plant science*, 8, 525.
- Vermeulen, K., Berneman, Z. N. & Van Bockstaele, D. R.** 2003a. Cell cycle and apoptosis. *Cell proliferation*, 36, 165-175.
- Vermeulen, K., Van Bockstaele, D. R. & Berneman, Z. N.** 2003b. The cell cycle: a review of regulation, deregulation and therapeutic targets in cancer. *Cell proliferation*, 36, 131-149.
- Vikal, Y. & Kaur, D.** 2017. Nucleus. *Plant Cells and their Organelles*, 146-208.
- Vitrat, N., Cohen-Solal, K., Pique, C., Lecouedic, J. P., Norol, F., Larsen, A. K., Katz, A., Vainchenker, W. & Debili, N.** 1998. Endomitosis of human megakaryocytes are due to abortive mitosis. *Blood, The Journal of the American Society of Hematology*, 91, 3711-3723.
- Waadt, R. & Kudla, J.** 2008. In planta visualization of protein interactions using bimolecular fluorescence complementation (BiFC). *Cold Spring Harbor Protocols*, 2008, pdb. prot4995.
- Walhout, A. J., Temple, G. F., Brasch, M. A., Hartley, J. L., Lorson, M. A., Van Den Heuvel, S. & Vidal, M.** 2000. GATEWAY recombinational cloning: Application to the cloning of large numbers of open reading frames or ORFeomes. *Methods in enzymology*. Elsevier.
- Wang, H., Dittmer, T. A. & Richards, E. J.** 2013. Arabidopsis CROWDED NUCLEI (CRWN) proteins are required for nuclear size control and heterochromatin organization. *BMC plant biology*, 13, 1-13.
- Wang, N., Gent, J. I. & Dawe, R. K.** 2021. Haploid induction by a maize cenH3 null mutant. *Science Advances*, 7, eabe2299.
- Watanabe, R., Hara, M., Okumura, E.-I., Hervé, S., Fachinetti, D., Ariyoshi, M. & Fukagawa, T.** 2019. CDK1-mediated CENP-C phosphorylation modulates CENP-A binding and mitotic kinetochore localization. *Journal of Cell Biology*, 218, 4042-4062.
- Weisshart, K., Fuchs, J. & Schubert, V.** 2016. Structured Illumination Microscopy (SIM) and Photoactivated Localization Microscopy (PALM) to Analyze the Abundance and Distribution of RNA Polymerase II Molecules on Flow-sorted Arabidopsis Nuclei. *Bio-protocol*, 6, e1725-e1725.
- Wenda, J. M., Prosée, R. F., Gabus, C. & Steiner, F. A.** 2021. Mitotic chromosome condensation requires phosphorylation of the centromeric protein KNL-2 in *C. elegans*. *Journal of Cell Science*, 134, jcs259088.

- Wu, J. 1999. *Mutant analysis of endosperm development in Arabidopsis*. Oklahoma State University.
- Wu, Y., You, H.-L. & Li, X.-Q. 2018. Dinosaur-associated Poaceae epidermis and phytoliths from the Early Cretaceous of China. *National Science Review*, 5, 721-727.
- Xie, X., Backman, D., Lebedev, A. T., Artaev, V. B., Jiang, L., Ilag, L. L. & Zubarev, R. A. 2015. Primordial soup was edible: abiotically produced Miller-Urey mixture supports bacterial growth. *Scientific reports*, 5, 14338.
- Yadala, R., Camara, A. S., Yalagapati, S. P., Jaroschinsky, P., Meitzel, T., Ariyoshi, M., Fukagawa, T., Rutten, T., Bui, T. T. G. & Lermontova, I. 2024. Structural Basis of betaKNL2 Centromeric Targeting Mechanism and Its Role in Plant-Specific Kinetochore Assembly. *bioRxiv*, 2024.07. 30.605747.
- Yadala, R., Ratnikava, M. & Lermontova, I. 2022. Bimolecular Fluorescence Complementation to Test for Protein-Protein Interactions and to Uncover Regulatory Mechanisms During Gametogenesis. *Methods in Molecular Biology (Clifton, N.J.)*, 2484, 107-120.
- Yalagapati, S. P., Ahmadli, U., Sinha, A., Kalidass, M., Dabravolski, S., Zuo, S., Yadala, R., Rutten, T., Talbert, P. & Berr, A. 2024. Centromeric localization of α KNL2 and CENP-C proteins in plants depends on their centromere-targeting domain and DNA-binding regions. *Nucleic Acids Research*, gkae1242.
- Yamagishi, Y., Sakuno, T., Goto, Y. & Watanabe, Y. 2014. Kinetochore composition and its function: lessons from yeasts. *FEMS Microbiology Reviews*, 38, 185-200.
- Yang, F., Fernández Jiménez, N., Majka, J., Pradillo, M. & Pecinka, A. 2021. Structural maintenance of chromosomes 5/6 complex is necessary for tetraploid genome stability in *Arabidopsis thaliana*. *Frontiers in Plant Science*, 12, 748252.
- Yeung, E. C. & Meinke, D. W. 1993. Embryogenesis in angiosperms: development of the suspensor. *The Plant Cell*, 5, 1371.
- Yu, H.-G., Dawe, R. K. & Hiatt, E. N. 2000. The plant kinetochore. *Trends in plant science*, 5, 543-547.
- Yuan, Z., Riera, A., Bai, L., Sun, J., Nandi, S., Spanos, C., Chen, Z. A., Barbon, M., Rappsilber, J. & Stillman, B. 2017. Structural basis of Mcm2–7 replicative helicase loading by ORC–Cdc6 and Cdt1. *Nature structural & molecular biology*, 24, 316-324.
- Zasadzińska, E., Huang, J., Bailey, A. O., Guo, L. Y., Lee, N. S., Srivastava, S., Wong, K. A., French, B. T., Black, B. E. & Foltz, D. R. 2018. Inheritance of CENP-A nucleosomes during DNA replication requires HJURP. *Developmental cell*, 47, 348-362. e7.
- Zhang, D., Martyniuk, C. J. & Trudeau, V. L. 2006. SANTA domain: a novel conserved protein module in Eukaryota with potential involvement in chromatin regulation. *Bioinformatics (Oxford, England)*, 22, 2459-2462.
- Zhang, M., Zheng, F., Xiong, Y., Shao, C., Wang, C., Wu, M., Niu, X., Dong, F., Zhang, X. & Fu, C. 2021. Centromere targeting of Mis18 requires the interaction with DNA and H2A–H2B in fission yeast. *Cellular and Molecular Life Sciences*, 78, 373-384.
- Zhang, W., Lukyanova, N., Miah, S., Lucas, J. & Vaughan, C. K. 2018. Insights into centromere DNA bending revealed by the cryo-EM structure of the core centromere binding factor 3 with Ndc10. *Cell reports*, 24, 744-754.
- Zickler, D. & Kleckner, N. 1999. Meiotic chromosomes: integrating structure and function. *Annual review of genetics*, 33, 603-754.
- Zuo, S., Yadala, R., Yang, F., Talbert, P., Fuchs, J., Schubert, V., Ahmadli, U., Rutten, T., Pecinka, A., Lysak, M. A., . . . Lermontova, I. 2022. Recurrent Plant-Specific Duplications of KNL2 and its Conserved Function as a Kinetochore Assembly Factor. *Molecular Biology and Evolution*, 39, msac123.

Chapter 10: Appendix

Appendix Table 1. List of all primers used in the study

Cloning	
EMD1674_fw	ATGACGACGACGAGGGCGAAGTC
EMD1674_rev	CCAACCGAAACTTCTTCTCCTATTCTTCTTC
EMD1674-attB1	GGGGACAAGTTTGTACAAAAAAGCAGGCTTCATGACGACGACGAGGGCGAAGTC
EMD1674-attB2	GGGGACCACTTTGTACAAGAAAGCTGGGTCCCAACCGAAACTTCTTCTCCTA
Analysis of T-DNA insertion mutants	
LB Primer	ATT TTG CCG ATT TCG GAA C
SALKseq_13577 8.1-LP	CAT TCC TTT AGC TAA CGT GCG
SALKseq_13577 8.1-RP	CCA ACA ACA TCG TCC AAA ATC
SALKseq_09105 4.2-LP	TGACAACATCATCCAAAGCC
SALKseq_09105 4.2-RP	TGA TTC GGT TCC ATT TGA AAC
SALKseq_13577 8.2-LP	ACGCCAAGAATCTTGTCCAG
SALKseq_13577 8.2-RP	TTGCTTTCACCATATGCCAG
SALKseq_13577 8.0-LP	ATAGGCACGTGGATTTGTCC
SALKseq_13577 8.0-RP	ACCAGGCGTAAGGTTGATTG
Primers used for site directed mutagenesis	
β KNL2 Δ N-For	ATGGTCACATTATCCGATTGGTGGCTAAC
β KNL2 Δ N-Rev	GAAGCCTGCTTTTTTGTACAAAGTTGGC
β KNL2 Δ SANTA-For	AATGAAGAAGAAGAAGAGAAGAAGAAGAAGAATGTTG
β KNL2 Δ SANTA-Rev	GGATTTTAGGGTTTTGATTGGAGTGATGACAG
β KNL2 Δ C-For	GACCCAGCTTTCTTGTACAAAGTTGGC

β KNL2 Δ C-Rev	GTAATCTTCCCAATCATAAGGAAACCCTAAACG
β KNL2(C)-For	ATGAATGAAGAAGAAGAAGAGAAGAAGAAG
β KNL2 Δ Motif I-For	TGTTTGAAAGATAAGATTTTGGACGATG
β KNL2 Δ Motif I-Rev	CTTCTTCTTCTTCTTCTTCTTCTTCTTC
β KNL2 Δ Motif II-For	AAATCTGATAAGGCATGTGAGAAATCAAG
β KNL2 Δ Motif II-Rev	ACAACCCTCAAGAGAATAAAGATCCTG
β KNL2 Δ Motif III-For	TATGAAGCTTCTATTGGGAAAAGAGTTG
β KNL2 Δ Motif III-Rev	ATCATCATCATCATCATCATCATCAAC
β KNL2 Δ Motif III new-Rev	AACTCTTTTCCCAATAGAAGCTTCATAC
Primers used for EMSA	
KNL2pf3aF	GGTTGCGATCGCATGGATTACAAGGATGACGATGACAAGGCAGCCGGT ATGACGACGACGAGGGCGAAGTCCAA
KNL2pf3aR	GTGTGTTTAAACTTACCAACCGAACTTCTTC
pAL1_f	GGTTAGTGTTTTGGAGTCGAATATG
pAL1_r	TTGCTTCTCAAAGATTTCATGGT
Primers used for genotyping and sequencing of constructs, colonies and transformants	
<i>attB1</i>	GGGGACAAGTTTGTACAAAAAAGCAGGCT
<i>attB2</i>	GGGGACCACTTTGTACAAGAAAGCTGGGT
Primers used for BiFC vectors construction	
BamHI 35S-For	ATGGATCCGTAAAACGACGGCCAGTGCCTAGC
MCS-35S-Rev	CTCGCATATCTCATTAAGCAGTCTAGAACTAGTGAATTCGCGAAAGC TCGAGAGAGATAG
MCS-tocs-For	CTATCTCTCTCGAGCTTTCGCGAATTCAGTCTAGACTGCTTTAAT GAGATATGCGAG
PstI-tocs-Rev	TACTGCAGCTGCTGAGCCTCGACATGTTGTCG
Eco-VenN-For	TAGAATTCATGGTGAGCAAGGGCGAGGAGC
Spe-VenN-cMYC-Rev	TAAC TAGTAAGATCCTCCTCAGAAATCAACTTTTGCTCCTCGATGTTGT GGCGGATC

Eco-VenC-For	TAGAATTCATGGACAAGCAGAAGAACGGCA
Spe-VenC-HA-Rev	TAACTAGTAGCGTAATCTGGAACATCGTATGGGTACTTGTACAGCTCGTCCATGCCGAGA
SpeI-cMYC-VenN-For	TAACTAGTATGGAGCAAAAGTTGATTTCTGAGGAGGATCTTATGGTGA GCAAGGGCGAGG
VenN-XbaI-Rev	TATCTAGACTACTCGATGTTGTGGCGGATCTTG
SpeI-HA-VenC-For	TAACTAGTATGTACCCATACGATGTTCCAGATTACGCTGACAAGCAGA AGAACGGCATC
VenC-XbaI-Rev	TATCTAGATTACTTGTACAGCTCGTCCATGCCG
SpeI-attR1-For	ATACTAGTTCAACAAGTTTGTACAAAAAAGCTG
SpeI-attR2-Rev	ATACTAGTAACCACTTTGTACAAGAAAGCTGAA

Appendix Table 2. Characterization and identification of the KNL2 variants in plants.

Species	Number of KNL2(s)	Database
Algae		
<i>Chlamydomonas reinhardtii</i>	1	JGI13
<i>Dunaliella salina</i>	1	JGI13
<i>Ostreococcus lucimarinus</i>	1	JGI13
<i>Coccomyxa subellipsoidea</i>	1	JGI13
<i>Chondrus crispus</i>	1	JGI13
Ferns		
<i>Azolla filiculoides</i>	2	ftp://ftp.fernbase.org/
<i>Salvinia cucullata</i>	2	ftp://ftp.fernbase.org/
<i>Ceratopteris richardii</i>	1	ftp://ftp.fernbase.org/
Lycophytes		
<i>Selaginella moellendorffii</i>	1	Ensembl plants; JGI; NCBI
Mosses		
<i>Physcomitrella patens</i>	1	Ensembl plants; JGI; NCBI
Liverworts		
<i>Marchantia polymorpha</i>	1	Ensembl plants; JGI; NCBI
Hornworts		
<i>Anthoceros angustus</i>	1	Ensembl plants; JGI; NCBI
Gymnosperms		
<i>Picea glauca</i>	1	https://bioinformatics.psb.ugent.be/plaza/versions/gymno-plaza/
<i>Picea abies</i>	1	ftp://plantgenie.org/Data/ConGenIE/
<i>Picea sitchensis</i>	1	Ensembl plants; JGI; NCBI
<i>Pinus pinaster</i>	1	Ensembl plants; JGI; NCBI
<i>Pinus sylvestris</i>	1	Ensembl plants; JGI; NCBI
<i>Pinus taeda</i>	1	Ensembl plants; JGI; NCBI
<i>Pseudotsuga menziesii</i>	1	Ensembl plants; JGI; NCBI

<i>Gnetum montanum</i>	1	Ensembl plants; JGI; NCBI
<i>Taxus baccata</i>	1	Ensembl plants; JGI; NCBI
<i>Cycas micholitzii</i>	1	Ensembl plants; JGI; NCBI
<i>Ginkgo biloba</i>	1	Ensembl plants; JGI; NCBI
Angiosperms		
<i>Aegilops tauschii</i>	2	Ensembl plants; JGI; NCBI
<i>Amaranthus hypochondriacus</i>	1	Ensembl plants; JGI; NCBI
<i>Amborella trichopoda</i>	1	ftp://ftp.ncbi.nlm.nih.gov/genomes/Amborella_trichopoda/
<i>Ananas comosus</i>	1	Ensembl plants; JGI; NCBI
<i>Aquilegia coerulea</i>	2	Ensembl plants; JGI; NCBI
<i>Asparagus officinalis</i>	1	Ensembl plants; JGI; NCBI
<i>Brachypodium distachyon</i>	3	JGI13
<i>Brachypodium stacei</i>	3	Ensembl plants; JGI; NCBI
<i>Colocasia esculenta</i>	1	Ensembl plants; JGI; NCBI
<i>Cinnamomum kanehirae</i>	1	https://www.ncbi.nlm.nih.gov/genome/57158
<i>Cucumis sativus</i>	1	Ensembl plants; JGI; NCBI
<i>Citrus sinensis</i>	2	Ensembl plants; JGI; NCBI
<i>Daucus carota</i>	1	Ensembl plants; JGI; NCBI
<i>Elaeis guineensis</i>	1	Ensembl plants; JGI; NCBI
<i>Eucalyptus grandis</i>	2	Ensembl plants; JGI; NCBI
<i>Fragaria vesca</i>	3	Ensembl plants; JGI; NCBI
<i>Glycine max</i>	3	Ensembl plants; JGI; NCBI
<i>Gossypium raimondii</i>	2	Ensembl plants; JGI; NCBI
<i>Hordeum vulgare</i>	3	Ensembl plants; JGI; NCBI
<i>Lactuca sativa</i>	2	Ensembl plants; JGI; NCBI
<i>Manihot esculenta</i>	1	Ensembl plants; JGI; NCBI
<i>Musa acuminata</i>	1	https://banana-genome-hub.southgreen.fr/
<i>Nelumbo nucifera</i>	2	https://www.ncbi.nlm.nih.gov/genome/?term=APLB0000000
<i>Oryza sativa</i>	2	JGI13
<i>Populus trichocarpa</i>	4	Ensembl plants; JGI; NCBI

<i>Phoenix dactylifera</i>	1	Ensembl plants; JGI; NCBI
<i>Setaria italica</i>	1	Ensembl plants; JGI; NCBI
<i>Solanum lycopersicum</i>	2	Ensembl plants; JGI; NCBI
<i>Sorghum bicolor</i>	3	Ensembl plants; JGI; NCBI
<i>Spirodela polyrhiza</i>	1	Ensembl plants; JGI; NCBI
<i>Triticum urartu</i>	1	Ensembl plants; JGI; NCBI
<i>Vitis vinifera</i>	2	JGI13
<i>Zea mays</i>	1	https://www.ncbi.nlm.nih.gov/genome/12
<i>Zostera marina</i>	1	Ensembl plants; JGI; NCBI
Brassicales		
<i>Tarenaya hassleriana</i>	2	ftp://ftp.ncbi.nlm.nih.gov/genomes/Tarenaya_hassleriana
<i>Carica papaya</i>	1	JGI_13
<i>Moringa oleifera</i>	2	http://herbalplant.ynau.edu.cn/html/Genomes/2.html
<i>Arabis alpina</i>	2	http://www.arabis-alpina.org/
<i>Aethionema arabicum</i>	1	http://brassicadb.org/brad/datasets/pub/BrassicaceaeGenome/
<i>Arabidopsis halleri</i>	2	JGI_13
<i>Arabidopsis lyrata</i>	2	JGI_13
<i>Arabidopsis thaliana</i>	2	JGI_13; TAIR10
<i>Brassica juncea</i>	4	http://brassicadb.org/brad/datasets/pub/Genomes/
<i>Brassica napus</i>	4	http://brassicadb.org/brad/datasets/pub/Genomes/
<i>Brassica nigra</i>	2	http://brassicadb.org/brad/datasets/pub/Genomes/
<i>Brassica oleracea</i>	2	plants.ensembl.org
<i>Brassica rapa</i>	2	http://brassicadb.org/brad/datasets/pub/Genomes/
<i>Brassica cretica</i>	2	https://www.ncbi.nlm.nih.gov/genome/70253?genome_assembly_id=384099
<i>Boechera retrofracta</i>	2	http://public.dobzhanskycenter.ru/ad89dedc8b4674276c9b0760f29b07af/
<i>Boechera stricta</i>	2	JGI
<i>Barbarea vulgaris</i>	2	185.45.23.197:5080/Barbarea_data/
<i>Capsella grandiflora</i>	1	JGI_13
<i>Cardamine hirsuta</i>	2	http://chi.mpipz.mpg.de/

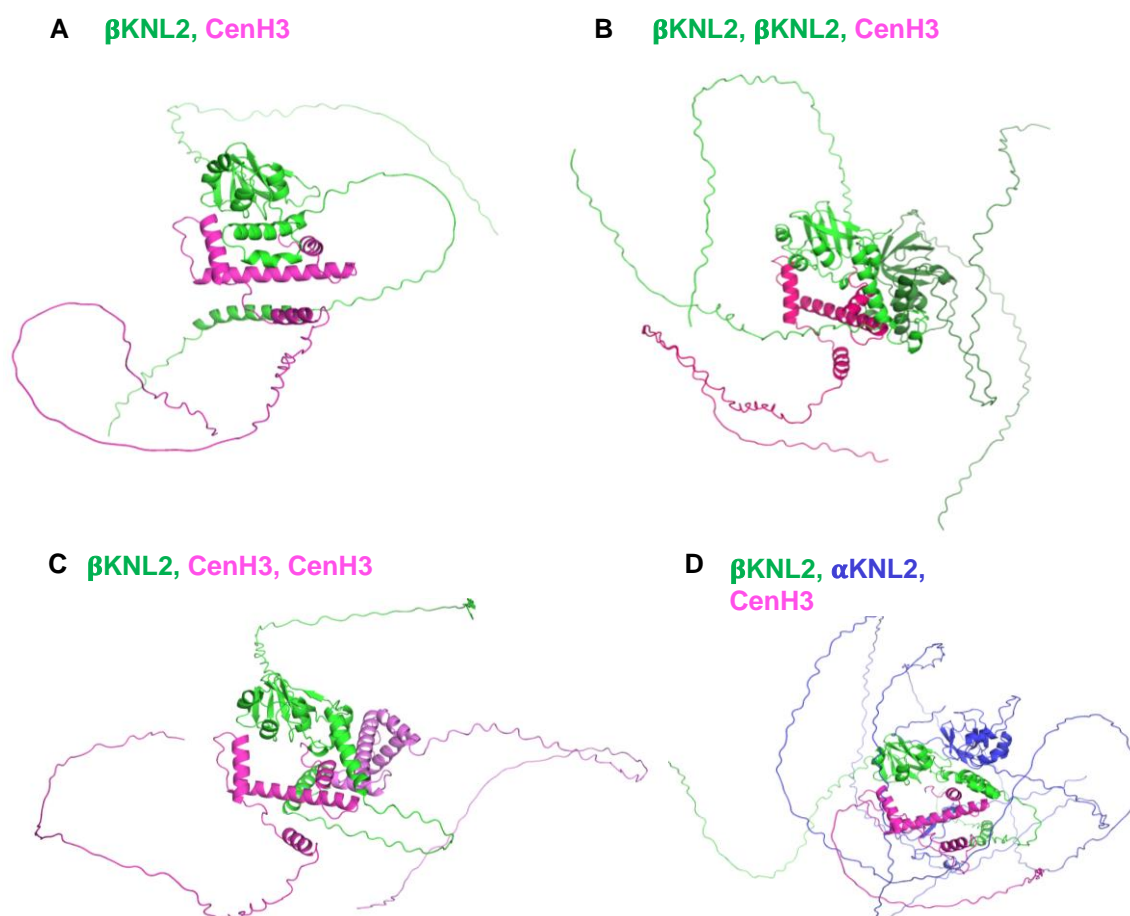
<i>Conringia planisiliqua</i>	1	JGI_13
<i>Capsella rubella</i>	2	JGI_13
<i>Camelina sativa</i>	6	ftp://ftp.ncbi.nlm.nih.gov/genomes/Camelina_sativa/
<i>Eutrema heterophyllum</i>	2	PKMM000000000
<i>Eutrema salsugineum</i>	2	JGI_13
<i>Euclidium syriacum</i>	2	JGI_13
<i>Eutrema yunnanense</i>	2	JGI_13
<i>Leavenworthia alabamica</i>	1	http://brassicadb.org/brad/datasets/pub/BrassicaceaeGenome/
<i>Lepidium meyenii</i>	6	http://maca.eplant.org/index.html
<i>Raphanus raphanistrum</i>	2	https://www.ncbi.nlm.nih.gov/genome/34361?genome_assembly_id=212223
<i>Raphanus sativus</i>	2	https://www.ncbi.nlm.nih.gov/genome/12929?genome_assembly_id=249276
<i>Sisymbrium irio</i>	2	http://brassicadb.org/brad/datasets/pub/BrassicaceaeGenome/
<i>Schrenkiella parvula</i>	2	http://brassicadb.org/brad/datasets/pub/BrassicaceaeGenome/
<i>Thlaspi arvense</i>	2	http://pennycress.umn.edu/download.html

Appendix Table 3. Reciprocal crossing of mutants with WT to confirm zygosity of mutation causing phenotype

Genotype	Number of seeds	% Normal seeds	% Aborted ovules	% Abnormal seeds
WT	745	94.6%	3.2%	2.1%
$\beta knl2-1 \times \beta knl2-1$	788	85.0%	0.8%	14.2%
$\beta knl2-2 \times \beta knl2-2$	565	87.3%	1.2%	11.5%
$\beta knl2-1 \times WT$	795	96.1%	2.6%	1.3%
$WT \times \beta knl2-1$	567	93.3%	1.7%	2.8%
$\beta knl2-2 \times WT$	819	95.5%	1.7%	2.8%
$WT \times \beta knl2-2$	646	92.4%	5.3%	2.3%

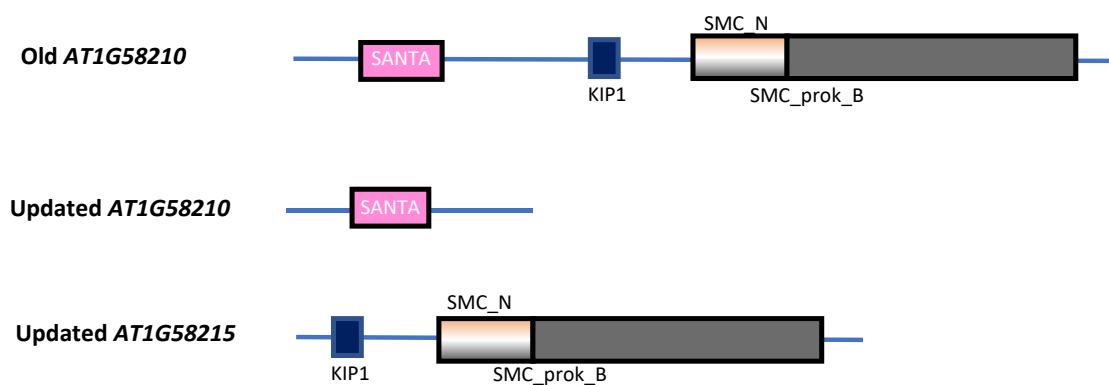
Appendix Table 4. Single silique genotyping of heterozygous $\beta knl2$ mutants

	$\beta knl2-1$ (n)	Percentage	$\beta knl2-2$ (n)	Percentage
Homozygous	29	16.0221	51	24.63768
Heterozygous	94	51.9337	106	51.20773
Wildtype	41	22.65193	35	16.90821
Missing data	17	9.392265	15	7.246377
Total (n)	181		207	



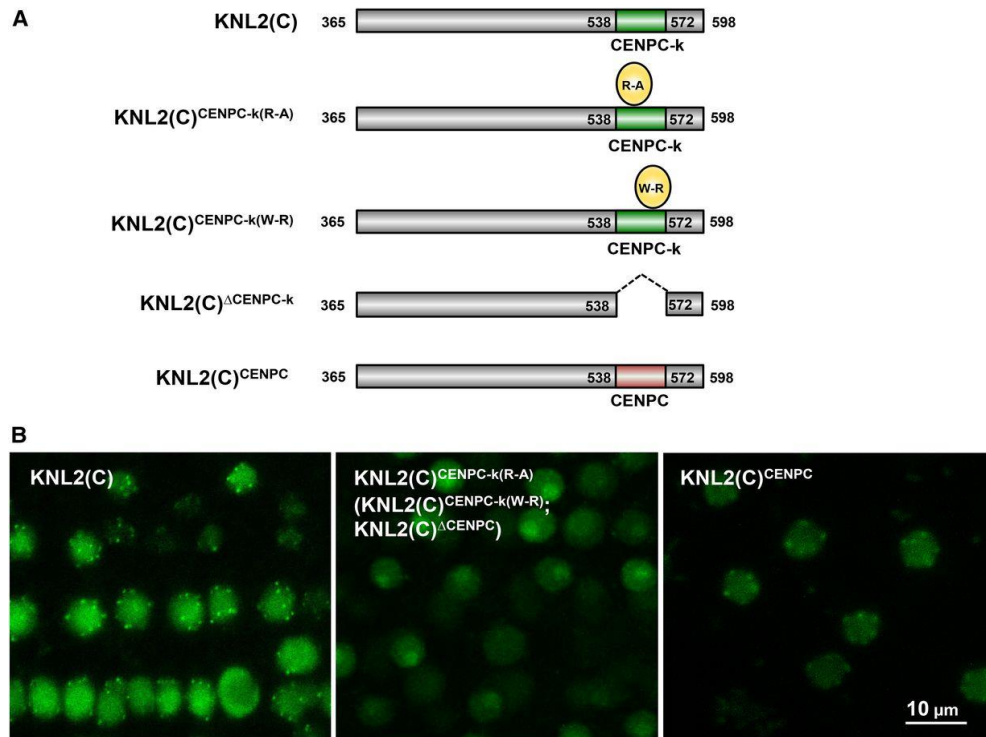
Appendix Figure 1. Predicted models of β KNL2 and CENP-A/CENH3 interactions

(A-C) Different combinations of β KNL2 and CENH3 in dimer and trimer forms. (D) Heterotrimer model of β KNL2, α KNL2, and CENH3, showing how these proteins might coalesce in a complex molecular assembly. Each model's left panels show the monomer colored in above referred color, varying degrees of the same color in case of homodimer.

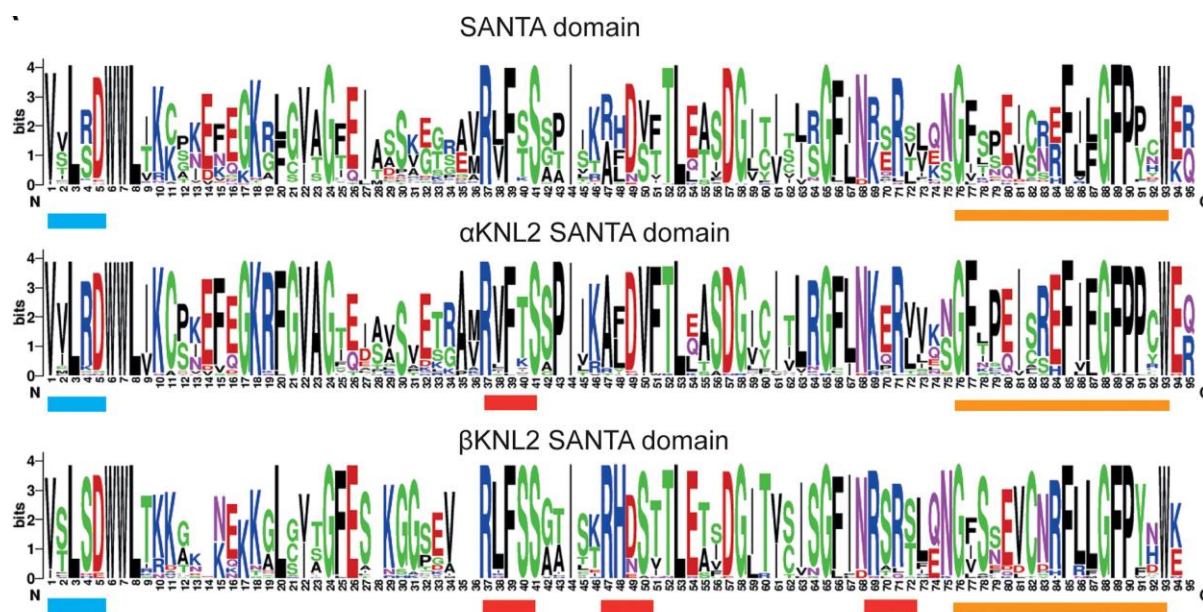


Appendix Figure 2. Re-annotation and updated domain structures of AT1G58210 genes in Arabidopsis.

This figure illustrates the re-annotation of the *AT1G58210* gene and the updated domain structure based on recent data from TAIR, Araport-11, and Phytozome 13. Updated *AT1G58210* gene encodes a 281 AA protein containing only the SANTA domain, now designated as β KNL2. The other gene *AT1G58215* with KIP1 and SMC_Prok_B domains, as NET2A.



Appendix Figure 3. Mutagenesis of conserved AA at the CENPC-k motif as well as its complete deletion results in KNL2 mislocalization that can be restored by the CENPC motif. Figure modified from Sandmann et al. (2017). **(A)** Schematic view of EYFP-tagged KNL2 constructs: KNL2(C), KNL2(C)^{CENPC-k(R-A)}, KNL2(C)^{CENPC-k(W-R)}, KNL2(C)^{ΔCENPC-k}, and KNL2(C)^{CENPC}. **(B)** Subnuclear localization of KNL2(C) (left panel), KNL2(C)^{CENPC-k(R-A)} (middle panel), and KNL2(C)^{CENPC} (right panel) fused to EYFP in root tip nuclei of Arabidopsis transformed with corresponding constructs. KNL2(C)^{CENPC-k(W-R)} and KNL2(C)^{ΔCENPC-k} proteins (indicated in brackets in the middle panel) showed the same localization pattern as KNL2(C)^{CENPC-k(R-A)}. The C-terminal part of KNL2 fused to EYFP showed nucleoplasmic and centromeric localization (Lermontova et al., 2013), while protein variants carrying the point mutations within the CENPC-k motif or lacking this motif completely lost an ability to localize at centromeres and were detected only at nucleoplasm and nucleolus. However, the C terminus of KNL2 with the substitution of CENPC-k by the CENPC motif was targeted to centromeres.



Appendix Figure 4. Alignments of SANTA domain and CENPC-k motif in KNL2 homologs presented in LOGO format.

Variation map of the SANTA domain in the KNL2 homologs. The upper panel aligns SANTA domains of all KNL2 homologs from Brassicales, whereas the middle and bottom panels represent SANTA domain alignments of α KNL2 and β KNL2 homologs, respectively. The conserved N-terminal and C-terminal hydrophobic motifs are marked by blue and orange bars, respectively. Putative Aurora kinase phosphorylation consensus sites are underlined with red bars. Figure modified from Zuo, et al. 2022.



Appendix Figure 5. Conservation of the CDK Consensus Motif (TPV/IK) in the N-Terminal Tail of β KNL2.

The figure presents a WebLogo illustrating the conservation of the CDK consensus motif (TPV/IK) in the N-terminal tail of β KNL2. This motif is critical for interactions and phosphorylation-dependent regulation. β KNL2 and α KNL2 form an intermonomeric β -sheet via the β SANTA domain and conserved AA preceding the SANTA domain of the TPV/IK motif. The TPV/IK motif is predicted to serve as a phospho-dependent CDK motif, a finding corroborated in other vertebrates (Pan et al., 2017, French and Straight, 2019, Watanabe et al., 2019).

Chapter 11: Curriculum vitae

Ramakrishna Yadala

<https://orcid.org/0000-0002-8731-7822>

Education

11/2020-Current	PhD: Martin Luther University Halle-Wittenberg Halle, Germany and Leibniz Institute of Plant Genetics and Crop Plant Research (IPK), Gatersleben
2018- 2020	Master of technology: Biotechnology& Bioprocess engineering VFSTR University, Guntur, India GPA: 9.56/10
2013 – 2017	Bachelor of technology: Biotechnology VFSTR University, Guntur, India GPA: 8.91/10

Research experience

11/2020-Current	PhD thesis: Leibniz Institute of Plant Genetics and Crop Plant Research, Gatersleben, Germany Thesis title: Identification and Characterization of EMB1674, as a Novel KNL2 Variant: Revealing Its Centromere Targeting Mechanism and Critical Role in Plant-Specific Kinetochore Assembly
09/2020-10/2020	Research assistant: Leibniz Institute of Plant Genetics and Crop Plant Research, Gatersleben, Germany
07/2019- 08/2020	Master thesis (Research assistant): Leibniz Institute of Plant Genetics and Crop Plant Research, Gatersleben, Germany Thesis title: <i>Small lateral spikelet1 (sls1)</i> candidate gene identification and characterization in barley
10/2017- 06/2018	Research assistant: VFSTR deemed to be university, & Prof. P B Kavi Kishor Lab, Hyderabad, India
06/2016- 12/2016	Bachelor thesis: Prof. Rajeev K Varshney lab, ICRISAT, India Thesis title: Molecular diversity analysis in Chickpea

Grants

09/2023- 09/2023	COST Action Grant, EPICATCH, STSM grant – CA19125
06/2021- 09/2021	COST Action Grant, ECOST, STSM–CA16212-47992

Publications

1. **Yadala, Ramakrishna***, Amanda Souza Camara, Surya Prakash Yalagapati, Pascal Jaroschinsky, Tobias Meitzel, Mariko Ariyoshi, Tatsuo Fukagawa, Twan Rutten, Thi Thu Giang Bui, and Inna Lermontova. "Structural Basis of betaKNL2 Centromeric Targeting Mechanism and Its Role in Plant-Specific Kinetochore Assembly." *bioRxiv* (2024): 2024-07.

2. Yalagapati, Surya Prakash, Ulkar Ahmadli, Aditya Sinha, Manikandan Kalidass, Siarhei Dabravolski, Sheng Zuo, **Ramakrishna Yadala** et al. "Centromeric localization of α KNL2 and CENP-C proteins in plants depends on their centromere-targeting domain and DNA-binding regions." *Nucleic Acids Research* (2024): gkae1242.
3. Zuo, Sheng¹, **Ramakrishna Yadala**¹, Fen Yang, Paul Talbert, Joerg Fuchs, Veit Schubert, Ulkar Ahmadli et al. "Recurrent plant-specific duplications of KNL2 and its conserved function as a kinetochore assembly factor." *Molecular Biology and Evolution* 39, no. 6 (2022): msac123.
4. **Yadala, Ramakrishna**, Maryia Ratnikava, and Inna Lermontova. "Bimolecular Fluorescence Complementation to Test for Protein–Protein Interactions and to Uncover Regulatory Mechanisms During Gametogenesis." In *Plant Gametogenesis: Methods and Protocols*, pp. 107-120. New York, NY: Springer US, 2022.
5. Jain, Ankit, Manish Roorkiwal, Sandip Kale, Vanika Garg, **Ramakrishna Yadala**, and Rajeev K. Varshney. "InDel markers: An extended marker resource for molecular breeding in chickpea." *PLoS One* 14, no. 3 (2019): e0213999.
6. **Ramakrishna, Y.**, J. Chittaranjan, S. Krupanidhi, and N. Jalaja. "Molecular Phylogenetic Affinities of Endangered Trombidium Grandissim Using Mitochondrial 16S rDNA Sequence." *RESEARCH JOURNAL OF PHARMACEUTICAL BIOLOGICAL AND CHEMICAL SCIENCES* 8, no. 2 (2017): 2001-2007.

Manuscripts under preparation

7. **Yadala, Ramakrishna**^{1*}, Fen Yang¹, Ales Pecinka and Inna Lermontova "βKNL2 needs to be localized at centromeres for proper mitosis and plant growth"

*Co-corresponding author & ¹Equal contribution author

Achievements

1. **Full merit scholarship** for the Master studies from VFSTR, Guntur (2018 -2020)
2. **Best paper presentation** prize in National conference on Biodiversity conservation at Sree Narayana Guru College, Coimbatore, 2017
3. **Several prizes** in university level competitions like worthy scrap, caroms, cooking, etc. at VFSTR University, Guntur, 2015

Selected Conferences

1. Poster presented in Plant genome stability and change 2024
2. Oral presentation in PSSC 2023, Gatersleben
3. Poster presented in EMBL Conference Chromatin and Epigenetic, 2023
4. Oral presentation in Chromosome Biology Retreat 2023
5. Lightning talk in EWPC 2022
6. Poster presented in ICAR 2022 (virtual)

Chapter 12: Eidesstattliche Erklärung / Declaration under oath

Ich erkläre an Eides statt, dass ich die Arbeit selbstständig und ohne fremde Hilfe verfasst, keine anderen als die von mir angegebenen Quellen und Hilfsmittel benutzt und die den benutzten Werken wörtlich oder inhaltlich entnommenen Stellen als solche kenntlich gemacht habe.

I declare under penalty of perjury that this thesis is my own work entirely and has been written without any help from other people. I used only the sources mentioned and included all the citations correctly both in word or content.

Datum / Date

*Unterschrift des Antragstellers /
Signature of the applicant*